UNIVERSIDADE DA CORUÑA

Development of alternative strategies for preservation and generation of corneal tissues for transplantation

Silvia Rodríguez Fernández

UDC Doctoral Thesis 2022

Programa de Doutoramento en Ciencias da Saúde

Directoras:

Silvia María Díaz Prado
María Esther Rendal Vázquez

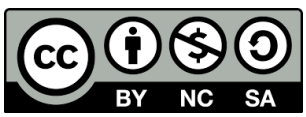

A Dra. Silvia María Díaz Prado, profesora titular da Área de Anatomía e Embrioloxía Humana do Departamento de Fisioterapia, Medicina e Ciencias Biomédicas da Universidade da Coruña, e a Dra. María Esther Rendal Vázquez, bióloga do Establecemento de Tecidos – Área de Criobioloxía do Complexo Hospitalario Universitario da Coruña,

Certifican

Que Dna. Silvia Rodríguez Fernández, graduada en Bioloxía pola Universidade da Coruña e con mestrado en Asistencia e Investigación Sanitaria con especialidade en Fundamentos de Investigación Biomédica pola Universidade da Coruña, realizou baixo a nosa dirección o traballo "Desenvolvemento de estratexias alternativas para a conservación e creación de tecidos corneais para transplante", e que dito traballo reúne as condicións necesarias de orixinalidade e rigor científico para ser defendido publicamente e optar á mención de doutora internacional en Ciencias da Saúde.

A Coruña, 20 de xullo de 2022

Dra. Silvia María Díaz Prado

Dra. María Esther Rendal Vázquez

Parte da investigación incluída nesta tese de doutoramento foi realizada no laboratorio da Dra. Stéphanie Proulx, baixo a súa supervisión, no *Centre de Recherche du Centre Hospitalaire Universitaire de Québec – Université Laval* de Québec (Canadá), durante unha estadía de investigación predoutoral de tres meses no ano 2019.

"The cake is a lie"

Portal, 2007

Para comezar, quero e debo expresar o meu agradecemento a todas aqueles familiares que permitiron a doazón de córneas dos seus seres queridos falecidos, pois sen eles, esta tese doutoral non sería posible.

Quero agradecer ás miñas directoras de tese, á Dra. Silvia Díaz Prado, do grupo de Terapia Celular e Medicina Rexenerativa (TCMR) da Universidade da Coruña (UDC), e á Dra. Esther Rendal Vázquez, bióloga da Unidade de Criobioloxía co Complexo Hospitalario Universitario da Coruña (CHUAC), a posibilidade que me deron de realizar este traballo dentro do grupo de TCMR, no Instituto de Investigación Biomédica de A Coruña (INIBIC). Grazas por ensinarme o que é a investigación e o mundo que o rodea. Grazas por apoiarme e por guiarme.

Dou as grazas tamén a todas aqueles profesionais, clínicos e investigadores, que me axudaron nalgún momento para sacar adiante a miña tese. Así, pola parte do CHUAC, quero dar as grazas ó Servizo de Criobioloxía e a Jacinto Sánchez Ibáñez, responsable da colección de córneas para investigación. Ó oftalmólogo Marcelino Álvarez Portela, que me axudou a aprender a manipular unha córnea como un clínico. A Purificación Filgueira Fernández e Beatriz Cruz Caamaño, técnicos de histoloxía do INIBIC. A Isidoro Baltar, biólogo da Unidade de Xenética, polo seu humor e as súas magníficas ideas, e a Arantxa García, bióloga tamén da Unidade de Xenética, sempre sincera e perseverante e sempre portadora de bos consellos. E sobre todo, grazas a Álex Montero Salinas, responsable das extraccións de córneas do Complexo Hospitalario Universitario da Coruña e compañeiro nestes estudos de doutoramento. Teño que dicirche que sempre tiñas razón, xa que me facías caer da burra mostrándome a realidade antes de que os demais a admitisen.

Pola parte da UDC, os meus máximos agradecementos a Catalina Sueiro López e a Ada Castro Couceiro, da Unidade de Microscopía do Servizo de Apoio á Investigación (SAI), que me asesoraron en todo o posible neste traballo cargado de imaxes; e do SAI tamén, a Jorge Otero Canabal, da Unidade de Espectroscopía Molecular, que me fixo ver o bonita que poder ser a química, o cal foi un sopro de aire fresco cando estaba atoada coa bioloxía. Tamén agradezo a Julián Yáñez, por atender ós correos desesperados de "se busca osmómetro", e deixarme as portas abertas do seu laboratorio para realizar os meus experimentos.

Merci aussi à la Dr. Stéphanie Proulx pour m'avoir reçu dans son laboratoire à Québec, et pour m'avoir montré comment travailler avec un tissu pour lequel je n'avais que peu de connaissance.

C'était ma première année d'étude au doctorat et même ainsi, vous m'avez fait pleinement confiance. Merci pour votre aide et pour votre enthousiasme scientifique.

E voltando ó laboratorio, teño moito que agradecer a María *senpai* (¿ou debería dicir *sensei*?), que sen dúbida, foi a que sempre estivo disposta a axudarme en todo, a que sempre me animou e me deu bos consellos, e a que (sorte que teño), o segue a facer. Grazas por esa graciosa ironía túa e pola teu racionalismo e sinceridade. Quero agradecer tamén a toda aquelas persoas que estiveron comigo, traballando nos mesmos proxectos e/ou aturando ás miñas desgrazas e queixas continuas. Grazas, Miriam, Paula *ma camarade*, Nati, Paz, rapazas de "Onco", Rocío e Clara, por estar aí para compartir o día a día, as tristezas, os desacougos, as alegrías e as tolerías (alleas) que nos fixeron e fan tolear a nós tamén.

Grazas á Consellería de Cultura, Educación e Ordenación Universitaria (Xunta de Galicia) e ó Fondo Social Europeo polo financiamento do meu contrato de investigadora predoutoral (ED481A-2019-206). Ó programa inMOTION INDITEX-UDC por financiarme unha estadía predoutoral, coa que puiden completar a miña tese e optar á mención internacional. Tamén quero agradecer o apoio financeiro que permitiu levar a cabo esta tese doutoral proporcionado polas Axudas da Xunta de Galicia para Grupos con Potencial de Crecemento (ED431B 2020/55).

E para terminar, quero dar as "gracias" a varias persoas e outros mamíferos alleos ó laboratorio, que foron os pilares principais que me sostiveron durante esta etapa. A Mathieu, persoa positiva onde as haxa, por aturarme moito, moito, moito a pesar das pequenas dificultades de comunicación por mor do español-galego-francés-inglés. Só che faltan os pompóns de animador cando me falas do futuro que haberá despois da tese doutoral, que tal como o presentas, mala pinta non ten. Grazas ós meus pais e ós meus "irmaos", sempre preocupados, sempre apoiándome, sempre animándome a "aguantar e avanzar", como tamén o fixeron os meus amigos máis próximos que se atopan espallados polo mundo. E como non, gracias ós peludos de catro patas, pero en especial, ó meu toxiño, Isa, que nos atopamos no camiño cando quizais máis nos necesitábamos.

Grazas por todo.

Index

List of abbreviations

$(CH_3)_2SO$: Dymetil sulfoxide

µL: Microliter

µM: Micromolar

µm: Micrometer

^1H: Proton

AM: Acetoxymethyl ester

BK: Bullous keratopathy

BSA: Bovine serum albumin

CDKI: Cyclin-dependent kinase inhibitor

CF: Calcium Free

CO_2: Carbon dioxide

CPA: Cryoprotective agent

CS: Cryoprotectant solution

CS1.1: Cryoprotectant solution 1 of protocol 1

CS1.2: Cryoprotectant solution 2 of protocol 1

CS1.3: Cryoprotectant solution 3 of protocol 1

CS2.1: Cryoprotectant solution 1 of protocol 2

CS2.2: Cryoprotectant solution 2 of protocol 2

CS2.3: Cryoprotectant solution 3 of protocol 2

D_2O: Deuterium oxide

DAPI: 4 ',6-diamidino-2-fenilindole

dDM: decellularized Descemet's membrane

DiIC18(5)-DS: 1,1'-Dioctadecyl-3,3,3',3'-Tetramethylindodicarbocyanine-5,5'-Disulfonic Acid

DiI: DiIC18(5)-DS

DiO: SP-DiOC18(3)

DM: Descemet's membrane

DMEK: Descemet's membrane endothelial keratoplasty

DMEM: Dulbecco's modified Eagle's medium

DMSO: Dimethyl sulfoxide

DNA: Deoxyribonucleic acid

DPX: Dibutylphthalate Polystyrene Xylene

DSAEK: Descemet's stripping automated endothelial keratoplasty

EBAA: Eye Bank Association of America

ECD: Endothelial cell density

ECM: Extracellular matrix

ECs: Endothelial cells

EDTA: Ethylenediaminetetraacetic acid

EGF: Epidermal growth factor

EK: Endothelial keratoplasty

E_K: Kinetic energy

FBS: Fetal bovine serum

FD: Fuchs' dystrophy

FISH: Fluorescence *in situ* hybridization

g: Gram

GAG: Glycosaminoglycan

GMP: Good manufactures practices

h: Hour

H_2O: Water

hCEnT-21T: Human corneal endothelial transformed cell line 21T

hECs: Human endothelial cells

HEPES: 4-(2-hydroxyethyl)-1-piperazineethanesulfonic acid

INIBIC: Instituto de Investigación Biomédica de A Coruña

IOP: Intraocular pressure

L: Liter

LK: Lamellar keratoplasty

M: Molarity

mg: Milligram

min: Minute

mL: Milliliter

mm: Millimeter

mm^2: Millimeter square

mOsmol/kg: Milliosmole/kilogram

N/A: Not available

Na^+/H^+: Sodium – proton exchanger

Na^+/HCO_3^-: Sodium – bicarbonate cotransporter

Na^+/K^+ ATPase: Sodium – potassium-adenosine triphosphatase

NMR: Nuclear magnetic resonance

npCPA: Non-permeating CPA

°C: Degree Celsius

°: Degree

OsO_4: Osmium tetroxide

P/S: Penicillin/streptomycin

P1: Protocol 1

$p16^{INK4a}$: Protein 16 kDa cyclin-dependent kinase inhibitor 2A

P2: Protocol 2

$p21^{Cip1}$: Protein 21 kDa cyclin-dependent kinase inhibitor 1

$p27^{Kip}1$: Protein 27 kDa Cyclin-dependent kinase inhibitor 1B

P3: Protocol 3

P4: Protocol 4

PBS: Phosphate buffered saline

PSS-L: Phosphate buffered saline solution *"di lavaggio"*

pCPA: Permeating CPA

pH: Potential hydrogen

PK: Penetrating keratoplasty

ppm: Particles per million

RT: Room temperature

s: Second

SAI: *Servizo de Apoio á Investigación*

SD: Standard deviation

Seg: Segments

SP-DiOC18(3): 3,3'-Dioctadecyl-5,5'-Di(4-Sulfophenyl)Oxacarbocyanine

TE: Tissue engineering

TE-EK: Tissue engineered-endothelial keratoplasty

TEM: Transmission electron microscopy

T_g: Glass transition temperature

TGF-β2: Transforming Growth Factor β2

TK: Tectonic keratoplasty

T_m: Melting temperature

***UDC**: Universidade da Coruña*

v/v: volume per volume

WS: Wash solution

WS1: Wash solution 1

WS2: Wash solution 2

WS3: Wash solution 3

x *g*: Times gravity

ZO-1: Zonula ocludens 1

List of figures

List of tables

Resumo

A queratoplastia ou transplante de córnea é o único tratamento dispoñible para moitas enfermidades corneais. Sen embargo, o acceso ás queratoplastias vese limitado pola dispoñibilidade das córneas doadas para transplante.

Para incrementar o número de tecidos corneais, nesta tese investigáronse métodos de preservación de córneas alternativos e outras fontes de tecido corneal para queratoplastias. O primeiro obxectivo consistiu en analizar o efecto, en córneas humanas, de protocolos de criopreservación convencional con dimetil sulfóxido (DMSO) con (P1) e sen albúmina (P2), e de protocolos de vitrificación sen (P3) e con formamida (P4). O segundo obxectivo consistiu no desenvolvemento dun enxerto mediante enxeñaría de tecidos empregando membranas de Descemet como andamios e células endoteliais (CEs) para construír o endotelio. Tanto células como andamios procederon de córneas descartadas para o seu uso en clínica.

Os resultados obtidos para o primeiro obxectivo mostran que só o P1 proporcionou córneas criopreservadas con CEs viables e unha estrutura xeral deformada. Sen embargo, a variabilidade dos resultados impide aplicar este protocolo na clínica. Os resultados do segundo obxectivo mostraron que é posible crear un enxerto a partir de córneas descartadas. Non obstante, a duración do estudio impediu que se crease un endotelio completamente funcional.

Estas dúas prometedoras metodoloxías representan alternativas coas que, nun futuro, e tras máis estudos para a súa mellora, se podería reciclar e incrementar o número de tecidos corneais transplantables e mellorar o acceso ás queratoplastias.

Resumen

La queratoplastia o trasplante de córnea es el único tratamiento disponible para muchas enfermedades corneales. Sin embargo, el acceso a las queratoplastias se ve limitado por la disponibilidad de las córneas donadas para trasplante.

Para incrementar el número de tejidos corneales, en esta tesis se investigaron métodos de preservación de córneas alternativos y otras fuentes de tejido corneal para queratoplastias. El primer objetivo consistió en analizar el efecto, en córneas humanas, de protocolos de criopreservación convencional con dimetil sulfóxido con (P1) y sin albúmina (P2), y de protocolos de vitrificación sin (P3) y con formamida (P4). El segundo objetivo consistió en el desarrollo un injerto mediante ingeniería de tejidos empleando membranas de Descemet como andamios y células endoteliales (CEs) para construir el endotelio. Tanto células como andamios procedieron de córneas descartadas para su uso en clínica.

Los resultados obtenidos para el primer objetivo muestran que sólo el P1 proporcionó córneas criopreservadas con CEs viables y una estructura general deformada. Sin embargo, la variabilidad de los resultados impide aplicar dicho protocolo en la clínica. Los resultados del segundo objetivo mostraron que es posible crear un injerto a partir de córneas descartadas. No obstante, la duración del estudio impidió que se crease un endotelio completamente funcional.

Estas dos prometedoras metodologías representan alternativas con las que, en un futuro, y tras más estudios para su mejora, se podría reciclar e incrementar el número de tejidos corneales trasplantables y mejorar el acceso a las queratoplastias.

Abstract

Many corneal diseases can only be treated through keratoplasty, a corneal transplantation whose access is dependent on the limited availability of transplantable donor corneas. To increase the number of corneal tissues, this thesis investigated alternative preservation methods and alternative sources of transplantable corneal tissues.

The first objective was to investigate the effect, on human corneas, of cryopreservation protocols using dimethyl sulfoxide (DMSO) with (P1) and without albumin (P2), and of vitrification protocols without (P3) and with formamide (P4). The second objective was to engineer new transplantable tissues using Descemet's membranes (DMs) and human endothelial cells (hECs) isolated from discarded corneas which were unfit for clinical use.

Results showed that only P1 provided corneas with viable ECs and a slightly distorted general structure, but variability among C1-cryorpeserved corneas did not allow to use this protocol in the clinical practice. A corneal graft was successfully engineered using discarded corneas with an intact decellularized DM seeded with primary hECs. However, a fully functional endothelium was not observed within the timeframe used in this study. Consequently, additional research will be needed to improve both approaches for clinical applications.

In the future and after further studies, these approaches would represent promising alternatives to improve the availability of transplantable corneal tissues and the access to keratoplasty.

I. Introduction

1. Anatomy of the human cornea

The cornea is a transparent and curved tissue located in the anterior part of the eyeball. The corneal tissue is avascular (di Zazzo *et al.*, 2021) and highly innervated (Al-Aqaba *et al.*, 2019). An adult human cornea has a thickness of approximately 500-550 μm, at his central part, and has a diameter of around 12 mm horizontally and 11 mm vertically (DelMonte and Kim, 2011; Dua and Said, 2019a). The main role of the cornea is to protect the intraocular space from external agents and to provide two thirds of the eye refractive power needed to direct the light toward the retina (Meek and Knupp, 2015).

The human cornea presents a specific structure that includes the epithelium, the Bowman's layer, the stroma, the Descemet's membrane, and the endothelium (**Figure 1**).

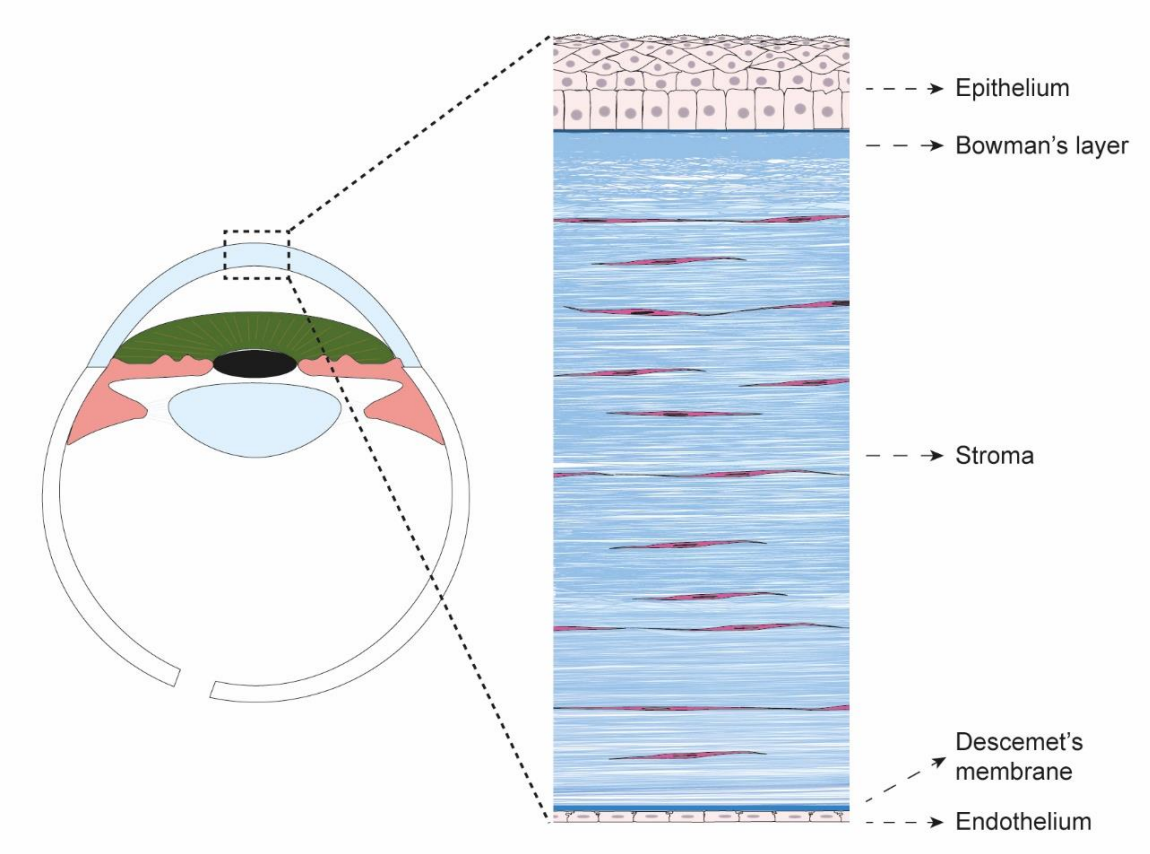

***Figure 1**. Anatomic illustration of the human cornea and its main corneal layers.*

1.1. Epithelium

A non-keratinized squamous stratified epithelium covers the anterior part of the cornea. The epithelium is made of 4 to 6 layers of cells with different shapes and with a thickness of 40-50 µm (**Figure 2**) (Dua and Said, 2019b). Columnar basal cells lie on their own secreted basal membrane composed mainly of type IV collagen and laminin (Eghrari, Riazuddin and Gottsch, 2015). Over those basal cells, polyhedral or oval cells with lateral extensions, called "wing" cells, form two to three layers. The most external superficial flat cells emit microvilli, that provides more surface to the glycocalyx, which interacts with the tear film to produce a smooth surface (Dua and Said, 2019b). Together with the external tear film, the epithelium acts as a physical barrier that protects the eye against external factors (Bashir, Seykora and Lee, 2017; Dua and Said, 2019b). This layer prevents an excessive fluid loss and allows the selective diffusion of oxygen (Dua and Said, 2019b).

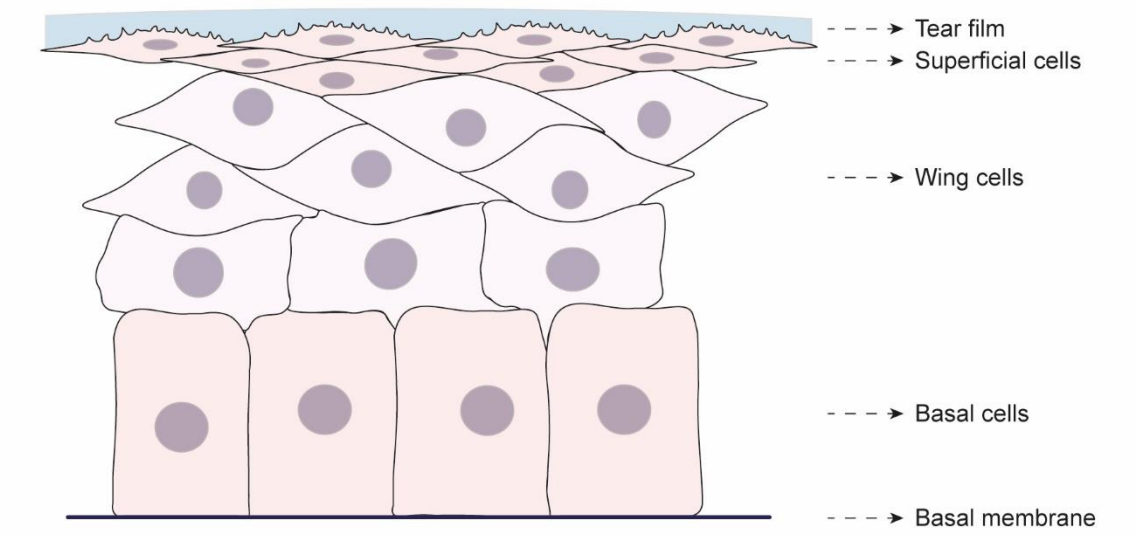

***Figure 2**. Illustration of the corneal epithelium, with the three types of epithelial cells (superficial, wing and basal cells) lying on the epithelial basal membrane. A tear film covers the superficial epithelial cells.*

The epithelium is routinely renewed as apical cells are lost due to desquamation. This renewal depends on the epithelial stem cells located at the corneal periphery, in the limbal epithelial crypts (Dua *et al.*, 2005). They produce new cells that migrate centripetally on the epithelial basal cell layer (Joyce *et al.*, 1996), and then vertically toward the surface layers (Figueiredo *et al.*, 2019).

1.2. Bowman's layer

The Bowman's layer is located between the epithelial basal membrane and the stroma. This layer consists of a thin, compact, and dense matrix of randomly disposed type I and

type III collagen fibers, with a thickness of 8-10 μm. Fibers of the posterior face of the Bowman's layer are woven into the anterior stroma. Although its function is not clear, it has been suggested that this layer provides rigidity and facilitates the optimum shape of the cornea. If damaged, the Bowman's layer is not able to regenerate (Dua and Said, 2019a).

1.3. Stroma

The stroma is the thickest corneal layer, measuring approximately 500 μm and confers most of refractive power of the cornea (**Figure 3**). This layer is a highly organized connective tissue in which keratocytes and nerves are embedded. In normal conditions, the stroma is in a relative deturgescent (dehydrated) state, with only 78% of its water absorption capability being filled (Dua and Said, 2019a).

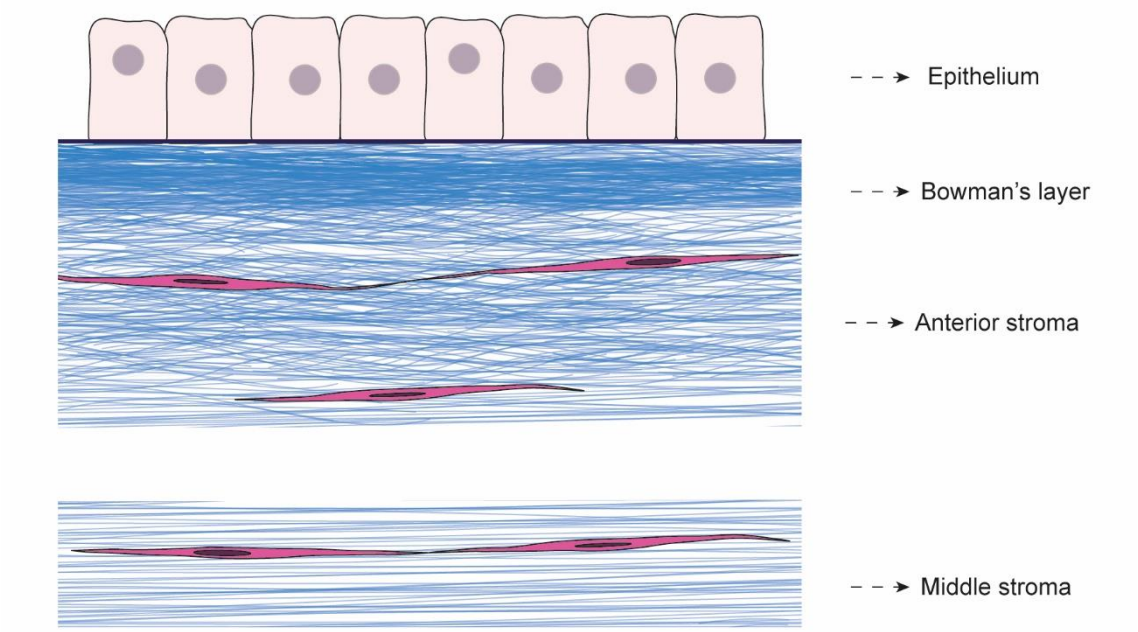

***Figure 3**. Illustration of a transversal section of the corneal stroma. Dense Bowman's layer shows woven fibers with the anterior stroma. Keratocyte's density (with fuchsia cytoplasm and purple nuclei) is higher in the anterior part compared to the middle stroma, where collagen forms lamellae disposed more uniformly.*

The matrix is mainly composed of type I and type V collagens. They form fibers with an uniform diameter that are disposed in parallel, equidistant to each other, and form 200 to 250 sublayers named lamellae (Massoudi, Malecaze and Galiacy, 2016; Dua and Said, 2019a). In the central and posterior part of stroma, those lamellae are disposed parallelly to the corneal surface and in an angle of 45° to each other (Radner *et al.*, 1998). However, in the anterior stromal face, fibers are randomly oriented to each other, and some fibers from the Bowman's layer penetrate in this area and *vice versa*. The anterior stromal face

is, therefore, highly interconnected, giving a compact appearance to this area and providing resistance to shear forces and stiffness (L. Müller, Pels and Vrensen, 2001).

Collagen fibers are surrounded by proteoglycans, which are composed of a core protein to which glycosaminoglycans (GAGs) are covalently bound. Water molecules bind to the polar GAGs, and this provides an accumulation of water in the tissue. In the stroma, the principal GAGs are chondroitin sulphate, dermatan sulphate, and keratan sulphate (Meek and Knupp, 2015). Due to their water attraction capability, proteoglycans modulate the distance between collagen fibers, ensuring the parallel disposition of the collagen fibers to reduce light scattering. This structural organization, as well as the physicochemical properties of their extracellular matrix (ECM) constituents, confer to the stroma its curvature, transparency, and tensile strength, and ensure the correct light refraction (Lewis *et al.*, 2010; Winkler *et al.*, 2013; Meek and Knupp, 2015; Dua and Said, 2019a).

The stromal cells are named keratocytes. These cells secrete stromal matrix components and are responsible for their maintenance. Cell density decreases from the anterior to the posterior stroma. If damage is caused to the stroma, keratocytes are activated and migrate to the injured site where they transform into myofibroblasts. There they secrete ECM proteins and metalloproteinases that degrade collagen to remodel and repair the damaged area. The result is often a fibrotic-like tissue with reduced transparency, which affects the visual acuity (Myrna, Pot and Murphy, 2009; Meek and Knupp, 2015; Dua and Said, 2019a).

1.4. Descemet's membrane

The Descemet's membrane (DM) is the specialized basal membrane of the corneal endothelium which supports the endothelial cells (ECs) (**Figure 4**). In an adult DM, it is possible to identify two sublayers. This differentiation is based on the moment in life where they were secreted, their components' arrangement, and their composition (Ali *et al.*, 2016; de Oliveira and Wilson, 2020). The prenatal striated anterior sublayer is composed of type VIII collagen, type IV collagen α1-α6 chains, fibronectin and vitronectin. The postnatal non-striated posterior sublayer of the DM is composed of type IV collagen α1-α6 chains, laminin 411 and 511, perlecan and nidogen (Murphy, Alvarado and Juster, 1984; Kabosova *et al.*, 2007). The postnatal sublayer never stops growing, achieving more than 10 μm of thickness at old age (Murphy, Alvarado and Juster, 1984).

1.5. Endothelium

The corneal endothelium is a 4 µm thick packed cobblestone-like cell monolayer that lies on the DM and is in contact with the aqueous humor of the anterior chamber (**Figure 4**). The role of this layer is to supply the cells of the other layers with nutrients, to eliminate metabolic waste and ions, and to maintain the corneal transparency through the control of the stromal (de)hydration (Bonanno, 2012; Klyce, 2020).

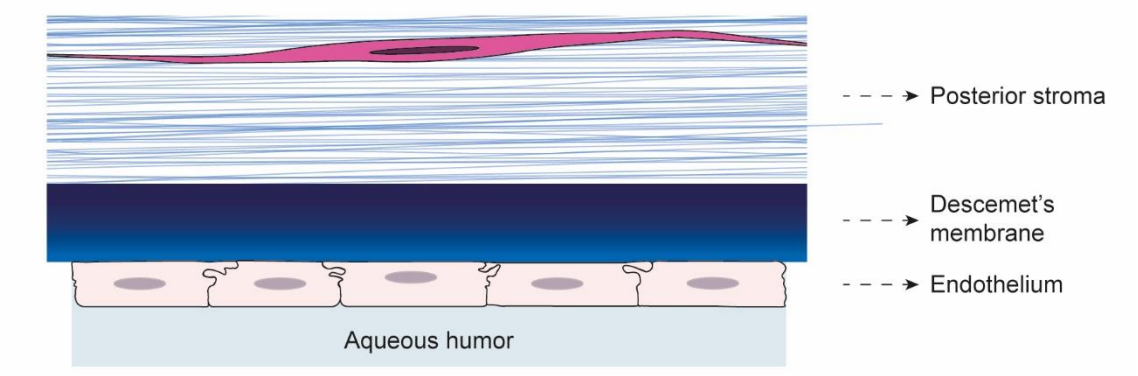

***Figure 4**. Illustration of the posterior stroma, the Descemet's membrane (DM), and the endothelium. The posterior stroma presents less keratocytes (fuchsia cytoplasm, purple nucleus). The DM possess two sublayers, secreted prenatally (dark blue) and after birth (lighter blue). The endothelial cells morphology varies from the apical part in contact with the aqueous humor toward the basal part, in contact with DM, where interdigitations are more numerous.*

1.5.1. Endothelium as a leaky barrier

The ECs are known for their particular morphology and their protein disposition. ECs have a hexagonal-like morphology in their apical part, created by the cytoskeletal actin, myosin IIA and vimentin proteins, which provide tensile strength to the cells. This structure is connected to the tight junctions through the scaffolding protein zonula occludens 1 (ZO-1). This combination of cytoskeletal structure and tight junctions provides resistance to the intraocular pressure (IOP), regulating the water stromal intake through the endothelium.

Just below the apical-lateral level and toward the DM, ECs' hexagonality is progressively lost and the cell membrane begins to present finger-like protrusions that become more complex near the DM, where a blossom-like morphology is observed. Adherens junctions and gap junctions are located below the apical surface in the lateral side of the ECs (Joyce, 2003; He, Forest, Gain, *et al.*, 2016).

The endothelium uses this stratified system of junctions and interdigitations to regulate EC-EC interaction and to generate a semipermeable or "leaky" barrier that controls the passage of molecules from the aqueous humor to the stroma, and *vice versa* (Joyce, 2003; Klyce, 2020).

1.5.2. Endothelium as a "pump" barrier

To counteract the water entering the stroma and, therefore, to maintain a dehydrated and transparent cornea, it was hypothesized that the endothelium acts as an active pump barrier that allows ions and other molecules to be evacuated from the stroma through ECs, which consequently cause a passive water movement into aqueous humor (Maurice, 1972; Bonanno, 2012). To date, the mechanism of the "endothelial pump" and how the endothelium regulates the dehydrated state of stroma is not fully understood (Klyce, 2020).

This pump mechanism uses several transmembrane transporters, including the sodium-potassium adenosine triphosphatase (Na^+/K^+ ATPase) pump (He, Forest, Gain, *et al.*, 2016), the lactate cotransporters (Nguyen and Bonanno, 2012), the sodium-proton (Na^+/H^+) exchangers, and the sodium-bicarbonate ($Na^+/H_2CO_3^-$) cotransporters (Bonanno, 2012). The most popular hypothesis to describe the pump function was developed by Bonanno's *et al*. It consists in a relation among the bicarbonate buffer system, the lactate efflux to the aqueous humor, and the stromal deturgescence. They observed in animal models that the inhibition or downregulation of the aforementioned transports or of the bicarbonate buffering system led to a decrease in lactate efflux and to stromal swelling (Nguyen and Bonanno, 2012; Li, Kim and Bonanno, 2016; Li, Kim, *et al.*, 2020; Li, Shyam, *et al.*, 2020). Klyce *et al.* (2020) proposed the existence of a possible relation between the sympathetic innervation of the cornea and the regulation of the stromal swelling, as those fibers present a thermoregulatory role in other parts of the body. It was demonstrated in an *ex vivo* experiment that decreasing temperature caused stromal swelling. However, animals do not experiment stromal swelling when their temperature is reduced during hibernation.

1.5.3. Endothelial regenerative capacity

Human endothelium presents a limited regenerative capacity *in vivo*. ECs are commonly arrested in the G1 phase of cell cycle due to different but complementary mechanisms (Joyce *et al.*, 1996; Joyce, 2012). Those mechanisms are the cell-cell contact inhibition, the elevated concentration of cyclin-dependent kinase inhibitor (CDKI) $p27^{Kip1}$ (Senoo and Joyce, 2000; Senoo, Obara and Joyce, 2000; Joyce, Harris and Mello, 2002; Yoshida *et al.*, 2004), the presence of the transforming growth factor β2 (TGF-β2) in the aqueous humor, that inhibits $p27^{Kip1}$ degradation (Kim *et al.*, 2001), and the absence of effective positive growth factors like the epidermal growth factor (EGF), that can trigger cell division in the EC environment (Senoo and Joyce, 2000; Joyce, Harris and Mello, 2002; Joyce, 2012).

Despite all this, the ECs maintain the ability to divide. The division potential of ECs is dependent on their location within the endothelium and the age of the individual. Peripheral ECs seem to maintain an increased division capacity compared to the ECs located in the central part of the cornea. However, when ECs are isolated and cultured with supplementary growth factors, this difference disappears (Konomi *et al.*, 2005).

Regarding the age factor, ECs from older donors have a decreased ability to quickly react to growth factors (Mimura and Joyce, 2006). Furthermore, older corneal endothelia show more senescent cells than younger corneal endothelia, especially in the central part of the endothelium. Those central ECs have a high concentration of CDKIs $p21^{Cip1}$ and $p16^{INK4a}$, which are proteins related to the stress-induced premature senescence (Enomoto *et al.*, 2006; Song *et al.*, 2008; Cui and Wu, 2012; Joyce, 2012).

Due to the lack of *in vivo* endothelial regeneration, humans lose ECs from birth. The endothelial cell density (ECD) of a child decreases approximately from 3500 cells/mm^2 at 5 years old to 2500 cells/mm^2 at 10 years old (Nucci *et al.*, 1990). In an adult, ECD decreases at an average rate of 0.6%/year (Bourne, Nelson and Hodge, 1997). When a space is created on the DM following the death of a cell, the adjacent ECs spread and/or migrate. The junctional complex disappears to facilitate the changes in the cytoskeleton for the cell enlargement and movement to cover the empty space. Therefore, an adult human corneal endothelium can be characterized by its polymegathism (different cell sizes) and polymorphism (different cell shapes), both of which increase with aging (Bourne, Nelson and Hodge, 1997). Thanks to this process, the corneal endothelium can maintain its barrier function despite a continuous cell attrition.

1.5.4. The functional endothelial cell density and disease

It has been estimated that an endothelium becomes dysfunctional below a threshold of 500 cells/mm^2. Lower ECD leads to a stromal edema and a consequent corneal opacity (Mishima, 1982). Endothelial dysfunctions are caused by diseases that directly affect the endothelium or as a result of side effects of other diseases or ocular treatments (Feizi, 2018). One example of a primary etiology of endothelial dysfunction is Fuchs' dystrophy (FD). FD is a multifactorial endothelial disease characterized by the loss of ECs and the formation of abnormal depositions of ECM on the DM known as guttae. With the progression of the disease, guttae covers the DM, the stroma becomes edematous, and epithelial bullae appears, resulting in the opacification of the cornea (Jeang, Margo and Espana, 2021). Another example is the bullous keratopathy (BK), a condition created by a non-functional endothelium and characterized by the presence of bullae under the epithelium and a stromal edema (Feizi, 2018). BK can result from an endothelial trauma, like those produced during a cataract surgery, with an intraocular lens implantation, or with glaucoma implants. These surgical procedures can accelerate the EC loss, leading to a dysfunctional endothelium (Jeang, Margo and Espana, 2021).

There is no pharmacological treatment for endothelial dysfunctions. The only current solution is to replace the damaged endothelium with a new one through a corneal transplantation, also called keratoplasty.

2. Corneal transplant for the treatment of endothelial pathologies

After the first keratoplasty in 1905, different procedures for corneal transplant have been developed and improved (Price *et al.*, 2017; Singh, Said and Dua, 2018). Thus, nowadays, it is possible to transplant the whole cornea by penetrating keratoplasty (PK) (**Figure 5**, A-B), or to transplant only one or several corneal layers by lamellar keratoplasty (LK) (**Figure 5**, C-E).

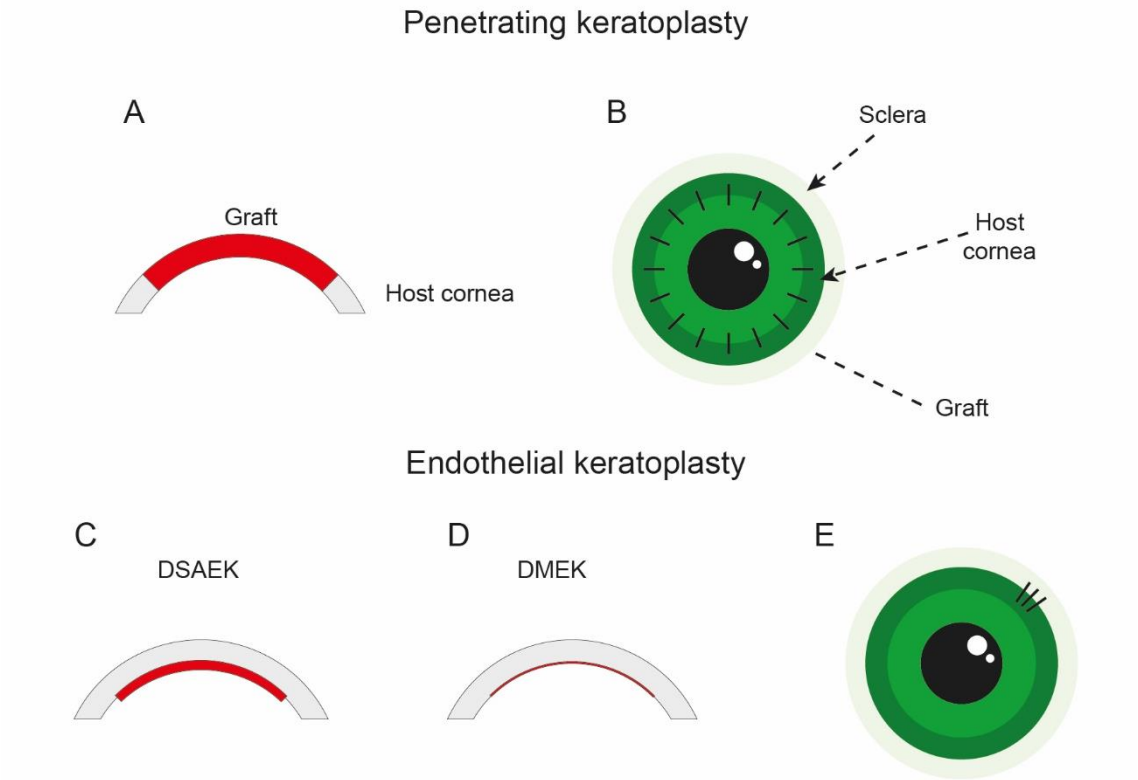

***Figure 5**. Illustration of the result of (A-B) a penetrating keratoplasty and of (C-E) the endothelial keratoplasties Descemet's stripping automatic endothelial keratoplasty (DSAEK) and Descemet's membrane endothelial keratoplasty (DMEK). In a penetrating keratoplasty, the graft (red) consists of a full-thickness corneal graft (A) that is sutured all around the periphery of the host cornea (grey) (B). In an endothelial keratoplasty, the endothelium-Descemet's membrane complex is removed, and a graft which consists of either the endothelium-DM complex with a thin layer of stroma (C, red) or only the endothelium-DM complex (D, red) is transplanted. EK grafts are inserted through a small opening within the limbus. The graft adhesion is realized by injecting an air bubble to push the graft toward the stroma. Sutures are only needed to close the limbal opening (E).*

LKs offer the possibility of being more selective and precise in the replacement of corneal layers, avoiding the unnecessary excision of intact parts of the cornea. Thus, an endothelial dysfunction as a result of FD or BK can be treated by replacing only the endothelium-DM complex with a LK named endothelial keratoplasty (EK). Different types of EKs were developed in the recent years. The two most common are the Descemet's stripping automated endothelial keratoplasty (DSAEK), where the graft consists of the donor endothelium with a thin layer of the posterior stroma (**Figure 5**, C), and the DM endothelial keratoplasty (DMEK), that replaces only the endothelium-DM complex (**Figure 5**, D) (Maharana *et al.*, 2017; Singh, Said and Dua, 2018; Liu, Wong and Walkden, 2022). The last is structurally identical to the removed endothelium-DM complex, while with DSAEK, the cornea thickness is increased due to the additional stromal layer.

2.1. Changes in corneal transplant's trends

Although PK is considered the gold standard in some countries, DSAEK and DMEK are increasingly challenging the place of PKs as the preferred surgery for endothelial disorders (Flockerzi *et al.*, 2018; Nishino *et al.*, 2019; Palma-Carvajal *et al.*, 2020). The reasons are the advantages that DSAEK and DMEK provide over PK, relative to the safer procedure, and the quicker and better postoperative outcomes. With these EKs, the common PK's complications related to an open-sky surgery and wound and suture problems are reduced (Hos *et al.*, 2019; Woo *et al.*, 2019). Induced refractive aberrations and graft rejection are also reduced (Singh, Said and Dua, 2018; Woo *et al.*, 2019; Liu, Wong and Walkden, 2022). Among both EKs, DMEK is the procedure that causes the lowest postoperative astigmatism complications due to the lack of stroma within the graft.

However, DSAEK and DMEK also present some disadvantages compared to PK. Both EKs are technically demanding with a steep learning curve. The DSAEK and DMEK graft manipulation is higher than with the PK, and the endothelium can be easily damaged with the consequent loss of ECs. This loss of cells can occur during graft preparation, graft positioning into the host anterior chamber, and graft adhesion to the stroma (Singh, Said and Dua, 2018). For this reason, some Eye Banks and surgeons established a minimal ECD requirement for EK donor cornea equal or superior to 2500 cell/mm^2 instead of 2000 cell/mm^2, which is the minimal ECD recommended for PK ('Plan Nacional de Córneas. 2016', 2016; European Directorate for the Quality of Medicines and Healthcare, 2017; Singh, Said and Dua, 2018; Woo *et al.*, 2019). Also, mainly between the first days and up to a few weeks after keratoplasty, the EK procedures are associated with a risk of graft detachment (Müller *et al.*, 2016; Price *et al.*, 2017; Parekh, Leon, *et al.*, 2018; Singh, Said and Dua, 2018). A complete graft detachment after DSAEK is more frequent than after DMEK, and a partial detachment is more frequent after DMEK (Price *et al.*, 2017; Woo *et al.*, 2019). It has been suggested that the edges of non-well attached DMEK graft can roll up and separate from the stromal surface (Price *et al.*, 2017; Woo *et al.*, 2019). Graft detachments are solved by spontaneous re-attachment, without any intervention (Price *et al.*, 2017; Woo *et al.*, 2019) or with a re-bubbling process, where the graft adhesion step is repeated with the injection of air (Price *et al.*, 2017; Parekh, Leon, *et al.*, 2018).

2.2. Troubles in worldwide cornea stock

With the aging population, the demand for corneal transplants, specifically for EKs, increases year after year (Röck, Bartz-Schmidt and Röck, 2018). The reason is that surgical treatments to reduce myopia or to treat cataracts and glaucoma are more frequent, and those procedures can damage the endothelium. Therefore, patients treated for these pathologies can develop an endothelial dysfunction, and, consequently, be a candidate for an EK (Feizi, 2018). Due to the excellent results of EKs and the technological improvement of those procedures reducing endothelial damages (Parekh, Baruzzo, *et al.*, 2017; Parekh, Borroni, *et al.*, 2018; Soma *et al.*, 2019), surgeons and patients are encouraged to realize an EK in earlier stages of the endothelial dysfunctions (Dickman *et al.*, 2016; Flockerzi *et al.*, 2018). That way, they can avoid the damage in the other corneal layers which, otherwise, would also have to be replaced by a full-thickness cornea. There is however a scarcity of available corneas internationally which do not satisfy the current demand (Gain *et al.*, 2016). This scarcity is increased as a result of the higher stringency requirement for the EKs, which selects only corneas with a higher endothelial density. Considering the elevated average donor age (*EBAA Eye banking statistical report 2019*, 2020) and the consequent reduction of ECD with aging, the compliance of all the requirements for an EK graft are harder to achieve.

2.3. Cornea donation for keratoplasty

Eye Banks are regulated establishments which orchestrate the processes of collecting, evaluating, storing, and distributing the donated corneas for transplantation (Lambert and Chamberlain, 2017; Moshirfar *et al.*, 2021). A general process of corneal donation is described below (**Figure 6**).

When a cornea donor is identified, the family consent is first obtained, and the social history is reviewed in a family interview. Then, medical history is reviewed, and the corpse is examined to complete the medical/social history and eliminate all the contraindications for corneal donation ('Plan Nacional de Córneas. 2016', 2016). Advantageously, the cornea is one of the most immune-privileged tissues for donation and transplantation. The reasons are the lack of blood and lymphatic vessels, the low presence of the major histocompatibility complex antigens and of ligands of immune cells in ECs, and the presence of secretory immunomodulatory factors that inhibit inflammatory cells (Hos *et al.*, 2019).

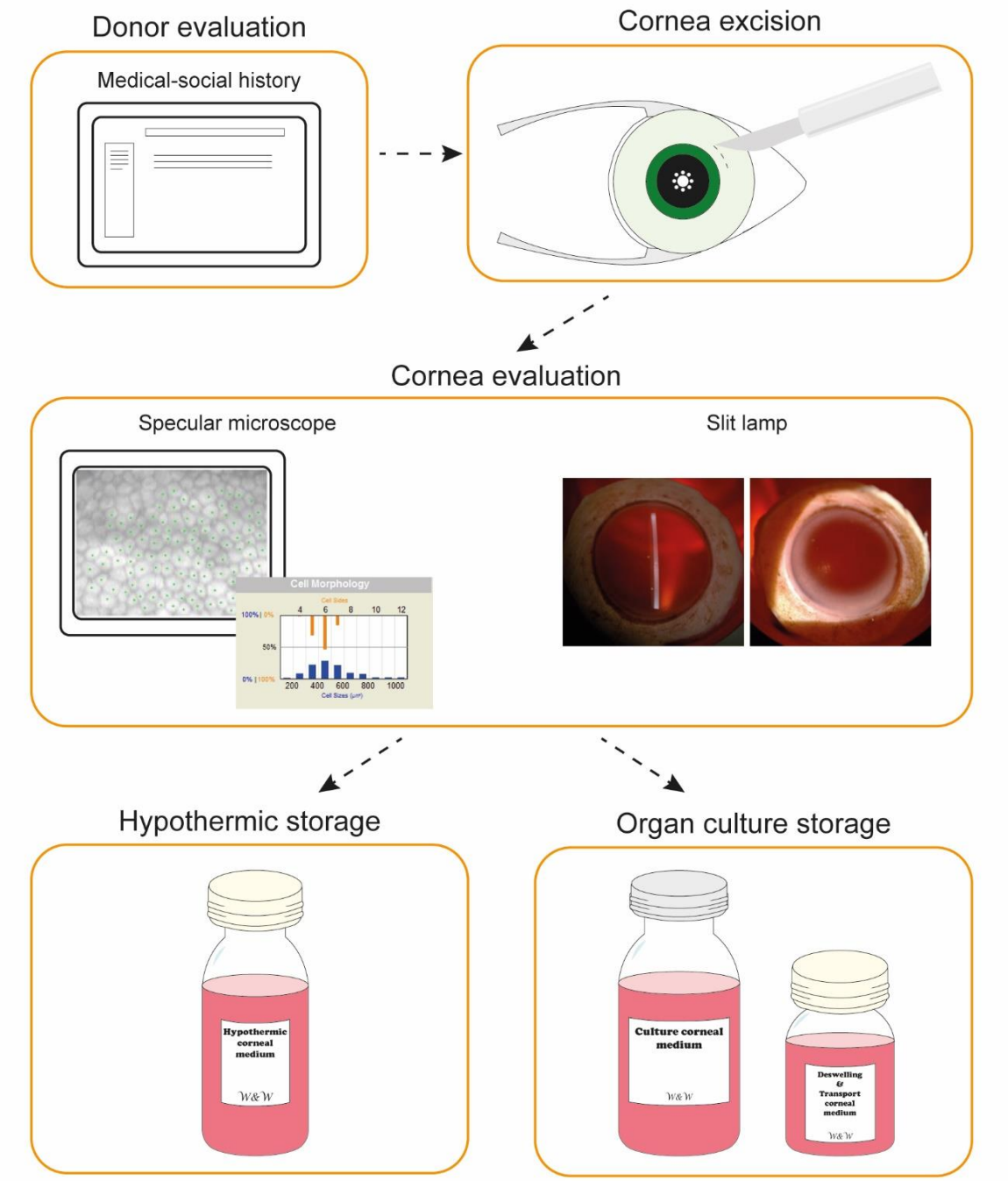

Figure 6. *Scheme of a general process of corneal donation after the obtention of the family consent. The donor medical and social history is reviewed before corneal excision to verify the absence of contraindications. Excised cornea is then evaluated with the specular microscope to validate the endothelial characteristics and with a slit lump to observe the general state of all the corneal layers. Once confirmed that the cornea is validated for transplantation, hypothermic storage or organ culture storage is employed for its conservation before being transplanted. For organ cultures storage, an extra medium is needed for corneal transportation.*

Once the donor is considered suitable for corneal donation, the corneal tissue is collected within 24 hours of death. The eyeball can be enucleated, placed in a moist chamber, and transported on ice to the Eye Bank for cornea excision. Another option is to perform the cornea excision *in situ* and immerse the cornea in storage medium with antibiotics and antifungals (European Directorate for the Quality of Medicines and Healthcare, 2017).

The corneas are then evaluated by specialized technicians to determine if the corneal tissue complies with the minimal requirements for transplantation. Quality criteria include the absence of microorganisms, the integrity and morphological state of the corneal layers, a high ECD, a low level of pleiomorphism and polymegathism of ECs, and an adequate diameter of the clear central area of the cornea. To do that, technicians use a slit lamp to visualize the corneal tissue, and a specular microscope to evaluate the ECD, the pleiomorphism and the polymegathism ('Plan Nacional de Córneas. 2016', 2016; European Directorate for the Quality of Medicines and Healthcare, 2017). Following this inspection, corneas suitable for transplantation are stored until surgery.

There are two main methods to store corneas before transplantation: the hypothermic storage and the organ culture storage. Hypothermic storage can provide an optimal storage for up to 2 weeks, while organ culture storage can provide an optimal storage for up to 4-5 weeks (Armitage, 2011; European Directorate for the Quality of Medicines and Healthcare, 2017). However, although the manufacturers recommend a maximum storage time when using their hypothermic or organ culture media, national institutions commonly enforce a stricter limitation (Moshirfar *et al.*, 2021). For example, the National Corneal Plan of Spain recommends only 7 days for hypothermic storage and 3 weeks for organ culture ('Plan Nacional de Córneas. 2016', 2016). What determines those delays is in direct consideration to the integrity and functionality of the endothelium, which quality decreases over time in the storage medium. If a donor cornea is not used within the selected timeframe, it is discarded.

When a stored cornea is needed for a keratoplasty, the Eye Bank usually takes in charge the logistic to deliver the tissue to the operating room where the surgeon prepares the graft *in situ*. Some Eye Banks offer a service of LK graft preparation. In the case of EK grafts, the Eye Bank can even send the graft preloaded into an injector, which reduces the manipulation of the graft, lowers the loss of ECs, and increases the speed of the surgery (Lambert and Chamberlain, 2017).

A third method of cornea storage is the cryopreservation. Cryopreservation is only recommended for the storage of corneas used in tectonic keratoplasty (TK), where a vitalized cornea is not needed (Brunette *et al.*, 2001; Armitage, 2011; 'Plan Nacional de Córneas. 2016', 2016; European Directorate for the Quality of Medicines and Healthcare, 2017). A TK is usually done for emergencies where a risk exists of losing the eye globe integrity. Therefore, the cryopreserved cornea is used like a temporary patch until the patient receives a cornea suitable for a permanent transplant. Corneas employed for patch-grafts can be preserved in glycerol, in 70% ethanol or in albumin, and then stored in liquid nitrogen (European Directorate for the Quality of Medicines and Healthcare, 2017).

3. Cryopreservation

Cryopreservation is a process that involves the cooling, the storage, and the warming of cells, tissues or any biological sample at temperatures under -80°C, normally at -196°C (Baust, Gao and Baust, 2009). The objective is to arrest any metabolic activity temporarily (Bakhach, 2009), and to restore such activity afterward upon warming. This technique is further used clinically to preserve gamete cells or embryonic tissues (Nagy, Shapiro and Chang, 2020). However, cryopreservation of viable tissues remains a challenge due to their greater structural complexity compared to single cell suspensions. Upon warming, the tissue must have conserved its functional structure and its cells must have survived the whole process before attempting any practicable clinical use (Pegg, 2015).

3.1. The physicochemical basis of cryopreservation

In an aqueous solution, water molecules present a high kinetic energy, and create dynamic structures that are continuously reorganizing. When temperature decreases below its melting temperature (T_m: temperature at which a substance changes from solid to liquid state and *vice versa*), and liquid water becomes supercooled, water molecules readjust to a new thermodynamic equilibrium of low energy, creating static structures. Consequently, water molecules start to bind each other helped by the container surfaces or solutes, such as salts, proteins, lipids, carbohydrates and even dust, which catalyze the process of ice nucleation. Then, those small ice nuclei grow and form a crystalline solid. This solidification process is called crystallization (Wowk, 2010; John Morris and Acton,

2013; Elliott, Wang and Fuller, 2017). It allows water to release energy in the form of latent heat (**Figure 7**).

The crystallization process causes the exclusion of solutes from the crystalline structure. These solutes become more and more concentrated in the remaining supercooled liquid water fraction. In this liquid fraction, the T_m decreases because of the increase of solutes that block the movement of water molecules to form ice crystals (Elliott, Wang and Fuller, 2017). The crystallization stops when a thermodynamic equilibrium is achieved between the progressively hypertonic liquid and the solid state (Baust, Gao and Baust, 2009).

If the aqueous solution presents an elevated concentration of solutes (high viscosity) and its temperature is decreased beyond T_m rapidly, water crystallization can be prevented (**Figure 7**). At this point, the aqueous solution achieves the glass transition temperature (T_g), where an amorphous non-crystalline solid is formed with molecules randomly oriented. This solidification process is called vitrification (Taylor, Song and Brockbank, 2004; Wowk, 2010).

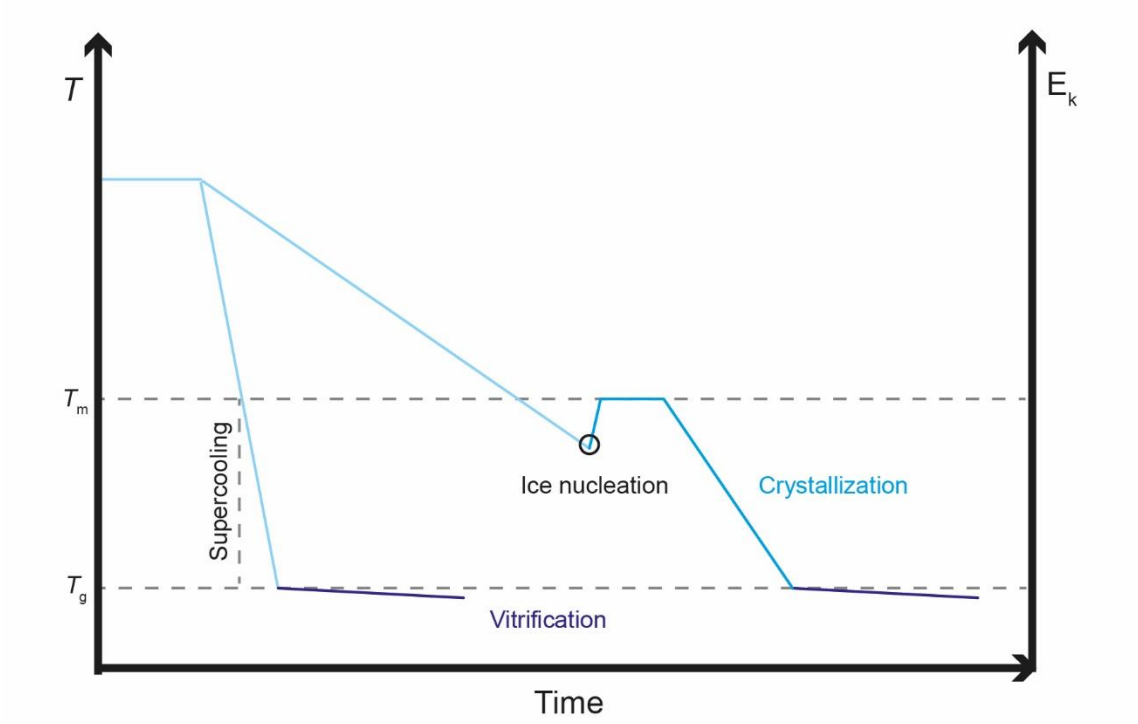

***Figure 7**. Simplified schematic of a liquid solution (light blue) crystallization (blue) and vitrification (dark blue). In a crystallization process, the kinetic energy (E_k) of water molecules decreases slowly following a slow decrease in temperature. Upon reaching the melting temperature (T_m) of the solution, the water becomes supercooled and ice nucleation is initiated (black circle), liberating latent heat and forming solid crystallized structure. In a vitrification process, the decrease of the temperature is so quick and the Ek decreases so fast that water in liquid state is not given the time to create ice crystals. Instead, the water arrives to the glass transition temperature (T_g) in a liquid state and forms an amorphous solid. Vitrification process can also take place after crystallization, in the viscous and supercooled liquid water that remains in this phase stage.*

Crystallization and vitrification can occur in the same aqueous solution and in the same freezing process: once crystallization lowest temperature is reached, additional cooling will instead generate vitrification in the fraction of the supercooled hypertonic liquid (Wowk, 2010).

3.2. The effect of ice crystals in cells and tissues

Ice crystals formed during a cryopreservation process can be harmful for cells and tissues, directly or indirectly (Taylor, Song and Brockbank, 2004; Bakhach, 2009; Baust, Gao and Baust, 2009; Pegg, 2010; Armitage, 2011; Elliott, Wang and Fuller, 2017).

In ideal conditions, if the cooling rate is gradual and the T_m is reached, crystallization starts in the extracellular environment instead of inside the cells. The increase of the solute concentration out of cells creates an osmotic gradient that is counteracted by the water exiting the cells, dehydrating themselves harmlessly. During cooling, the increase of intracellular solutes decreases the T_m, preventing the harmful intracellular crystallization, and favoring the less damaging intracellular vitrification (Bojic *et al.*, 2021; Raju *et al.*, 2021).

However, if the cooling rate is too slow, cells are led to an excessive dehydration and shrinkage, to a harmfully high concentration of solutes inside cells, and to changes in pH. All these changes caused by osmotic hypertonicity can be called "solution effects". They can irreversibly denature proteins, alter lipid membranes, or lead to an osmotic shock during warming due to the quick absorption of water into cells (Mazur, Leibo and Chu, 1972; Raju *et al.*, 2021).

On the contrary, if the cooling is too fast but stays within the range of crystallization temperature, intracellular crystals are formed causing cells to be subjected to mechanical damages as ice crystals can directly disrupt organelles and cell membranes (Mazur, Leibo and Chu, 1972; Pegg, 2010; Bojic *et al.*, 2021; Raju *et al.*, 2021).

Upon warming, ice crystals can also grow and damage cells (Bakhach, 2009). In a process where crystallization has occurred during cooling, small innocuous intracellular ice crystals can bind to each other instead of melting in a process called recrystallization, and create a large harmful crystalline structure (Bakhach, 2009; Raju *et al.*, 2021). Also, during the warming process after vitrification, ice crystals can be formed in a process called devitrification. In devitrification, a transition of vitreous to crystalline state occurs once

temperature is superior to the T_g. At this point, the water leans toward a more energetically stable structure, i.e., to ice crystal (Pegg, 2015; Bojic *et al.*, 2021; Fahy and Wowk, 2021), with the consequent disrupting effect of intracellular ice.

Ice crystals can also affect tissues extracellularly, disrupting the ECM components and their functional arrangement (Armitage and Rich, 1990). Extracellular ice crystals can disrupt the cells organization by breaking for example their cell-cell and cell-matrix interactions (Ebertz and McGann, 2004; Pegg, 2015). Additionally, if a tissue possesses different types of cells, those can react differently to decreasing temperature and display distinct tolerance to dehydration or osmotic changes (Bojic *et al.*, 2021).

3.3. The cryoprotectant agents

For cell and tissue cryopreservation in clinical practice and research, biological samples are embedded in solutions that contain molecules that play the role of cryoprotective agents (CPAs) through the reduction of ice-related injuries (**Figure 8**).

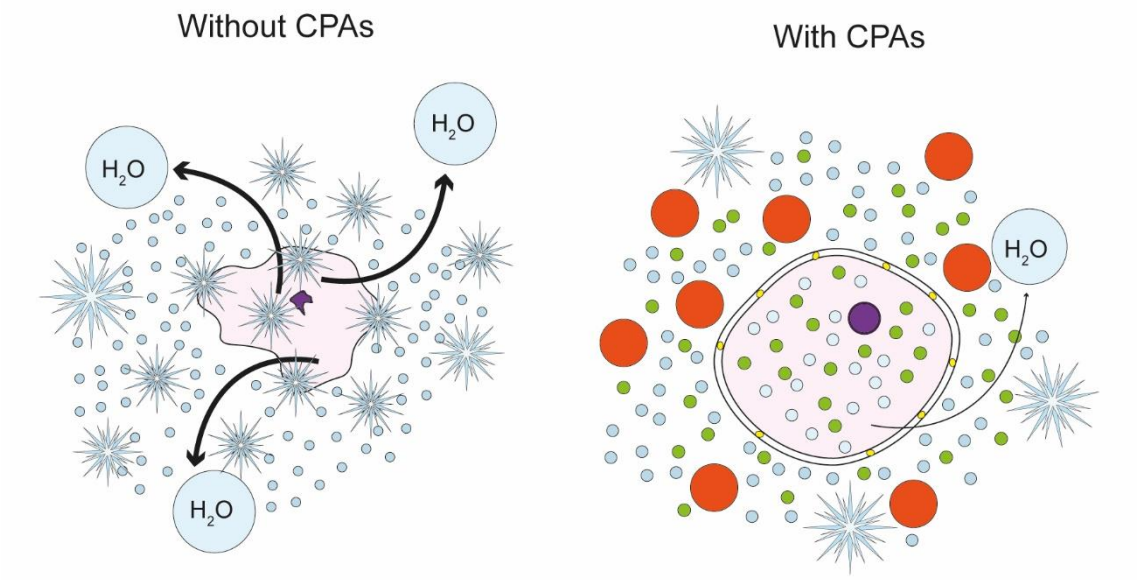

***Figure 8**. Illustration of a conventional cryopreservation process without and with cryoprotective agents (CPAs). Without CPAs, the cells are subjected to osmotic shocks, quickly shrink, and lose of a high volume of water. Ice crystals are randomly formed intracellularly and extracellularly, generating fractures in the cells and organelles membranes. With CPAs, cell osmosis and water exit are better regulated, avoiding damaging osmotic shocks. Ice crystals are also mainly generated extracellularly. Addition of non-permeating cryoprotective agents (npCPAs) (red circles) reduces the movement of water molecules, which regulates the formation of the crystals and increases the viscosity. As a result, supercooled liquid water vitrifies. Addition of permeating cryoprotective agents (pCPAs) protects the cell structural integrity, such as lipidic membranes (yellow dots), and increases the viscosity in the cytoplasm (green dots), favoring a vitrification process inside cells.*

For conventional cryopreservation, where the crystallization is allowed but controlled, the use of CPAs helps to control the ice crystal formation. In cryopreservation by vitrification, CPAs are used at increased concentrations to prevent ice crystals formation (Bakhach, 2009; Elliott, Wang and Fuller, 2017; Raju *et al.*, 2021). CPAs can be classified as permeating CPAs (pCPAs) or non-permeating CPAs (npCPAs) according to their capacity to enter the cells. The mechanisms through which CPAs protect cells during cryopreservation are not well understood yet (Elliott, Wang and Fuller, 2017; Bojic *et al.*, 2021).

The first identified pCPAs were glycerol and dimethyl sulfoxide (DMSO). DMSO is the most studied and the most used in cryopreservation protocols (Bakhach, 2009; Best, 2015; Elliott, Wang and Fuller, 2017; Jang *et al.*, 2017). DMSO and glycerol can increase the dehydration of cells at subzero temperatures and modulates the temperature of the cell membrane liquid-gel phase transition (Akhoondi *et al.*, 2012; Bojic *et al.*, 2021; Wolkers and Oldenhof, 2021). DMSO can also help to avoid the protein denaturalization at low temperatures (Wolkers and Oldenhof, 2021). Other examples of pCPAs are ethylene glycol, propylene glycol, formamide, and methanol (Best, 2015).

The main problem of pCPAs is their cytotoxicity, that is dependent on cell type, concentration, and temperature. They are more cytotoxic at high temperatures and at high concentrations. They can alter metabolic pathways or cell transport. Nonetheless, combinations of some pCPAs can neutralize this cytotoxicity. For example, DMSO can neutralize the cytotoxicity of formamide (Best, 2015; Bojic *et al.*, 2021).

Regarding npCPAs, these comprise sugar molecules like trehalose, dextrose and sucrose, proteins like albumin, GAGs like chondroitin sulfate, and synthetic polymers like polyvinyl pyrrolidone or povidone. It has been observed that they prevent ice-related damages if they are used in combination with pCPAs (Elliott, Wang and Fuller, 2017; Bojic *et al.*, 2021; Wolkers and Oldenhof, 2021). They can increase the T_g and help to avoid recrystallization during warming (Wolkers and Oldenhof, 2021), and can decrease the use of pCPAs to reduce their cytotoxicity (Elliott, Wang and Fuller, 2017).

3.4. Attempts of corneal cryopreservation

Cryopreservation of cells in suspension allows a long-term cell storage with limited damage to the cells. However, tissue cryopreservation is still problematic (Taylor *et al.*,

2019). Tissues are complex structures formed by several types of matrices and, frequently, with several types of cells. Those cells present different cytotoxicity thresholds and different ice-related injury tolerance, which limits the number of compatible CPA preparations. Additionally, optimal tissue cryopreservation relies on CPAs that should reach, equilibrate with, and be easily removable from all tissue areas. Temperature variations should also be homogeneous to prevent localized damage (Elliott, Wang and Fuller, 2017).

Tissues are more sensible to extracellular ice because ice crystals can damage the tissue and alter its optimal and functional structure. For this reason, vitrification has been postulated as the best cryopreservation technique to preserve the viability of tissues such as cornea and cartilage (Armitage, Hall and Routledge, 2002; Brockbank, Chen and Song, 2010; Elliott, Wang and Fuller, 2017; Taylor *et al.*, 2019). However, with vitrification, cytotoxicity is increased due to the higher concentration of CPAs that is needed (Best, 2015; Elliott, Wang and Fuller, 2017; Taylor *et al.*, 2019).

Regarding corneas, cryopreservation can potentially increase the preservation capacity of viable corneas, increasing the quantity of available donor tissues and reducing corneal waste in periods of low demand (Taylor, 1986). The first attempt for the cryopreservation of a corneoscleral disc was published during the mid-20th century. The most successful ones, which, at first, seemed to provide a well conserved cornea, were the conventional cryopreservation methods developed by Capella, Kaufman and Robbins (1965) and by O'Neill, Mueller and Trevor-Roper (1967). Those methods (or close variations of them) were then subsequently employed in additional studies. It was however observed that the corneal endothelium integrity was not sufficiently maintained and thus could not to be used as a viable transplant for keratoplasty (Taylor, 1986). In the 80s, corneal vitrification was also considered (Armitage, 1989), and different protocols were investigated (Rich and Armitage, 1991, 1992; Bourne and Nelson, 1994).

Corneal cryopreservation processes, conventional or through vitrification, were analyzed thoroughly. Different cryopreservation parameters of a protocol were studied, such as the cell tolerance to CPAs and/or the cryoprotectant solutions (Armitage, 1989; Madden, 1989; Taylor and Hunt, 1989), the corneal permeability to CPAs (Taylor and Busza, 1992; Walcerz, Taylor and Busza, 1995), and the cooling and warming rates (Routledge and Armitage, 2003). Cryopreservation protocols were thus improved step by step by

adjusting those parameters in response to the endothelial reaction or the general corneal state compared with those of previous attempts.

Rabbit corneas are generally the most used tissues to evaluate the cryopreservation protocols (Taylor, 1986; Fong, Hunt and Pegg, 1987; Armitage, 1989; Madden *et al.*, 1993; Armitage, Hall and Routledge, 2002; Routledge and Armitage, 2003; Wusteman *et al.*, 2008). Other animal and human corneas are usually harder to obtain; the latter being used in priority for clinical use before being available to research. This can be problematic considering that the same cryopreservation protocol applied to a human cornea often provides a different result compared to what was observed previously in the animal model. For example, rabbits cornea can hide the endothelial damages caused by cryopreservation, as they conserve the endothelial regeneration capability (Van Horn *et al.*, 1977; Wusteman *et al.*, 1999; Canals *et al.*, 2000).

The implementation of a preservation method to store viable corneas for keratoplasty must be well defined with a reproducible outcome. So far, and despite all attempts, an optimized human corneal cryopreservation protocol has yet to be developed.

4. Tissue engineering: development of an endothelial keratoplasty graft

Tissue engineering (TE) is a discipline whose aim is to create, using cells, scaffolds and biomolecules, a substitute for a damaged tissue, to restore, regenerate, and/or recover its normal functionality. In the field of ophthalmology, tissue engineering is proposed as an alternative strategy to treat corneal defects such as endothelial dysfunctions. The idea would be to create a engineered EK-graft with a high density endothelium using human ECs (hECs) isolated from low density corneas which were not deemed suitable for transplantation (Rodríguez-Fernández *et al.*, 2021).

4.1. Scaffolds

To build an EK-graft, scaffolds are used to seed the ECs and create a functional endothelium. A suitable scaffold for an EK-graft must be biocompatible and have a strong cell adhesion capacity. It should have suitable physical and mechanical properties with the transparency, shape, strength, and flexibility of the cornea, in order to maintain the correct light refraction and to resist the IOP. Furthermore, the EK-graft should be sufficiently permeable to allow molecules to pass through selectively. Finally, it should

be adaptable to the current EK surgery techniques and have good adhesion to the stroma to prevent graft detachment (Rodríguez-Fernández *et al.*, 2021).

Several authors have tested different scaffolds for EK-grafts. In the literature, the most frequent ones are those composed essentially of proteins that are part of a typical ECM or basement membrane providing binding sites for cells integrins. Thus, collagen-based scaffolds have been thoroughly studied. Some examples are decellularized fish scale (Parekh, Ahmad, *et al.*, 2017), collagen polymeric scaffolds (Vázquez *et al.*, 2016; Li *et al.*, 2017; Yoshida *et al.*, 2017) or crystalline lens capsules (Van den Bogerd, Ní Dhubhghaill and Zakaria, 2018). Among the collagen-based scaffolds, those with a human corneal origin, like stromal lamellae (He, Forest, Bernard, *et al.*, 2016) or DM (Liu *et al.*, 2019; Spinozzi *et al.*, 2020), showed promising results. These scaffolds, once decellularized by employing physical or chemical methods, provide a biocompatible ECM for ECs seeding with multiple cell adhesion points, with optimal transparency and shape, and with a predictable flexibility and strength (Rodríguez-Fernández *et al.*, 2021; Català *et al.*, 2022). However, the successful implementation of these type of EK-grafts is limited to the donor tissue availability (Català *et al.*, 2022).

Other polymeric biomaterials tested for EK were substances of natural origin such as agarose (Seow *et al.*, 2019) and silk fibroin (Vázquez *et al.*, 2017; Kim *et al.*, 2018; Ramachandran *et al.*, 2020), and scaffolds made with synthetic biomaterials, like gelatin methacrylate (Rizwan *et al.*, 2017), poly(lactic-co-glycolic acid) (Kruse *et al.*, 2018), or combinations of glycine and silk fibroin (Song *et al.*, 2019). Although these materials offer greater customization at the physical-mechanical level, with an optimal topography for cell adhesion (Muhammad *et al.*, 2015), their biocompatibility with hECs should be tested (Català *et al.*, 2022).

4.2. Human endothelial cells

For the engineering of EK grafts, hECs are needed. The main source are the donor corneas from which primary hECs can be successfully isolated and expanded, thanks to the culture protocols developed in the last decades (Engelmann, Böhnke and Friedl, 1988; Peh *et al.*, 2011, 2015; Chen *et al.*, 2019). Primary cultured hECs are the most similar, at a proteomic level, to *ex vivo* hECs (Frausto, Le and Aldave, 2016). However, the use of primary hECs in TE presents some limitations.

First, hECs undergo an endothelial-mesenchymal transition around the third passage, losing their functional morphology and phenotype (Peh *et al.*, 2011; Roy *et al.*, 2015; Frausto *et al.*, 2020). This dedifferentiation limits the number of cells that can be potentially obtained from one cornea before cells become unqualified for TE due to the loss of the endothelial phenotype (Rodríguez-Fernández *et al.*, 2021; Català *et al.*, 2022). Additionally, there is great variability among donor corneas, and not all are going to generate a hEC population with an optimal quality. Depending on factors like donor age or donor health condition, hECs can respond differently to the media, and have different doubling times, different cell yield before dedifferentiation or different phenotype (Soh, Peh and Mehta, 2016; Rodríguez-Fernández *et al.*, 2021).

Regarding the translation of the TE approach to clinical application, there is currently no consensus on the biomarkers to be used to specifically identify hECs. A biomarker set need to be developed for the creation of homogeneous populations of hECs qualifiable for clinical TE practice (Soh, Peh and Mehta, 2016; Van den Bogerd *et al.*, 2019). Some researchers have made progress in identifying genes and proteins that could be valid candidates for hECs biomarking (Okumura *et al.*, 2014; Masahito *et al.*, 2015). At present, the most used are nonspecific biomarkers, like ZO-1 and Na^+/K^+ ATPase pump (Van den Bogerd *et al.*, 2019). Parallelly, research is also continuously developing new hEC isolation and expansion protocols, and EK-graft engineering methods to replace the commonly used animal derived products (Peh *et al.*, 2017). Animal tissues used in research could transfer animal pathogens to the hECs or to the engineered grafts, and could possibly cause xenorejection (Soh, Peh and Mehta, 2016). They must be eliminated to fulfill the good manufactures practices (GMP) requirements for the construction of an engineered-EK graft (Soh, Peh and Mehta, 2016; Peh *et al.*, 2017), and to comply to all the safety and quality standards of the different regional legislations.

Despite the described challenges of using primary hECs from human donor corneas to engineer EK-graft, it remains currently the only admissible source, since the use of animal ECs, human immortalized ECs or human induced pluripotent stem cell-derived ECs are prohibited for clinical practice due to safety reasons (Soh, Peh and Mehta, 2016; Rodríguez-Fernández *et al.*, 2021).

II. Justification and Objectives

Corneal transplantation is the only effective treatment for most of corneal endothelial diseases and trauma. Unfortunately, disparity exists between the limited availability of donor corneas and the increasing number of patients who need a corneal transplant. This situation is meant to deteriorate with the aging population, that carries a higher risk of developing eye-related illnesses. It is also paradoxically complicated by the development of new improved keratoplasties that recommend earlier stages intervention and more specific donor characteristics. For example, corneas used for EKs require a high ECD (>2500 cell/mm^2) and must originate from donors over 60 years (parameters recommended in the *Plan Nacional de Córneas* (2016) of Spain). The current corneal storage methods also limit our ability to bank corneal tissues to only a few weeks. This cause logistical hurdles, and often, corneas do not get used within this established Eye Bank storage timeframe and are eventually discarded.

Many strategies can be envisioned to enhance our ability to treat patients using donor tissues. Replacing the current temporary preservation methods with a more permanent corneal cryopreservation method could offer an interesting solution to reduce or even eliminate the unused tissue as corneas would not be discarded after a few weeks in storage. Another strategy could be to develop tissue engineered corneal grafts. Such grafts could be generated by building an endothelium over a discarded cornea with an intact DM using cultivated and expanded ECs from another discarded cornea. Being engineered, these grafts could be made to fit and even surpass the characteristics that LK transplantation requires.

On that account, the general aims of this doctoral thesis were to investigate the use of corneal cryopreservation as a storage method to preserve corneas for functional keratoplasties, and to generate a tissue engineered-EK (TE-EK) graft using discarded corneas.

The specific objectives of the project were:

Objective 1:

1. Analysis of corneal cryopreservation protocols and of the resulting cryopreserved corneas.
   1.1. Development of two conventional cryopreservation protocols and two vitrification protocols to preserve corneas.

1.2. Evaluation of the endothelial integrity and viability and of the general corneal structure of the cryopreserved corneas.

1.3. Detailed characterization of the cryopreserved corneas when using the protocol that generated the best results.

1.4. Study of the cryopreservation parameters which influence the cryopreservation outcomes when using the protocol that generated the best results.

1.5. Development of an *in vitro* PK-model to study ECs migration and division on receptor and donor corneas.

Objective 2:

2. Development of an EK graft by TE endothelia with the use of discarded corneas.

2.1. Establishment of a protocol for the obtention of decellularized DM (dDM) scaffolds and for the isolation and culture of primary hECs.

2.2. Construction of the TE-EK grafts using cultured primary hECs and dDM scaffolds.

2.3. Analysis of the expression of endothelial-related structural proteins and of ECs morphometric parameters on the TE-EK grafts.

III. Materials and Methods:

Objective 1

1. Corneal samples collection

This study was reviewed and approved by the research ethics committee of A Coruña-Ferrol, Spain (2017/594) (**Annex I-II**). Corneas were obtained from the public collection C.0001265 located in the Tissue Establishment – Cryobiology Unit of the Teresa Herrera Hospital (A Coruña). This collection is composed of corneas that were discarded after the slit lamp and/or specular microscopy evaluation, by corneas that have not found a receptor within 7 days and had been stored at 4 °C in Corneal Chamber (AlchimiA, Padua, Italy) medium, or by the presence of donor contraindications checked after corneal excision. Normally, those corneas are directly cryopreserved using the cryopreservation protocol for tectonic keratoplasty (*Procesado de córnea criopreservada*; Ref.: UCBET-PE-PSS-CCP-00-17).

A total of 34 corneas were used (**Table 1**), 15 already cryopreserved and 19 in hypothermic storage.

***Table 1**. Data of corneal samples used in the Objective 1. The variables sex, age, discard reason, and endothelial cell density (ECD) were obtained from each cornea and its donor. The techniques in which each cornea was employed are indicated in the last column. HypoN: hypothermic stored cornea; CryoN: cryopreserved cornea; PN: tested cryopreservation protocol; MT: Masson's trichrome staining; En-DM: endothelium-Descemet's membrane complex; CAM: calcein AM; BR: trypan blue – alizarin red; TEM: transmission electron microscopy; NMR: nuclear magnetic resonance spectroscopy; PK: penetrating keratoplasty.*

Cornea code	Sex	Age	Discarded for	ECD	Techniques
Hypo1	Male	64	No receptor	2475	P1-cryopreservation + MT
Hypo2	Male	64	Infiltrates	N/A	P2-cryopreservation + MT
Hypo3	Female	72	Small clear area	N/A	P3-cryopreservation + MT
Hypo4	Female	63	Guttae	N/A	P4-cryopreservation + MT
Hypo5	Female	74	Infiltrates	2817	Hypothermic + MT
Hypo6	Male	73	Scar of previous ocular surgery	2110	P1-cryopreservation + En-DM extraction + CAM
Hypo7	Male	73	Low ECD	1493	P1-cryopreservation + En-DM extraction + CAM
Hypo8	Female	64	7 days in hypothermic storage	2674	P2-cryopreservation + En-DM extraction + CAM
Hypo9	Female	75	Small clear area	2315	P2-cryopreservation + En-DM extraction + CAM
Hypo10	Male	68	Infiltrates	2157	P3-cryopreservation + En-DM extraction + CAM

Hypo11	Female	72	Infiltrates	2106	P3-cryopreservation + En-DM extraction + CAM
Hypo12	Female	61	Low ECD	1618	P4-cryopreservation + En-DM extraction + CAM
Hypo13	Male	65	Infiltrates	2625	P4-cryopreservation + En-DM extraction + CAM
Hypo14	Female	67	Small clear area	2242	Hypothermic + En-DM extraction + CAM
Hypo15	Female	67	Infiltrates	2202	Hypothermic + En-DM extraction + CAM
Cryo1	Female	72	Small clear area	2342	P1-cryopreservation + BR
Cryo2	Male	71	Small clear area	2326	P1-cryopreservation + BR
Cryo3	Male	44	7 days in hypothermic storage	2618	P1-cryopreservation + BR
Cryo4	Male	76	Low ECD	1992	P1-cryopreservation + BR
Cryo5	Male	76	Low ECD	1894	P1-cryopreservation + BR
Cryo6	Male	74	Small clear area	2217	P1-cryopreservation + BR
Cryo7	Female	55	Leukoma	2488	P1-cryopreservation + BR
Cryo8	Female	55	Folds and small clear area	2451	P1-cryopreservation + BR
Cryo9	Female	74	Hemoculture positive	1608	P1-cryopreservation + BR
Cryo10	Female	76	Neurological disease	2227	P1-cryopreservation + BR
Hypo16	Male	76	Hemoculture positive	2500	Hypothermic + BR
Cryo11	Female	60	Leukoma in epithelium	N/A	P1-cryopreservation + TEM
Cryo12	Female	54	Small clear area	N/A	P1-cryopreservation + TEM
Hypo17	Male	57	Iris debris adhered	N/A	Hypothermic + TEM
Cryo13	Female	64	*Guttae*	N/A	P1-cryopreservation + NMR
Cryo14	Male	61	Surgery cancelled	2802	P1-cryopreservation + NMR
Cryo15	Male	62	Leukoma	2278	P1-cryopreservation + NMR
Hypo18	Male	73	"Slit lamp"	2353	PK Model
Hypo19	Female	79	Small clear area	2004	PK Model

2. Cryopreservation techniques

Four different cryopreservation protocols were assayed. Protocol 1 (P1) and protocol 2 (P2) were based on the conventional clinical cryopreservation protocols of the Tissue Establishment – Cryobiology Unit of the Teresa Herrera Hospital. P1 was the corneal cryopreservation protocol for tectonic keratoplasty (*Procesado de córnea criopreservada*; Ref.: UCBET-PE-PSS-CCP-00-17) and P2 was the heart valve cryopreservation protocol (*Protocolo de Tejidos Vasculares*; Ref.: UCBBT-PE-PSS-PTVS-00-10). Protocol 3 (P3) and protocol 4 (P4) were protocols for vitrification where the experimental solutions named VS55 and DP6 were employed. These solutions were previously tested in vitrification experiments of heart valves, cartilage, muscle, and blood vessels (Brockbank, Chen and Song, 2010; Eisenberg, Taylor and Rabin, 2012; Eisenberg *et al.*, 2014; Brockbank *et al.*, 2015).

2.1. Cryoprotectant solutions

Cryoprotectant solutions (CSs) from P1 and P2 consisted in DMSO (Sigma-Aldrich Química S.A., Madrid, Spain) diluted in Medium 199 (Gibco, Thermo Fisher Scientific, Madrid, Spain). Human Albumin Grifols® 200 g/L (Grifols, Barcelona, Spain) was added to the cryoprotectant solutions of P1. For each protocol, three CSs (CS1.1, CS1.2, CS1.3 and CS2.1, CS2.2, CS2.3) were prepared according to **Table 2**. For P1, pH and osmolality of each CS was measured with the pH-meter GLP21 (Hach Lange Spain, S.L.U, Barcelona, Spain) and the cryoscopic osmometer Osmomat 030 (ELITechGroup, Puteaux, France). Osmolalities results were expressed as a mean ± standard deviation (SD). CSs were stored at 4 °C.

Two CSs, named VS55 and DP6, were prepared for P3 and P4 respectively. For both CSs, the solvent was a modified Euro-Collins solution used previously by Brockbank *et al*. (2015). Euro-Collins consisted in an aqueous solution prepared with distilled water and 174.76 g/L dextrose (Panreac Química S.L.U., Barcelona, Spain), 10.2 g/L KH_2PO_4 (Merck, Madrid, Spain), 36.5 g/L K_2HPO_4 (Merck), 5.6 g/L KCl (Merck), 4.2 g/L $NaHCO_3$ (Panreac Química S.L.U.). This solution was filtered with a 0.22 μm-pore filter (Millipore, Madrid, Spain) and stored at 4 °C.

The components of DP6 and VS55 were DMSO, propylene glycol (Sigma-Aldrich Química S.A.) and 4-(2-hydroxyethyl)-1-piperazineethanesulfonic acid (HEPES) (Sigma-Aldrich

Química S.A.), added in the concentrations exposed in **Table 2**. Formamide (Sigma-Aldrich Química S.A.) was also added to the VS55. VS55 and DP6 were filtered with a 0.22 μm-pore filter and stored at 4 °C for at least one hour before the corneal cryoprotectant addition step.

***Table 2**. Composition of cryoprotectant solutions (CSs) of protocol 1, 2, 3, and 4. DMSO: dimethyl sulfoxide; HEPES: 4-(2-hydroxyethyl)-1-piperazineethanesulfonic acid; v/v: volume per volume.*

	Cryoprotectant solution	Human Albumin Grifols® 200 g/L	DMSO	Propylene glycol	Formamide	HEPES	Vehicular solution
		% (v/v)	Molarity (M)	Molarity (M)	Molarity (M)	Molarity (M)	
Protocol 1	*CS1.1*	25	0.3	–	–	–	Medium 199
	CS1.2	25	0.6	–	–	–	
	CS1.3	25	1	–	–	–	
Protocol 2	*CS2.1*	–	0.3	–	–	–	Medium 199
	CS2.2	–	0.6	–	–	–	
	CS2.3	–	1	–	–	–	
Protocol 3	*VS55*	–	3.1	2.2	3.1	0.01	Euro-Collins
Protocol 4	*DP6*	–	3	3	–	0.01	Euro-Collins

2.2. Cryoprotectant addition

For P1 and P2, corneal cryoprotectant addition was carried out using a non-adherent 6-well culture plate (ThermoScientific, Thermo Fisher Scientific) placed on ice. Approximately 10 mL of cold CS1.1, CS1.2 and CS1.3, and CS2.1, CS2.2 and CS2.3 solutions were added in respective wells.

Cryoprotectant addition was done gradually using the three CSs of each protocol at intervals of 3 min, from the CS with the lowest DMSO concentration to the CS with the highest DMSO concentration. For that, corneas were transferred from the hypothermic Corneal Chamber medium to the CS1.1 and CS2.1 solutions, submerging the cornea endothelium side-up and picking the cornea by the sclera rim with a curved smooth tip dissecting forceps without touching the endothelium. This process was repeated with

CS1.2 and CS2.2 and the CS1.3 and CS2.3. After 3 min embedded in CS1.3 or CS2.3, the corneas were transferred to a 5 mL pre-cooled cryovial (AstiK's Labbox, Barcelona, Spain) that contained 5 mL of cold CS1.3 and CS2.3. Using an orbital shaker, cryovials were gently shaken on ice for 10 min for tissue equilibration, which is, according to Taylor and Busza (1992), the process where the tissue achieves the same pCPA concentration as the surrounding CS.

For P3 and P4, corneas were transferred from the hypothermic Corneal Chamber medium to a pre-cooled cryovial by picking the cornea from the scleral rim with the dissecting forceps without touching the endothelium. The cold VS55 or DP6 CS was added dropwise until achieving a volume close to the cryovial maximum volume. Isopentane was added on the top of the solution to reduce the risk of ice nucleation.

2.3. Cooling process

For P1 and P2, after the cryoprotectant addition step, cryovials were immediately transferred to a precooled freezing chamber in a biological freezer CM-2010 (Carburos Medica, Barcelona, Spain) where they were subjected to the controlled cooling process typical of the conventional cryopreservation. To record the sample temperature during the cooling process, a thermocouple thermometer was introduced in a pre-cooled cryovial that contained the cold CS1.3 without any tissue, as it was described by Capella *et al*. (1965) that registered cooling rates with or without a cornea did not change significantly.

The used cooling program is represented in **Figure 9** and its segments are shown in **Table 3**. With this program, samples were first subjected to a process called shock cooling, which consisted in a rapid cooling to initiate ice nucleation, followed by different temperature segments to counteract the latent heat liberation during crystallization and avoid extreme variations of temperature in sample. Cryovials were then stored in the gas phase of a liquid nitrogen tank.

The programmed temperature and the sample temperature were recorded at each second of the cooling process using the biological freezer software. Sample cooling rates were calculated by subtracting the final temperature achieved at the end of a segment to the final temperature of a previous segment. The resulting values were then divided by the duration of the corresponding segment, and expressed as °C/min.

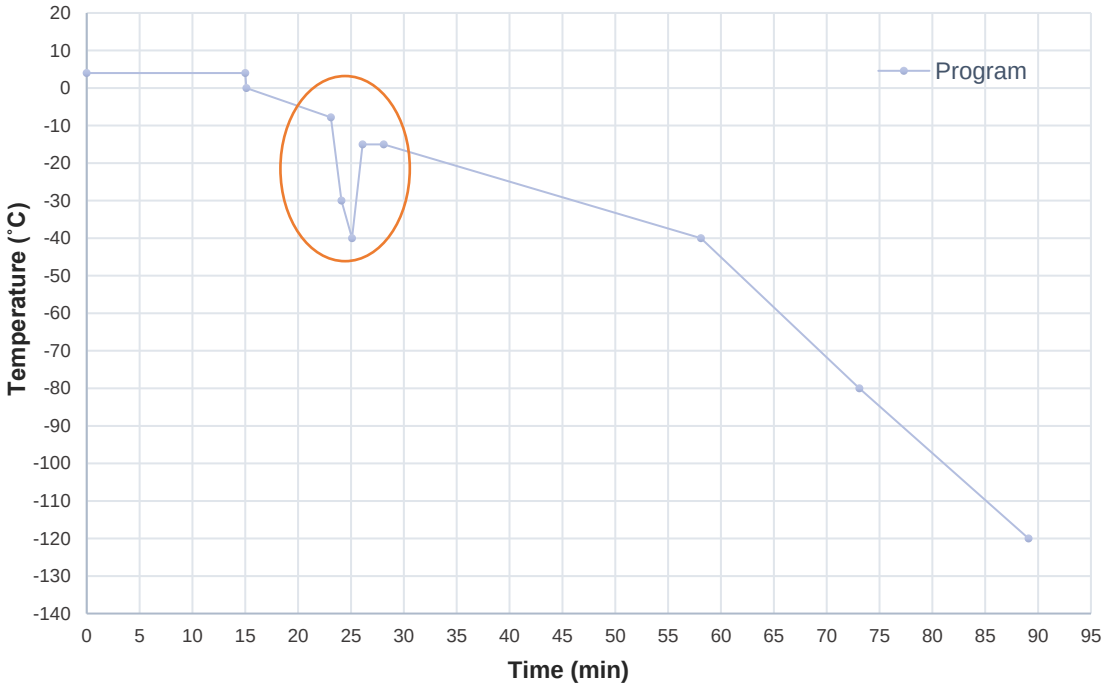

***Figure 9**. Graphic of the cooling program used in the cryopreservation protocols 1 and 2. The blue points represent the start and end of each segment. The shock cooling process for ice nucleation induction and heat latent release control is shown in the orange circle.*

***Table 3**. Segments (Seg) of the cooling program used in protocol 1 and protocol 2, with the duration and the final temperature achieved at the end of each segment.*

	Seg 1	**Seg 2**	**Seg 3**	**Seg 4**	**Seg 5**
Time (min)	15	0.1	8	1	1
Final Temperature (°C)	4	0	-7.8	-30	-40
	Seg 6	**Seg 7**	**Seg 8**	**Seg 9**	**Seg 10**
Time (min)	1	2	30	15	16
Final Temperature (°C)	-15	-15	-40	-80	-120

For P3 and P4, vitrification was achieved by using precooled isopentane (Sigma-Aldrich Química S.A.) to quickly freeze the cryovial's content to below -100 °C. Briefly, a beaker containing isopentane was partially immersed in liquid nitrogen. After several minutes, the isopentane formed a solid phase at the base of the beaker (meaning that a T_m of -160 °C was reached) with a liquid phase remaining in the upper part with a temperature of approximately −135 °C (near to isopentane T_m). After the cryoprotectant addition, cryovials were immediately transferred to the liquid phase of the isopentane where they

remained during 10 min. Then, the cryovials were stored in the gas phase of a liquid nitrogen tank.

2.4. Warming process and cryoprotectant removal

The cryovials containing the corneas and the CSs were removed from the nitrogen tank and left at room temperature (RT) for 1 min. Cryovials' content was then warmed in a water bath at 37 °C until the CSs became liquid.

For P1, the cryovials' content was poured in a well of a pre-cooled non-adherent 6-well culture plate, and corneas were carefully transferred, endothelium side-up, in 10 mL of cold wash solution (WS) consisting of Human Albumin Grifols® 200 g/L. To remove the DMSO, a total of three consecutive washes were carried out at intervals of 5 min.

For P2, P3 and P4, the cryovials' content was poured in a well of a pre-cooled non-adherent 6-well culture plate. Half of the CS was removed and an equal volume of cold sodium chloride (NaCl) 0.9% physiological solution (Braun, Barcelona, Spain) (P2) or cold Euro-Collins solution (P3 and P4) was added at intervals of 5 min. This washing process was repeated until the CS was entirely removed.

3. Spectroscopy techniques

3.1. Nuclear magnetic resonance spectroscopy

Proton (^1H) nuclear magnetic resonance (NMR) spectroscopy was used to detect the DMSO in warmed P1-cryopreserved corneas before and after each wash of the cryoprotectant removal step. NMR allows the detection of protons in molecules such as DMSO ($(CH_3)_2SO$) and water (H_2O). These molecules show a distinct specific peak in the chemical shift range of the NMR spectra at approximately 2.7 ppm and 4.8 ppm respectively. Concentration of each substance can be extrapolated using each peak area, as these areas are proportional to the number of protons, and thus, to the number of molecules.

For NMR analysis, three P1-cryopresereved corneas were cut in four pieces after thawing (**Figure 10**). The sample procedure preparation is described in **Figure 11**. Briefly, for each cornea, one piece was transferred to a vial with 600 µL deuterium oxide (D_2O, Sigma-Aldrich Química S.A.), and the remaining three were washed in Human Albumin Grifols® 200 g/L for cryoprotectant removal, as described in the section 2.4. Warming process and

cryoprotectant removal, once, twice and three times, respectively. Then, the pieces washed once, twice and three times were transferred immediately to vials with 600 μL D_2O. All pieces were incubated 24 h at RT for tissue equilibration. Then, the tissues were removed from the vials and the D_2O bathing solutions were frozen at -20 °C for ^1H NMR spectroscopy.

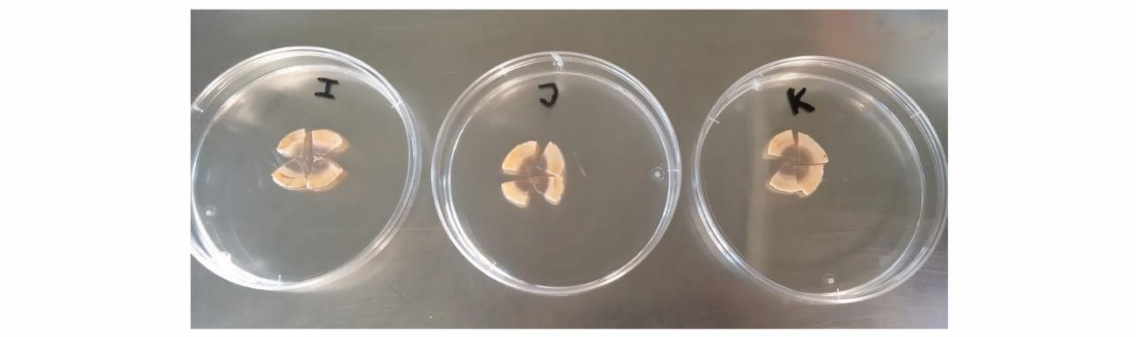

***Figure 10**. Warmed P1-cryopreserved corneas before being washed and/or immersed in deuterium oxide for proton nuclear magnetic resonance spectroscopy.*

The determination of DMSO concentration was performed by technicians of the Molecular Spectroscopy Unit at the *Servizo de Apoio á Investigación* (*SAI*) of *Universidade da Coruña* (*UDC*). Briefly, the D_2O bathing solution of each piece of cornea was thawed and transferred into a 5 mm NMR glass vial (Bruker, Massachusetts, USA) and analyzed with the spectrometer Bruker AVANCE III HD 400.1 (Bruker). Spectra were acquired after a strong pulse. All the spectra were Fourier - transformed with the software NMR MNova (Mestrelab Research; Santiago de Compostela, Spain) and automatically phased. Integrals of each water and DMSO peaks were calculated to obtain the absolute value. Concentrations of DMSO were extrapolated using a reference curve created with different concentrations of DMSO in milliQ water within a range of 0 M to 1.6 M. Results for each piece of cornea were expressed as mean ± SD.

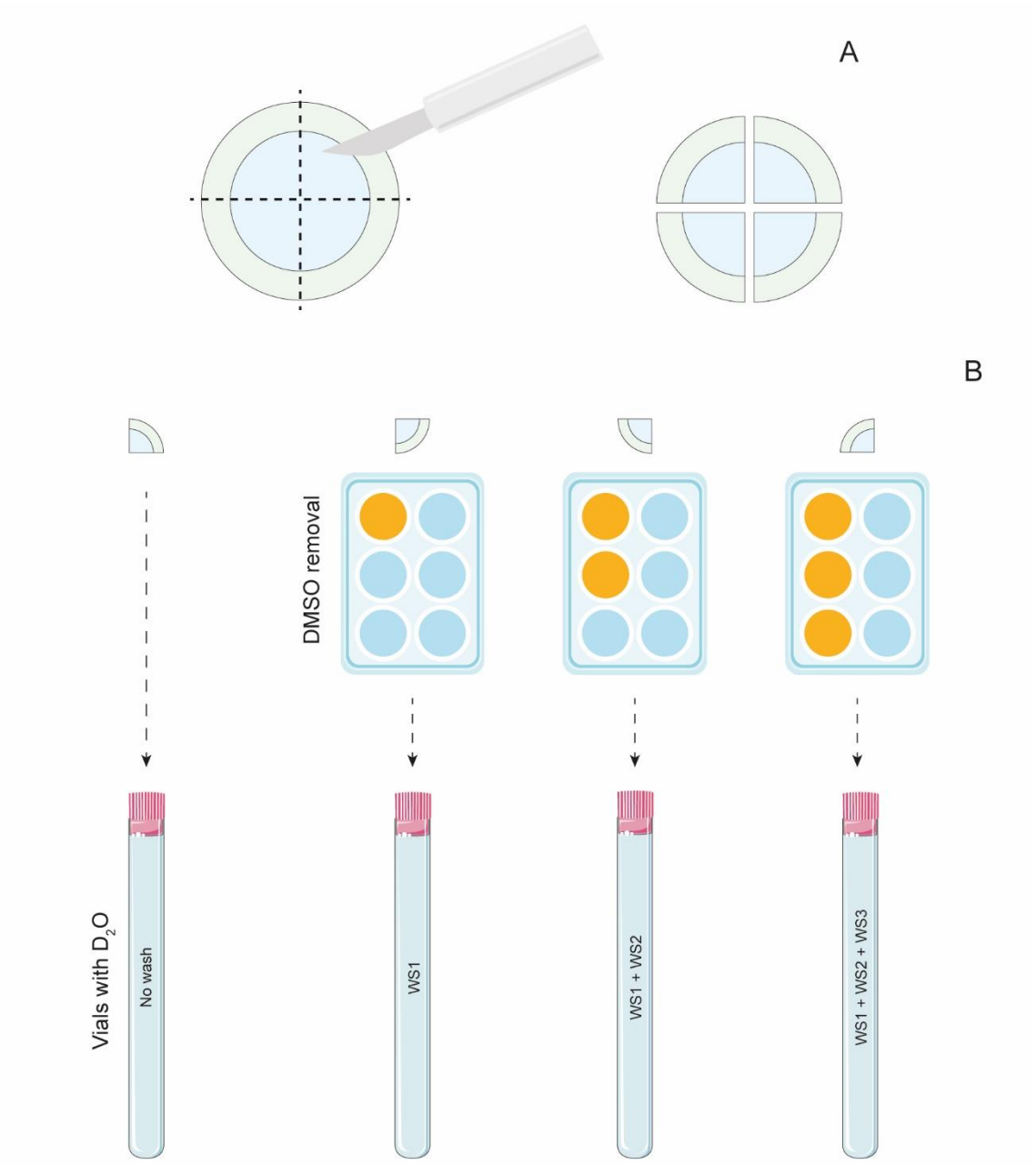

***Figure 11**. Schematic planning of the sample preparation procedure before proton nuclear magnetic resonance (NMR) spectroscopy. A warming cornea was cut in four pieces (A). One piece was transferred directly to the vials with deuterium oxide (D_2O), while the other three were washed once with the wash solution 1 (WS1), twice (WS1+WS2) or three times (WS1+WS2+WS3) with the albumin solution (orange), and then transferred to the vials with D_2O (B). WSn: wash solution 1, 2, 3.*

4. Clinical related techniques

4.1. Endothelium-Descemet's membrane complex extraction

To remove the endothelium-DM complex, the clinical method for DMEK graft peeling was followed (**Figure 12**).

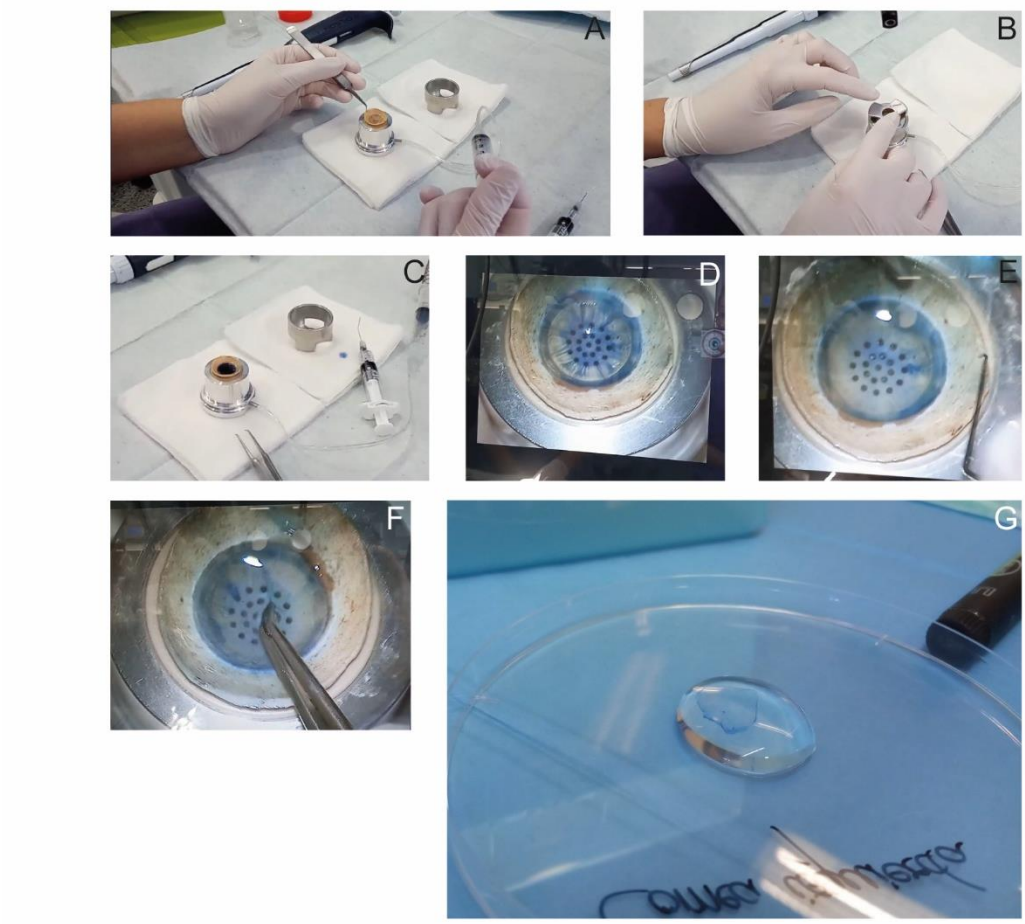

***Figure 12**. Representative images of the DMEK-graft excision process. The cornea is fixed to the vacuum base of the punch (A), cut with the blade of the punch cover (B), and stained with trypan blue (C) to visualize the circumferential cut (D). With a cleavage hook (E, right), the complex is carefully detached, using the spatula-Hockey stick (E, up) to hold the sclera and the cornea. With a pointed forceps, the complex is carefully peeled (F) and completely detached from the cornea (G).*

With a stereoscope, corneas were centered, endothelium side-up, on the base of a disposable 10 mm-diameter corneal vacuum guarded punch (Moria, Antony, France), and held in place by applying a suction under the cornea (**Figure 12**, A). Using the cover which contains a 10 mm-diameter circumferential blade, a cut was made through the posterior part of the cornea where the endothelium is located (**Figure 12**, B). The endothelium was stained for 1 min with an ophthalmic trypan blue solution (AJL BLUE 0.06%, AJL Ophthalmic, Álava, Spain), to visualize the circumferential cut (**Figure 12**, C). Trypan blue was poured-off, and the endothelium was rinsed once with the phosphate buffered saline

solution "*di lavaggio*" PSS-L (AlchimiA). The endothelium was kept moist using PSS-L for the subsequent manipulations (**Figure 12**, D). Seeing the trephined line stained in blue, the trephined edge of the complex was slightly lifted circumferentially with a cleavage hook (e.Janach, Como, Italy) (**Figure 12**, E). Then, with a spatula-Hockey stick, while the sclera was held using a straight and acute tip forceps specific for the donor lamella stripping (e.Janach), the complex endothelium-DM was carefully peeled longwise in one movement (**Figure 12**, F-G). If the DM was tightly attached to the stroma, the three-quadrant peeling off method was used to avoid tearing (Parekh *et al*., 2018).

4.2. *In vitro* penetrating keratoplasty

A male (Y) and female (X) corneas were used in an *in vitro* PK surgery at the *Centro Tecnológico de Formación* of the *Instituto de Investigación Biomédica de A Coruña* (*INIBIC*). The surgery was performed by the ophthalmologists Marcelino Álvarez Portela and Patricia Simón Alonso and assisted by the nurse Celestino Pérez Vayá.

The X cornea was placed on the base of a disposable Barron vacuum donor punch (Katena, New Jersey, EE.UU.) (**Figure 13**, A) and was entirely trepanned with the punch vacuum cover equipped with an 8 mm-diameter circumferential blade to obtain a corneal button and a perforated cornea (**Figure 13**, B).

The Y cornea was placed in a Barron artificial anterior chamber (Katena). The infusion of saline buffer through one port and the injection of viscoelastic (Provisc®; Alcon, Texas, USA) allowed the cornea to maintain its tension (**Figure 13**, C). The cornea was then firmly fixed to the artificial chamber using the locking cover ring (**Figure 13**, D) and trepanned with a disposable Barron trephine of 8 mm-diameter (Katena) (**Figure 13**, E). Corneal keratoplasty scissors were used to remove the XY button (**Figure 13**, F-G). Following the excision of the Y button, the X button was placed in the perforated Y corneoscleral ring (**Figure 13**, H-I) and sutured with the non-absorbable Mononylon Ethilon® 10.0 (Ethicon, Country) using a tying and stitch forceps and a needle holder for suture. 8 faced single sutures with double knots were done, starting for the first suture at 12 o'clock, the second at 6 o'clock, the third at 3 o'clock, the fourth at 9 o'clock, and the remaining sutures were done between the first four, to maintain the tension (**Figure 13**, J-K). The same procedure was carried out with the Y button and the perforated corneoscleral X cornea. As a results, two models were obtained: the PK model X^Y (X donor at the center and Y receptor at the

periphery) (**Figure 13**, L) and the PK model Y^X (Y donor at the center and X receptor at the periphery).

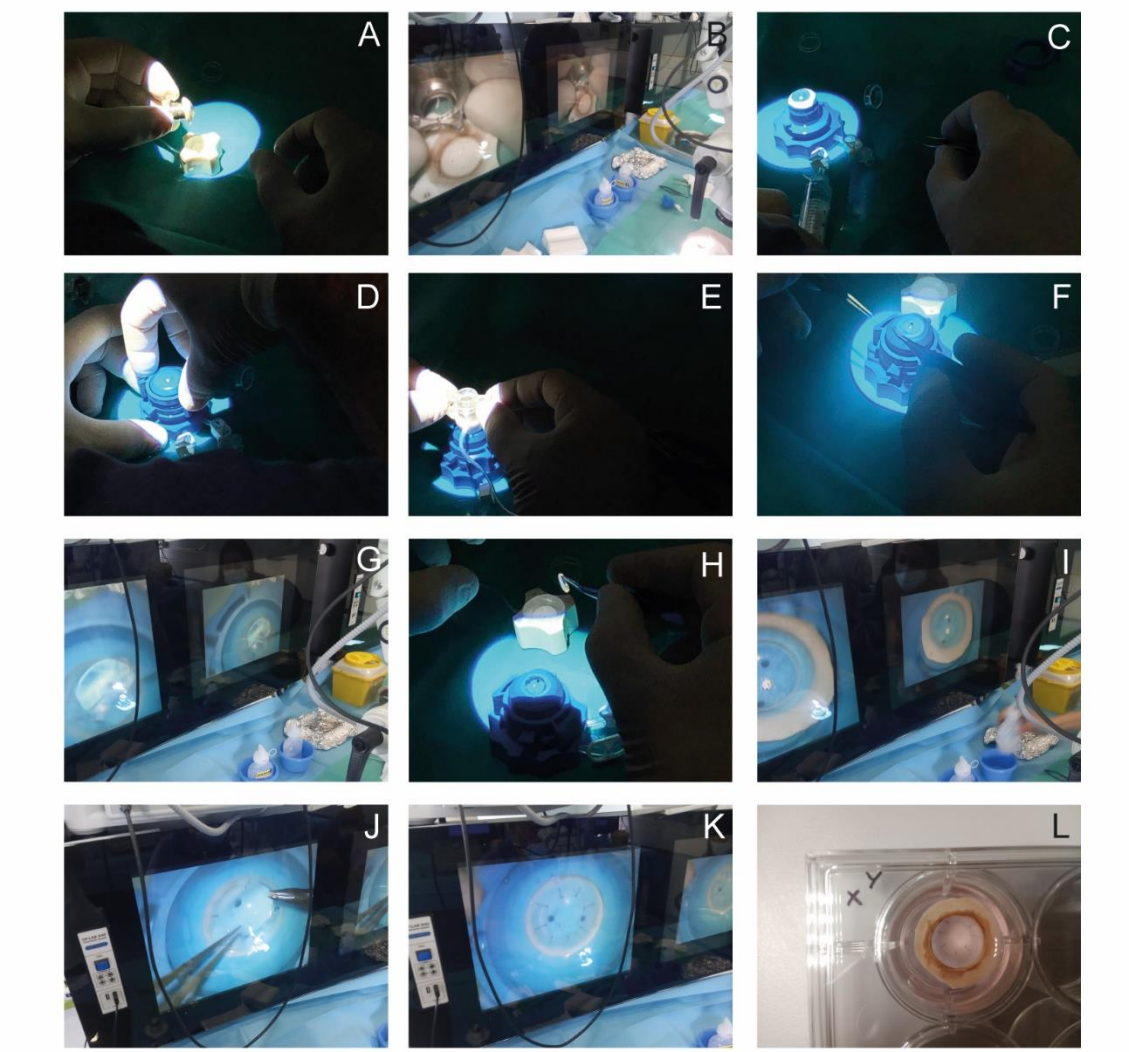

***Figure 13**. Steps of the penetrating keratoplasty model X^Y. The female X cornea was trephined (A-B). The male Y cornea was placed in an artificial chamber and correctly positioned (C), fixed (D) and trepanned (E), removing the Y bottom with a corneal keratoplasty scissors (F-G). The X corneal bottom was placed in the Y corneoscleral ring (H-I) and sutured (J-K). The model X^Y was removed from the artificial chamber and placed on a plastic support in a 12-well culture plate with endothelial medium (L).*

5. Cell culture techniques

5.1. Organ culture of penetrating keratoplasty models

The model X^Y and Y^X were disposed endothelial side-up on a plastic supports inside the wells of a 12-well culture plate (Falcon, Merck), and cultured at 37 °C and 5% CO_2 using an specific corneal endothelial medium which consisted in Opti-MEM (Gibco) supplemented with 8% fetal bovine serum (FBS; Gibco), 1% penicillin/streptomycin (P/S; Gibco), 5 ng/mL epidermal growth factor (EGF) (R&D, Minneapolis, EE.UU.), 0.08%

chondroitin sulfate (Y0000280; European Pharmacopoeia Reference Standard, Strasbourg, France) and 20 mg/mL ascorbic acid (Merck). This medium was changed each 2-3 days. X^Y model was cultured for 4 weeks and Y^X model was cultured for 9 weeks.

6. Microscopic techniques

6.1 Optical microscopy

6.1.1 Bright field microscopy

6.1.1.1. Masson's trichrome staining

Masson's trichrome staining is used to visualize the collagen fibers in blue with aniline blue dye, the cell cytosols in pink with Biebrich scarlet-acid fuchsin dye, and the cell nuclei in purple-black with Weigert's iron hematoxylin.

One warming and washed cornea from each cryopreservation protocol (P1, P2, P3 and P4) and one hypothermic stored cornea were fixed with 3.7% formaldehyde, embedded in paraffin, and cut in 4 μm sections using a microtome. Those sections were spread on microscope slides, deparaffined, hydrated, stained with Masson's trichrome, and mounted with Dibutylphthalate Polystyrene Xylene (DPX) mounting media (Surgipath®, Leica Microsistemas S.L., Barcelona, Spain). The slides were then observed and photographed using an Olympus DP70 digital camera (Olympus Iberia S.A., Barcelona, Spain) on an Olympus BX61 fluorescence microscope (Olympus Iberia S.A.) using the cellSens 1.16. software (Olympus Iberia S.A.).

The stromal thickness of cryopreserved corneas were measured using Fiji software (Schindelin *et al.*, 2012). For that, the stromal area was measured and divided between the width of the micrograph, as it remained constant for all images. This allowed to correct the measurement in rippled sections.

6.1.1.2. Hematoxylin-eosin staining

Hematoxylin-eosin staining is used to visualize cells, whose nuclei become purple in contact with Harris's hematoxylin and whose cytoplasm and collagen fibers become pink in contact with eosin.

PK models' pieces were fixed with 3.7% formaldehyde, embedded in paraffin, and cut in 4 μm sections with a microtome. After deparaffinization, hydration, and fluorescence *in*

situ hybridization (FISH) 98 °C pretreatment, slides were stained with hematoxylin-eosin dyes and mounted with DPX mounting media. The tissue was observed and photographed with an Olympus BX61 fluorescence microscope using the Olympus DP70 digital camera and the cellSens 1.16. software.

6.1.1.3. Trypan blue – alizarin red staining

The double stain with trypan blue and alizarin red is a dye-exclusion assay. Trypan blue stains nuclei of cells that present injured membranes, while alizarin red precipitate into the intercellular spaces, becoming a dye-lake in contact with calcium, and delineating the borders of cells in red.

The adapted corneal endothelium staining protocol by Taylor and Hunt (1981) was followed with some modifications (**Figure 14**, A). Briefly, ten warmed and washed P1-cryopreserved corneas and one hypothermic stored cornea were placed on plastic rings with the endothelium facing upward. They were gently rinsed twice with calcium free (CF) phosphate buffered saline (PBS) (Oxoid™, ThermoFisher, Spain). The endothelia were then stained for 90 s with a 0.2% trypan blue solution made by diluting 0.4% Trypan Blue Solution (Gibco) in distilled water. The trypan blue was poured off, and the endothelia were briefly rinsed twice with CF-PBS. Immediately, the endothelia were stained for 90 s with a 0.2% alizarin red solution (pH 4.2), prepared with alizarin red powder (Panreac Química S.L.U) in CF-PBS, and filtered with a 0.22 μm-pore filter. The alizarin red was poured off and the endothelia were briefly rinsed twice with CF-PBS. Several micrographs of each endothelium, with two magnifications (0.67X and 5X) were taken with the Nikon digital sight DS-Fi2 camera mounted on a Nikon SM7 745T stereoscope (Nikon Instruments Europe B.V., Amsterdam, Netherlands) (**Figure 14**, B). An overview image of the endothelia was obtained with the lower magnification and a detailed image of the central part of the endothelial monolayers were obtained by manually merging multiple images of the higher magnification with Photoshop software (Adobe; California, EE.UU.).

To evaluate the final ECD, the methodology employed by the Konan specular microscopy software was followed to calculate the ECD (**Figure 15**, A). This equipment and software are used routinely in clinical practice to evaluate the ECD of donor corneas. Briefly, using Fiji software, four areas of 66 mm^2 were randomly chosen in each of the merged images (**Figure 15**, B). In each area, a group of ECs which stayed together were rounded to

calculate their area, and cells with and without blue nuclei were manually counted inside (**Figure 15**, C-E). ECD was calculated subtracting the blue nuclei cells from the number of counted cells and by dividing the result to the area occupied by the counted cells. ECD was expressed as cells/mm².

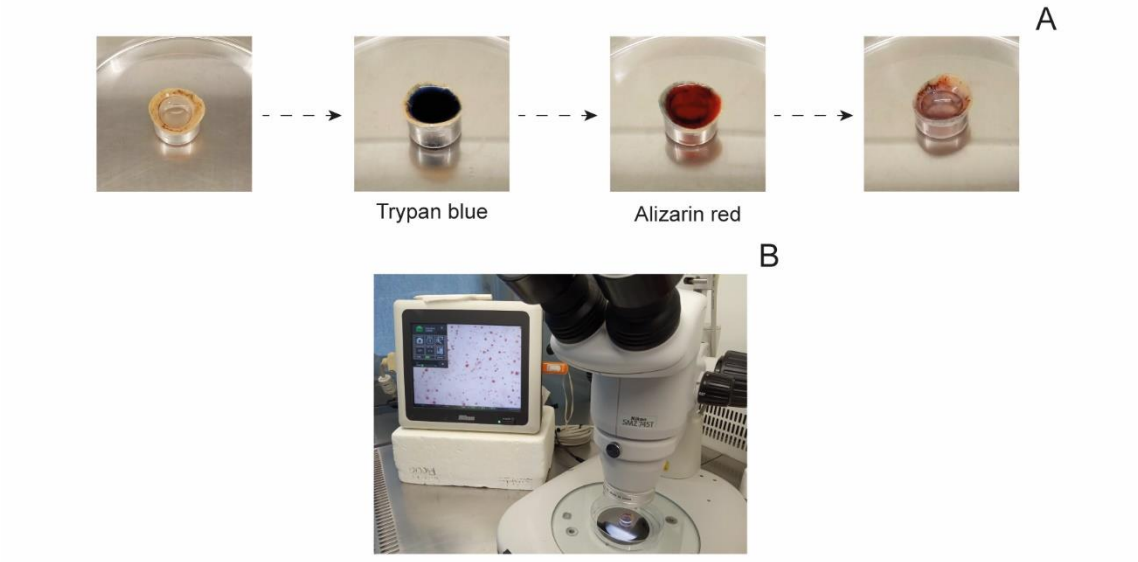

***Figure 14**. Methodology of the trypan blue – alizarine red staining. A) Steps of the live cells staining assay with trypan blue and alizarin red. B) Visualization of the stained endothelium in the screen of a stereoscope.*

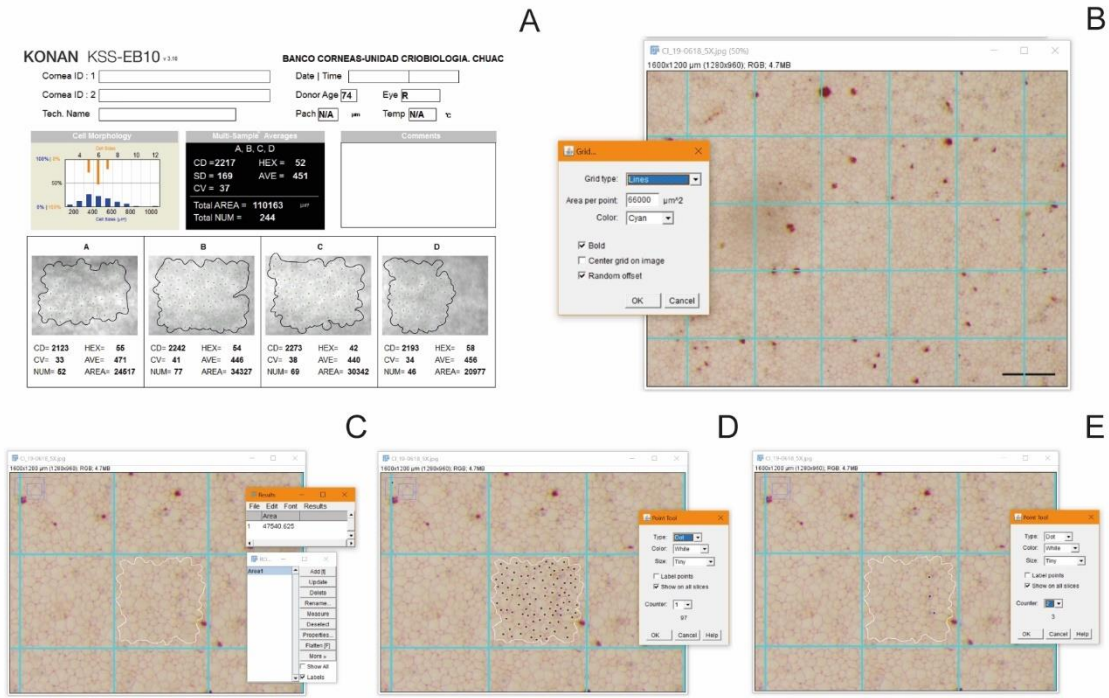

***Figure 15**. Calculation of the endothelial cell density after cryopreservation with P1 and trypan blue and alizarin red staining, imitating the methodology employed by the specular microscope Konan software. A) Example of data provided by the Konan KSS software, where endothelial cells are counted manually in four endothelium's photographs of 66 mm². B) For EC counting, a grid with areas of 66 mm² were created on a merged stained image of an endothelium. C) An area where ECs have recognizable cell membranes are delimitated. D) Total cells inside this area are counted. E) Cells with blue nuclei are counted inside the area, to calculate the endothelial cell density after P1-cryopreservation.*

6.1.2. Fluorescence microscopy

6.1.2.1. Calcein AM assay

The calcein acetoxymethyl ester (AM) enzymatic assay is used to visualize the enzymatic activity in living cells and the cell membrane integrity. The calcein AM is a non-fluorescent membrane-permeant dye that is hydrolyzed by esterase. The product is a fluorescent molecule which remains in the cytoplasm of living cells with an intact cell membrane.

The endothelium-DM complex of two cryopreserved corneas from each protocol (P1, P2, P3 and P4) was placed back onto the corneal stroma after stripping. Endothelium was stained with 300 µL of the calcein AM solution provided by LIVE/DEAD® Cell Imagine Kit (Invitrogen, Thermo Fisher Scientific), following the manufacturer's instructions. For EC nuclei visualization, the complex was counterstained for 45 min at RT with 3 µL/mL Hoechst 33342 (bisBenzimide H 33342 trihydrochloride, Sigma-Aldrich Química S.A.), which binds to deoxyribonucleic acid (DNA) (Romano *et al.*, 2018).

After removing the Hoechst dye, the complex was rinsed with PSS-L. While maintaining the endothelium moist with PSS-L, the complex was transferred on a microscope slide. The complex was spread over the slide using forceps and ophthalmic microsponges. Immediately, the endothelium was observed using the Olympus BX61 fluorescence microscope. Micrographs of the endothelium were taken with the Olympus DP70 digital camera, employing the cellSens 1.16. software.

6.1.2.2. Cell tracer staining

Endothelia of two hypothermic stored corneas of different sex, named X (female cornea) and Y (male cornea), were stained with two different cell tracers: SP-DiOC18(3) (3,3'-Dioctadecyl-5,5'-Di(4-Sulfophenyl)Oxacarbocyanine, Sodium Salt; Invitrogen), abbreviated as DiO, and DiIC18(5)-DS (1,1'-Dioctadecyl-3,3,3',3'-Tetramethylindodicarbocyanine-5,5'-Disulfonic Acid; Invitrogen), abbreviated as DiI. These lipophilic dyes, which exhibit green fluorescence in the case of DiO and orange fluorescence in the case of DiI, diffuse within the plasma membrane and allow the monitoring of cell movements and location.

Following the manufacturer's instructions and previous concentration's optimization, the X's endothelium was stained with 1.5 µM DiO and the Y's endothelium was stained with

2.5 μM Dil. The corneas were placed on a plastic support and immersed until the PK surgery in a specific corneal endothelial medium described in section 5.1. Organ culture of penetrating keratoplasty models. To observe cell tracers, the confocal microscope A1R (Nikon) was used by technicians of the Microscopy Unit the *SAI* facility.

6.1.2.3. Fluorescence *in situ* hybridization

FISH is a cytogenetic technique used to detect a specific DNA sequence in cell chromosomes using a fluorescence-labeled complementary DNA probe. This technique was realized within the Genetic Area of the *Centro Oncológico de Galicia* and of the Teresa Herrera Hospital.

Paraffined 4 μm sections of the models X^Y and Y^X were deparaffinated in xylene and progressively hydrated in solutions with decreasing ethanol concentrations down to distilled water. Then, different parameters were tested using the clinical FISH protocol for tissue as a starting point.

Following the clinical protocol, slides were incubated 30 min at 98-100 °C in a ceramic Coplin jar (Cytocell, Germany) (**Figure 16**, A) which contained prewarmed Heat Pretreatment Solution of the Aquarius® Tissue Pretreatment Kit (Cytocell). Slides were washed with distilled water twice for three minutes. An enzymatic solution (Enzymatic Reagent of the Aquarius® Tissue Pretreatment Kit) was added over tissue and incubated at 37 °C for 20 min in a Hybridizer (Dako, California, USA). The enzymatic solution was removed with two washes of 2 min in distilled water, and samples were dehydrated.

Tested variations of this protocol were:

a) Heat pretreatment solution for 5, 10 and 15 min in the Coplin jar at 98-100 °C.
b) Enzymatic treatment without previous heat pretreatment.
c) Heat pretreatment solution for 10 min in the Hybridizer at approximately 90 °C (**Figure 16**, B) and subsequent enzymatic treatment.

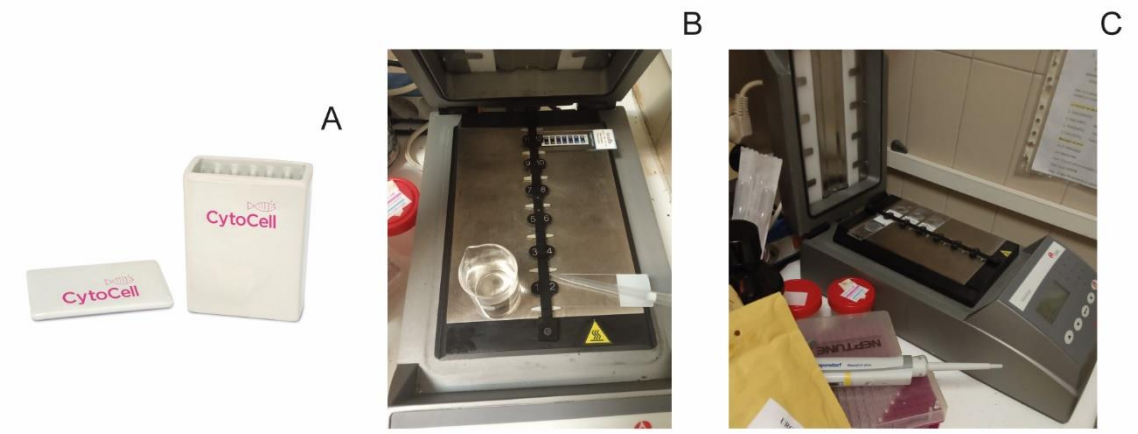

***Figure 16**. Tools and equipment used to test the variations of fluorescent* in situ *hybridization (FISH) clinical protocol. A) Ceramic Coplin jar used for the 98 °C pretreatment. B) Warming of the pretreatment solution in the Hybridizer hotplate and control of the plate temperature with a slide surface thermometer. Pretreatment solution was added to slides when the slide surface thermometer marked 90 °C. C) Slides with probes before hybridization on the hybridizer plate.*

After dehydration, Chromosome X Alpha Satellite Probe Green (LPE0XG; Cytocell) and Chromosome Y Alpha Satellite Probe Red (LPE0XR; Cytocell) were added to the tissues following the manufactures' recommendations. The tissues were covered with a round coverslip, and rubber solution glue (CytoCell) was added to the periphery of the coverslip for sealing. Slides were placed in the Hybridizer (**Figure 16**, C). The hybridization program consisted of a 2 min denaturalization of the double stranded DNA at 75 °C followed by overnight hybridization at 37 °C.

After hybridization, the dried rubber glue solution and the coverslip were removed, and the slides were incubated in a solution of 0.25% SSC (Cytocell) for 2 min at 72 °C. Then, the slides were immersed for 1 min in a solution made of 2% SSC and 0.05% Tween-20 (Sigma-Aldrich Química SA). Samples were counterstained with DAPI (4 ',6-diamidino-2-fenilindole) Antifade (Cytocell) and covered with a coverslip. For probes visualization, Nikon Eclipse E400 fluorescent microscope (Nikon) was employed, using an objective of 100X. Micrographs were obtained with the digital camera Nikon Ds Qi2 (Nikon) using the software Nis-Elements Basic Research 4.50 (Nikon).

6.1.2.4. Immunofluorescence assay

Pieces of the X^Y model were washed once with PBS, fixed with 4% paraformaldehyde (Sigma-Aldrich Química S.A.), permeabilized with 0.02% Triton-100 (Sigma-Aldrich Química S.A.) for 10 min, and washed twice with PBS. Cryosections of the Y^X model were treated using same process.

Samples were incubated for 2 hours at RT with mouse or rabbit antibodies directed against ZO-1 (33-9100; 1:50; Invitrogen), N-cadherin (33-3900; 1:100; Invitrogen), the marker of proliferation Ki-67 (550609; 1:100, BDBiosciences, USA), or p27 (703608; 1:100; Invitrogen). Those antibodies were used in 1% bovine serum albumin (BSA; Sigma-Aldrich) in PBS. Phalloidin conjugated to a fluorescent dye was added for actin counterstaining (A12381; 1:1000; Invitrogen).

After incubation, samples were washed three times with PBS and incubated for 1 h at RT in a 1% BSA solution containing the secondary antibodies Alexa Fluor 594 goat anti-mouse IgG, (A11032; 1:400, Invitrogen) or Alexa Fluor 594 goat anti-rabbit IgG (A11012; 1:400, Invitrogen). Nuclei were stained using Hoechst in combination with the secondary antibodies or with the conjugated phalloidin when used.

Pieces from the X^Y model were washed three times in PBS and stored at 4°C with 0.02% sodium azide diluted in PBS until visualization with the confocal microscope A1R (Nikon) of the *SAI* facility. For Y^X model cryosections, samples were washed three times with PBS, mounted with Glycergel aqueous mounting medium (Dako) and observed with the Olympus BX61 fluorescence microscope. Micrographs were taken with the Olympus DP70 digital camera, employing the cellSens 1.16. software.

6.2. Electron microscopy

6.2.1. Transmission electron microscopy

Transmission electron microscopy (TEM) is a microscopy technique that allows the visualization of the ultrastructure in ultrathin samples when a beam of electrons pass through the sample and interacts with it.

Two warmed and washed P1-cryopreserved corneas and one hypothermia stored cornea were prepared for TEM to analyze the integrity of the stroma. For that, 8 small pieces of cornea were cut from the central part of the tissue. Following the protocol of Müller *et al*. (2004), with some modifications, the pieces were initially prefixed for 30 min at RT with cacodylate buffer solution (1 M, pH 7.4; Acros Organic, Spain) containing 1.25% glutaraldehyde (Guimana, Valencia, Spain) and 0.1% paraformaldehyde (ThermoScientific). Those prefixed tissues were then fixed for 20 h at 4 °C in a 2.5% glutaraldehyde solution.

The next steps were performed by technicians at the Microscopy Unit of the *SAI* facility. Briefly, tissue pieces were postfixed with 1% osmium tetroxide (OsO_4), dehydrated with increasing concentrations of acetone solutions, and embedded in resin Spurr (Electron Microscope Science, Pennsylvania, USA). Ultrathin sections were processed (**Figure 17**) and visualized with the JEOL JEM 1010 transmission electron microscope (JEOL Ltd., Japan).

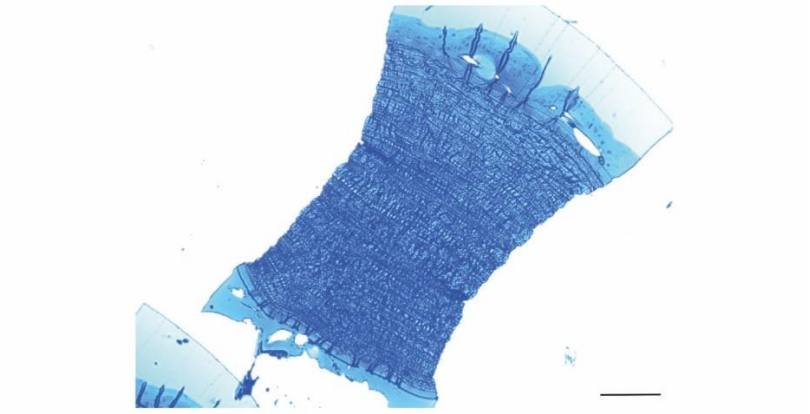

***Figure 17**. Semi thin section of a cryopreserved cornea stained with Toluidine blue. Scale bar: 100 µm.*

A total of 100 distances between transversal sectioned collagen fibers were measured using the open software Fiji. Results for each sample were expressed as mean ± SD.

7. Statistical analysis techniques

Statistical analyses were performed with the GraphPad PRISM 5 software (La Jolla, CA, USA). The nonparametric statistical Kruskal-Wallis test was used to analyze the osmolality (n=3) and DMSO (n=3) concentrations. Statistically significant differences between each group were determined by using the nonparametric Dunn's multiple comparison test. The parametric ANOVA test was used to analyze the distance between collagen fibers (n=3). Statistically significant differences between cryopreserved corneas and the hypothermic stored cornea collagen distances were determined by the Dunnett's multiple comparison test with hypothermic stored cornea data used as the control. The nonparametric Wilcoxon signed-rank test was used to analyze the difference between the ECD of corneas before cryopreservation with P1 and the ECD after warming and staining with trypan blue and alizarin red (n=9). The Spearman's rank correlation coefficient was calculated to analyze if a correlation existed between ECD before and after cryopreservation. A statistical difference was considered significant when the *p-value* was equal or inferior to 0.05 in every test.

III. Materials and Methods:

Objective 2

All these experiments were performed in the *Centre de Recherche du Centre Hospitalier Universitaire de Québec – Université Laval* (Quebec, Canada) under the supervision of Dr. Stéphanie Proulx (**Annex III**), in accordance with the guidelines of the institution and the Declaration of Helsinki and approved by the B*ureau de l'éthique de la recherche du CHU de Québec – Université Laval* ethics committee (DR-002-1382). Seven research-grade human corneal samples were provided by the local eye bank (*Banque d'yeux du Centre Universitaire d'Ophtalmologie, Hôpital St-Sacrement*, Quebec, Canada), through the infrastructure "Ocular tissues for vision health research" (Vision Health Research Network, Quebec, Canada). Next-of-kin consent was obtained from Héma-Québec (Quebec, Canada) for all tissues.

One pair of corneas from a 63-years old female donor was used for EC isolation and culture. One cornea from an 80-years old male donor and two pair of corneas from a 70-years old and 76-years old male donors were used for DM decellularization. Two corneas, one from a 79-years old female donor and one from a 58-years old male donor, were used as a positive control in the immunofluorescence assay.

1. Cell culture techniques

1.1. Isolation and culture of endothelial cells

1.1.1. Endothelium-Descemet's membrane complex extraction

Using sterilized forceps (**Figure 18**, A), two corneas stored in Optisol-GS Corneal Storage Media (Bausch and Lomb, Québec, Canada) (**Figure 18**, B) were transferred, endothelium facing up, to a 60 mm Petri dish (Corning, Massachusetts, USA) containing extraction media which consisted in Dulbecco's modified Eagle's medium (DMEM; Corning, Massachusetts, USA) supplemented with 1% P/S. Using the ZEISS SteREO Discovery.V8 binocular stereomicroscope (Zeiss, Toronto, Canada) (**Figure 18**, C), the sclera was held with a curved smooth tip dissecting forceps, while the complex endothelium-DM was scratched circumferentially with a straight pointed acute dissecting forceps, using the dark brown line of the trabecular meshwork as a guide. With the same forceps, the complex was then peeled in one movement or from different anchor points to prevent tissue tearing.

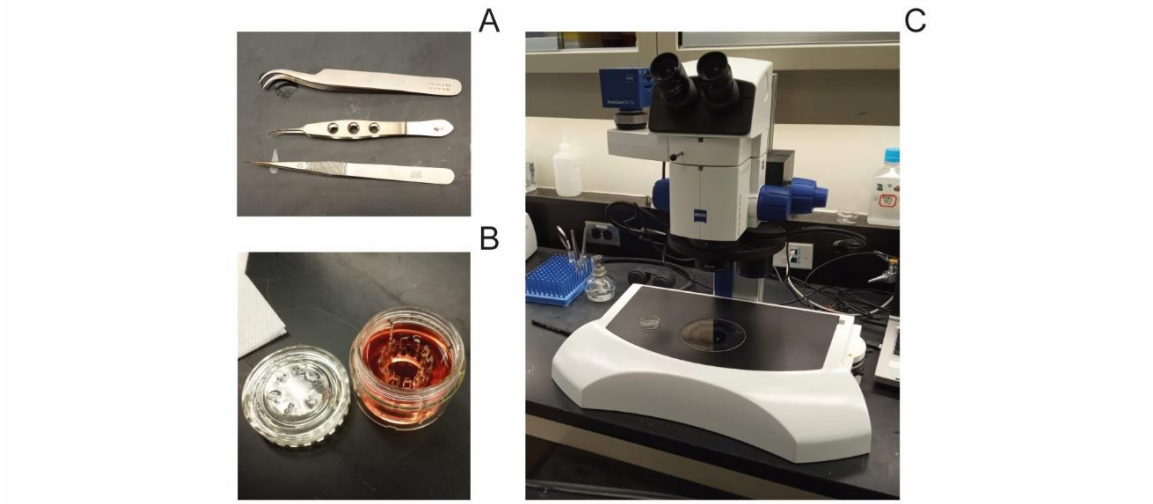

***Figure 18**. Tools for the endothelium-Descemet's membrane isolation. A) Curved smooth tip dissecting forceps to hold the corneal sclera and straight pointed acute dissecting forceps for the endothelium-DM complex peeling; B) Container with Optisol-C to store corneas at 4 °C; C) Stereomicroscope for the endothelium-Descemet's membrane peeling.*

1.1.2. Primary endothelial cells isolation and culture

The isolated endothelium-DM complexes were transferred to 15mL-tubes containing 10 mL of endothelial basal medium, which consisted in Opti-MEM-I medium (Gibco, Ontario, Canada) supplemented with 8% FBS (HyClone, Logan, Utah), 1% P/S (Sigma-Aldrich, Ontario, Canada), and 5 ng/mL human EGF (Austral Biologicals, San Ramon, Canada). The complex endothelium-DM was incubated overnight at 37 °C and 5% CO_2, with the tube cap slightly open.

After incubation, the endothelium-DM complex was centrifuged at 300 x *g* for 10 min. The supernatant was removed and replaced by 1 mL of 1 mg/mL collagenase A (Roche, Ontario, Canada) for an additional incubation of 3 hours at 37 °C and 5% CO_2. The collagenase solution was prepared in the previously described endothelial basal medium and filtered with a 0.22 µm-pore filter (Millipore, Ontario, Canada) before use.

The digested samples were centrifuged for 10 min at 300 x *g*, and after that, the supernatant was removed. The cell pellets were resuspended in completed endothelial medium made of endothelial medium supplemented with 0.08% chondroitin sulfate (Sigma-Aldrich) and 20 mg/mL ascorbic acid (Sigma-Aldrich). The cells were transferred to 6-well (cells from a corneal pair) or 12-well (cells from one cornea only) plates pre-coated for 1 min at RT with FNC coating mix® (Athena Enzyme Systems, Baltimore, MD). Medium was changed 3 times a week.

When they reached confluence, ECs were washed with prewarmed 0.05% trypsin/0.53 mM ethylenediaminetetraacetic acid (EDTA) (Corning) and trypsinized with 0.05% trypsin/0.53 mM EDTA for 5 to 10 min until complete cell detachment. Trypsin was inhibited with completed endothelial medium, and cells were counted using a Neubauer counting chamber and 0.4% trypan blue (Sigma-Aldrich). Cells were subcultured in adherent culture plates, without FNC coating, at a seeding density of 2 x 10^4 cells/cm^2.

1.1.3. Immortalized endothelial cells culture

Cells from a cryopreserved vial of an immortalized corneal endothelial cell line named HCEnC-21T (Schmedt *et al.*, 2012) (graciously given by Dr Ula Jurkunas (Mass. Eye and Ear, Boston, United States)) were thawed, transferred to 5 mL of basal endothelial medium and centrifuged for 10 min at 300 x *g* to eliminate the cryopreservation media. Cell pellet was resuspended in endothelial basal medium and cultured in a 6-well plate. Medium was changed three times a week and cells were subcultured when they reached confluence as described previously.

1.2. Descemet's membrane decellularization

Five research grade corneas stored in hypothermic corneal media Optisol-GS (Gibco, Ontario, Canada) were decellularized using three freeze-thaw cycles, as described by Proulx *et al.* (2009). Briefly, corneas were placed in a 50 mL tube and immersed in 5 mL extraction medium. Samples were frozen at -20 °C overnight. Then, corneas were thawed at 4 °C for 24 h, and medium was removed. DMs were washed with fresh medium to remove ECs debris, and new extraction medium was added. This freezing-thawing cycle was repeated twice. Corneas were stored frozen on the last cycle until use.

1.3. Endothelial keratoplasty graft engineering

1.3.1. Optimization of the graft engineering

The thawed dDMs were washed with fresh extraction medium to remove cell debris and visualized under the stereomicroscope to ensure complete decellularization. Then, dDMs were removed using the technique described in section 1.1.1. Endothelium-Descemet's membrane complex extraction, and transferred to an adherent 60 mm cell culture dish (Corning, Massachusetts, USA) where they were gently spread using a forceps.

For cell suspension volume optimization, HCEnC-21T cells were seeded on dDMs at a density of 2.35 x 10^5 cells/DM in 200 µL basal endothelium medium (calculated to obtain a cell density of 3 x 10^3 cell/mm^2 on a DM of Ø 10 mm). After 30 min of cell adhesion at RT, medium was added to the cell culture dish, and the HCEnC-21T-TE-EK graft was cultured for 5 days at 37°C. Medium was changed twice a week.

1.3.2. Endothelial keratoplasty graft engineering with primary cells

Primary ECs at passage 1 were seeded on four dDMs at a density of 2.35 x 10^5 cells/DM in 100 µL of complete endothelial medium. After 30 min of cell adhesion at RT, medium was added to the Petri dish. The four primary-TE-EK grafts were cultured at 37 °C for 7 days. Media was changed three times a week.

2. Optical microscopy techniques

2.1. Fluorescence microscopy

2.1.1. Phase-contrast microscopy

ECs become polygonal (hexagonal) cells when they create a confluent endothelium. Moving and spreading ECs tend instead toward a spindle fibroblast-like morphology. Following the method of Peh *et al*. (2013) to analyze the morphology of ECs, cell circularity was measured on the primary TE-EK grafts ECs and on the plastic-adhered ECs. Hexagonal ECs have a circularity closer to 0.8 while elongated ECs have a circularity close to 0. Micrographs were taken with the digital camera Zeiss Axiocam 105 Color (Zeiss) mounted on a Nikon Eclipse TS100 phase contrast microscope (Nikon), using the Zen Blue software (Zeiss). Areas and perimeters of at least 75 ECs from each sample were measured using the Fiji software (**Figure 19**, A). Circularity was calculated using the Excel software (Microsoft, USA), following the circularity formula (**Figure 19**, B). Results for each sample were expressed as mean ± SD.

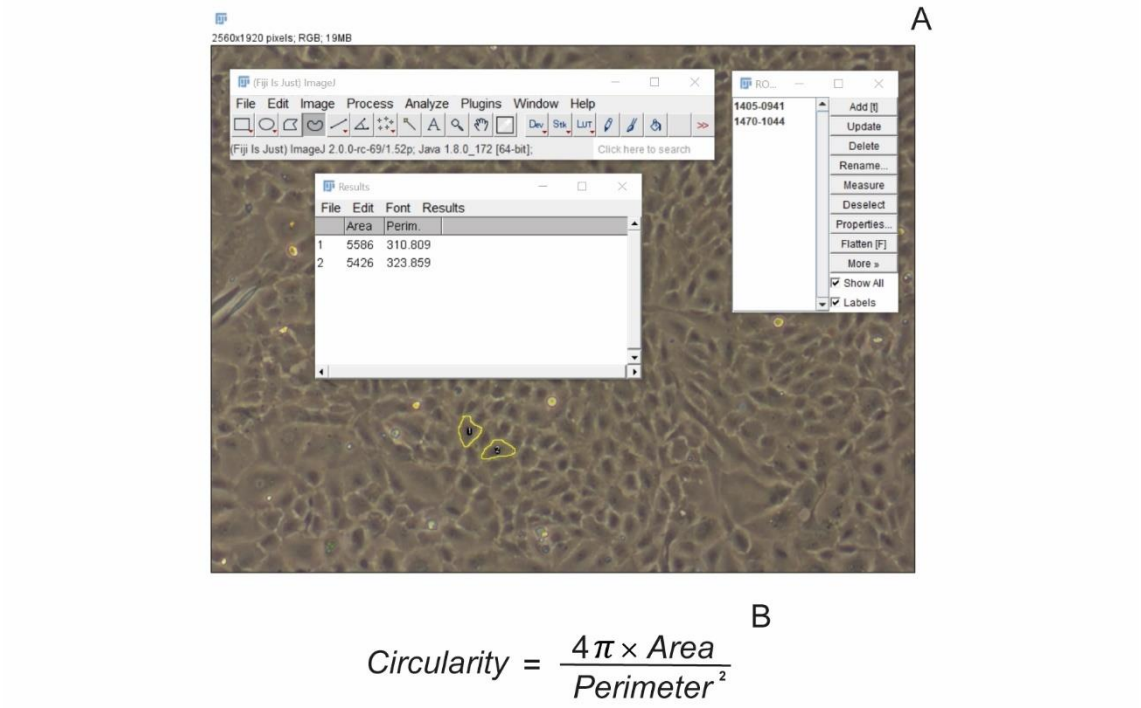

***Figure 19**. A) Fiji software illustration when measuring cell's morphometry. Each cell was manually surrounded to calculate the area and the perimeter. B) Circularity formula.*

2.1.2. Immunofluorescence assay

The TE-EK grafts and the native endothelium-DM complexes were washed once with PBS, fixed with 4% paraformaldehyde (Electron Microscopy Sciences, Hatfield, PA, USA) for 15 min, permeabilized with 0.02% Triton-X100 (Sigma-Aldrich) for 10 min, and washed twice with PBS. The same process was carried out with the same populations of primary ECs adhered on plastic in the Petri dishes.

During the permeabilization step, each TE-EK grafts and the native endothelium-DM complexes were cut into pieces and spread out in Petri dishes under the stereoscope. Primary-TE-EK grafts and primary ECs adhered in culture plastic were incubated for 2 hours with mouse antibodies directed against ZO-1 (Invitrogen, Ontario, Canada) N-cadherin (DAKO, Ontario, Canada), and β-catenin-1 (DAKO). For HCEnC-21T-TE-EK graft, only ZO-1 was used. Those antibodies were used at a dilution of 1:50 in PBS with 1% BSA (Sigma-Aldrich).

After incubation, samples were washed twice with PBS, spread out under stereomicroscopy, and incubated for 1 hour with a mixture containing the secondary antibody (Alexa Fluor 594 goat anti-mouse IgG, 1:400, Invitrogen), Hoechst (1:1000), phalloidin (Alexa Fluor 488 Phalloidin, 1:100, Invitrogen), and PBS with 1% BSA. After two additional washes with PBS, tissues were spread out on a slide under the

stereomicroscope and mounted with aqueous mounting medium. Plastic-adhered cells were also covered with the same aqueous mounting medium.

Slides were visualized with the confocal microscope Zeiss LSM800 (Zeiss) coupled to a Zeiss Axiocam 105 digital camera (Zeiss). Photographs were taken using the Zen Blue software (Zeiss). Plastic-adhered cells were visualized and photographed with the inverted fluorescent Nikon Eclipse TE2000-U microscope (Nikon, Ontario, Canada), coupled to a digital Axiocam MR3 camera (Zeiss), using the AxioVision software (Zeiss).

IV. Results:

Objective 1

1. Corneal integrity and viability using different cryopreservation protocols

1.1. Structural integrity of cryopreserved corneas

Masson's trichrome staining shows the cryopreserved corneal layers following warming and removal of CPAs. Representative photographs of the stained corneas and of epithelium and endothelium are shown in **Figure 20**, **Figure 21**, and **Figure 22**, respectively.

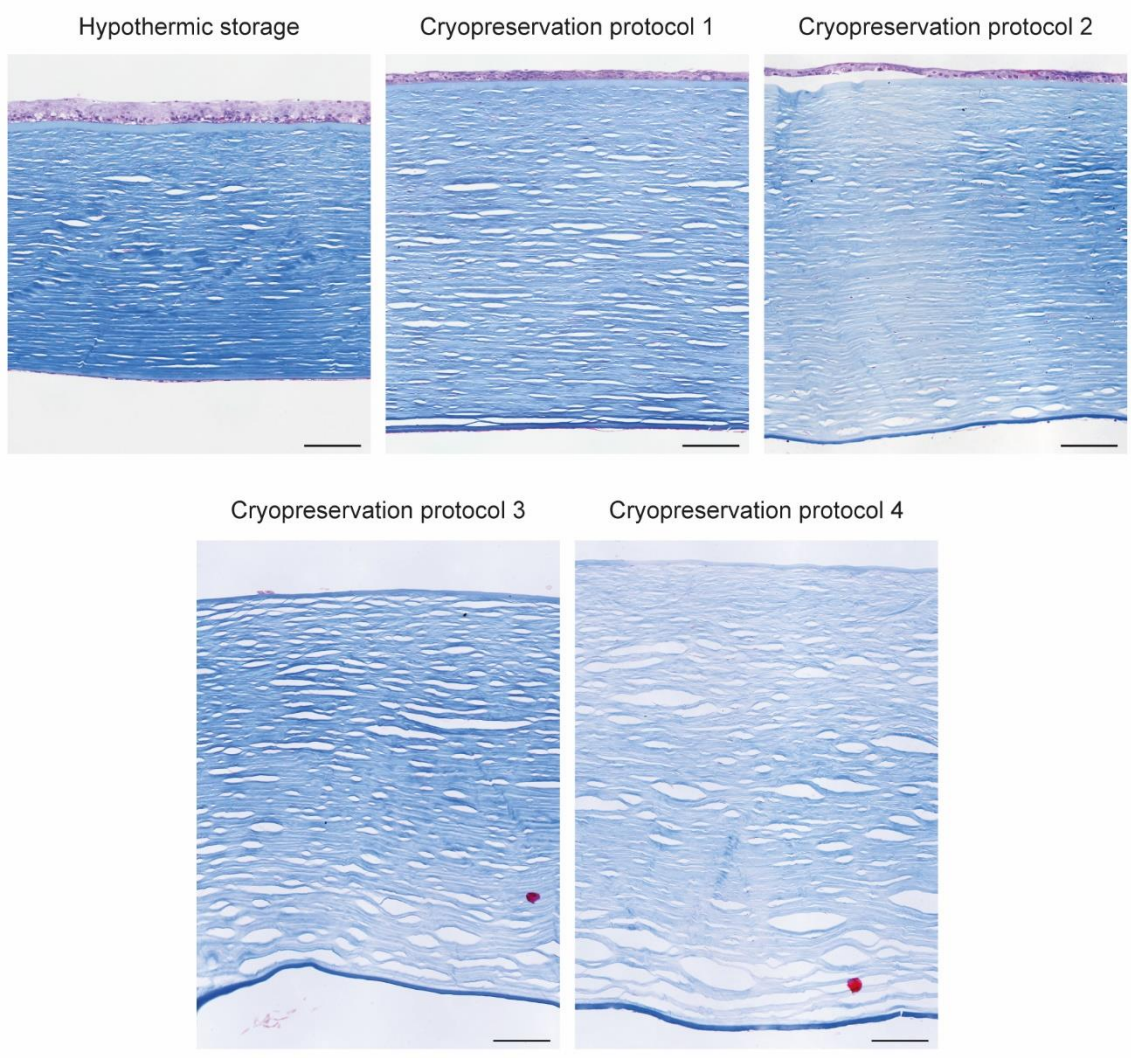

***Figure 20**. Transversal sections of hypothermic stored and cryopreserved corneas stained with Masson's trichrome. Scale bar: 100 μm.*

The thickness of all cryopreserved corneas was greater than that of the hypothermic stored cornea, which had a mean stromal thickness value of 452.5 μm. P1-cryopreserved cornea was the thinnest (616.8 μm), followed by P2-cryopreserevd cornea (617.2 μm) and P3-cryopreserved cornea (695.6 μm). P4-cryopreserved cornea was the thickest, with a mean stromal thickness of 807.3 μm.

With respect to stroma, collagen bundles were undulating in the posterior (epithelial) stroma of hypothermic stored cornea and of P1-, P2- and P3-cryopreserved corneas and were straighter in the middle and anterior (endothelial) stroma (**Figure 20**). In P4-cryopreserved cornea, the arrangement of parallel anterior collagen bundles could not be adequately visualized, but the arrangement of middle and posterior collagen bundles was similar to those of other cryopreserved corneas.

All cryopreserved corneas showed unstained areas of various sizes among the stromal collagen lamellae bundles, which were more noticeable in P2-, P3-, and P4-cryopreserved corneas and larger in the posterior stroma. In P1-cryopreserved corneas, keratocyte debris was observed attached to the sides of some unstained area perimeters. In P2-cryopreserved corneas, keratocytes were more abundant, with perceptibly shrunken nuclei. In P3- and P4-cryopreserved corneas, the presence of keratocytes or keratocyte debris was anecdotal.

Observing the epithelium in detail (**Figure 21**), while the epithelium of hypothermic stored cornea maintained its integrity, the epithelium of P1-cryopreserved cornea had an irregular surface, with two to three differentiated cell layers in the central portion of the cornea. Epithelial cells were small, flat, and deformed, creating an irregular and desquamated epithelium with a serrated appearance in one end and a smoother appearance at the other end. The epithelial surface of P2-cryopreserved cornea was smooth and slightly desquamated. Two to four layers of flat epithelial cells were retained throughout the epithelium, which was detached from the Bowman's layer at some points. Epithelial cells were flat and small. In P3- and P4-cryopreserved corneas, epithelium was lost in the central portion of the corneas but remained present at the corneal periphery. The epithelium showed two to five layers of small and flat cells, with a desquamated but smooth appearance on the surface.

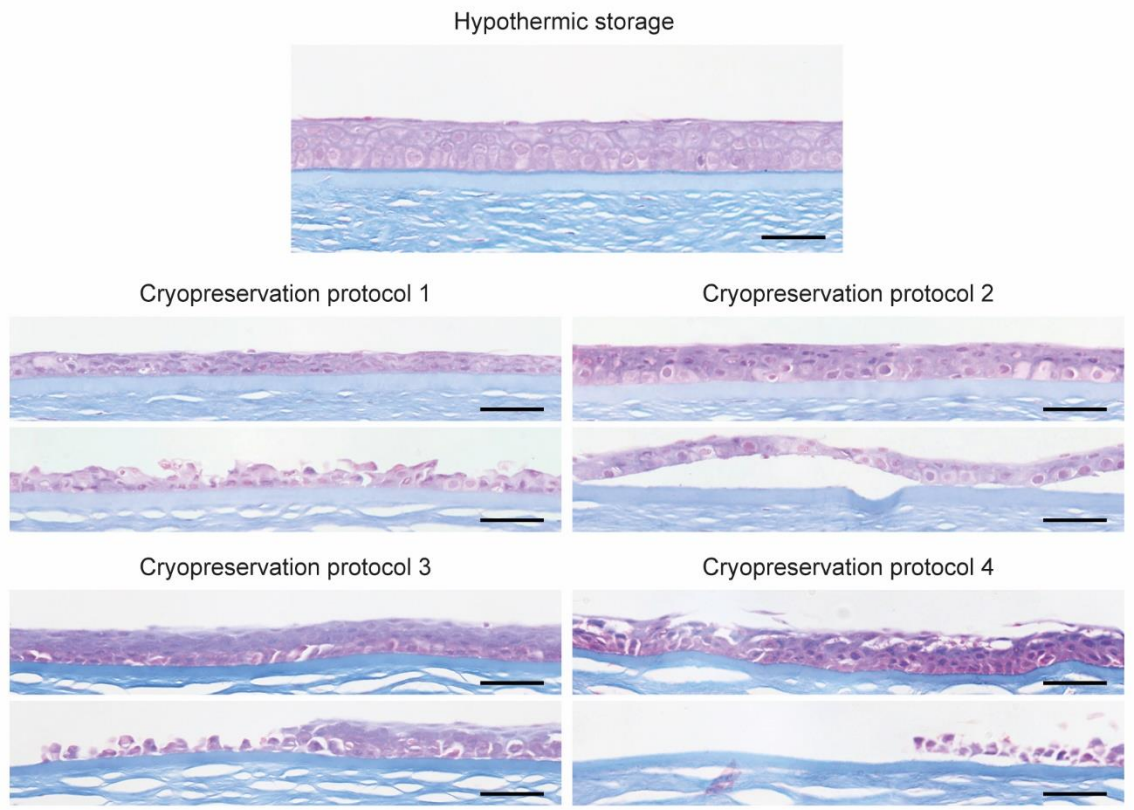

***Figure 21**. Images of cryopreserved corneal epithelia and hypothermic stored corneal epithelium stained with Masson's trichrome. Scale bar: 50 µm.*

Endothelium integrity was disrupted, and cells were irregularly shaped in all the cryopreserved corneas (**Figure 22**). Conversely, the endothelium was preserved in the hypothermic stored cornea. In P1-cryopreserved corneas, cytoplasm in ECs was attached to the DM, and very few nuclei were observed. In P2-cryopreserved corneas, continuous endothelium integrity was better preserved, although ECs were detached from the DM at some points. In P3- and P4-cryopreserved corneas, endothelium was widely detached from the DM, except for cell debris and some ECs with identifiable cytoplasm and nuclei.

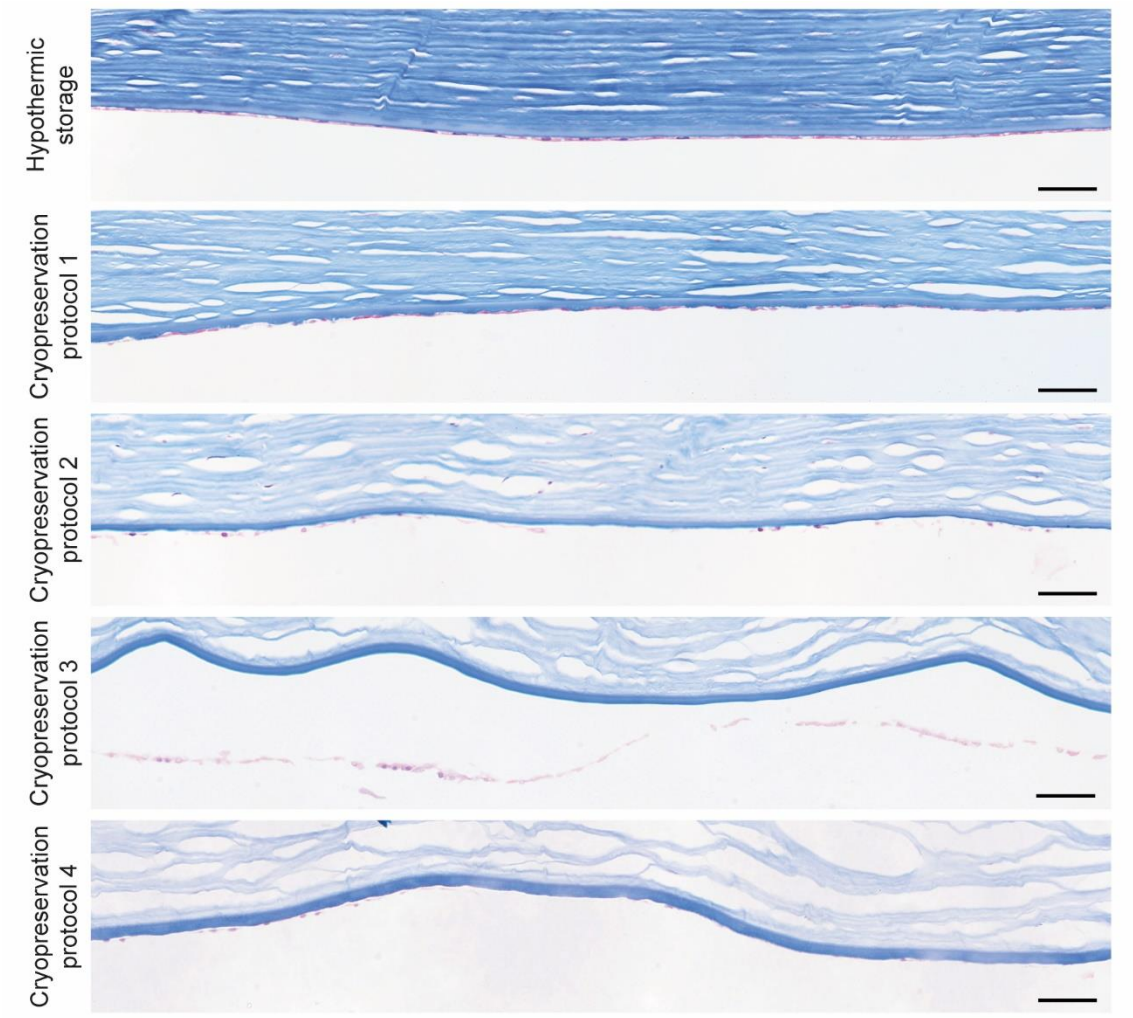

***Figure 22**. Transversal sections of a hypothermic stored cornea and of the P1-, P2-, P3-, and P4-cryopreserved corneas stained with Masson's trichrome. Scale bar: 50 µm.*

1.2. Endothelial cells viability and endothelial integrity

For the calcein-AM assay, endothelium-DM complexes were successfully peeled off from all the corneas. The unrolling and unfolding of the complexes on microscope slides were not damage-free and were accompanied with accidental sample tearing, partial loss, and tissue folding. One of the endothelium-DM complexes of P3-cryopreserved corneas was lost during the process. Thus, the evaluation of the whole complex was discarded. Photographs of unfolded areas were taken (**Figure 23**).

Loss of endothelium integrity was observed in all cryopreserved corneas. Decellularized areas were visualized on the DM using Hoechst counterstaining, which showed small, irregularly shaped non-fluorescent areas or striations. P3- and P4-cryopreserved corneas showed greater homogeneous areas of DM-adhered ECs, indicating a high degree of cellularity.

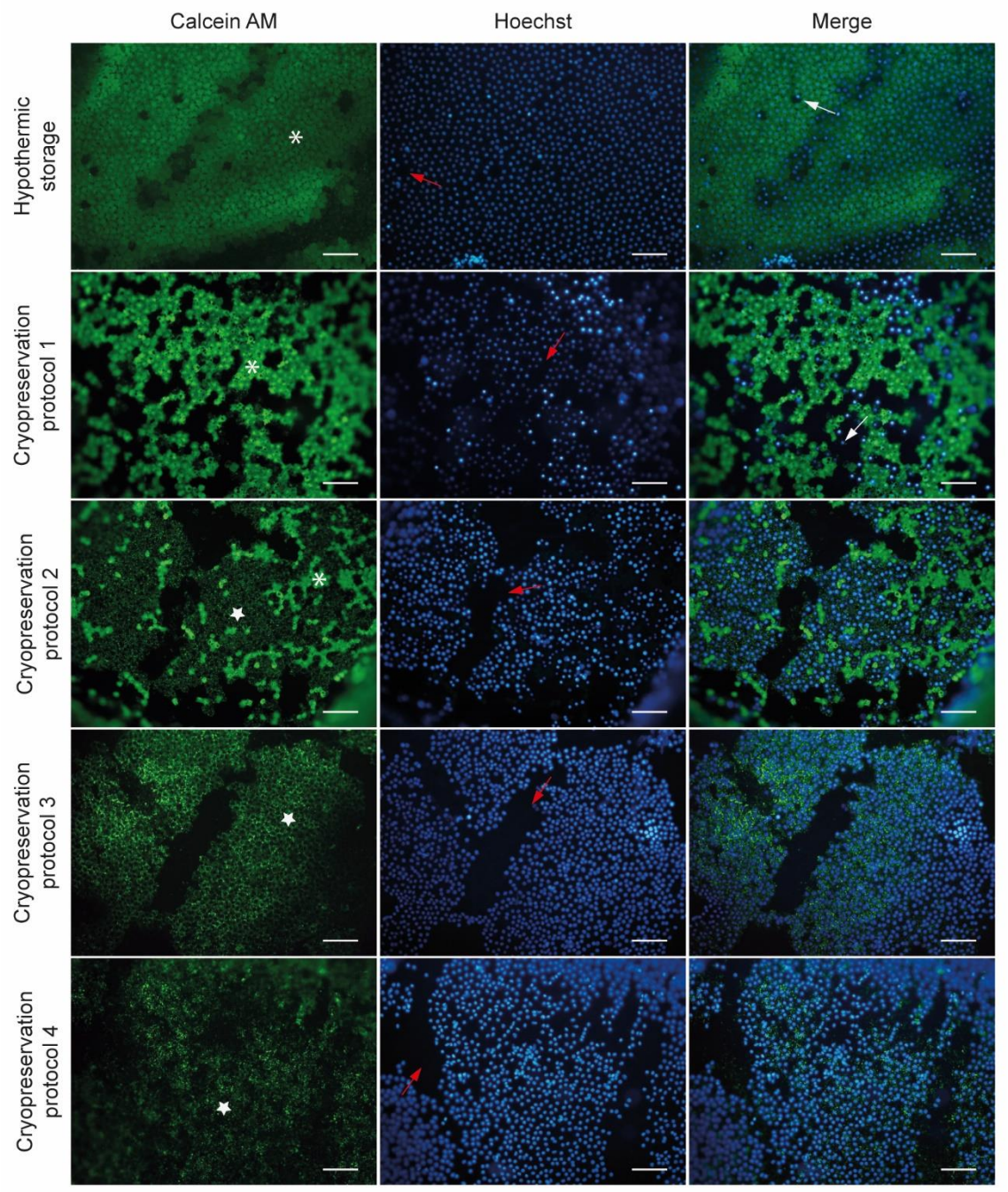

***Figure 23**. Endothelium-DM complex stained with Calcein AM (green) and Hoechst (blue) from a hypothermic store cornea (control), and from cryopreserved corneas using protocols P1, P2, P3, and P4. White asterisk: endothelial cells (ECs) with homogeneous green cytoplasm from the fluorescent signal of the accumulated calcein AM; white star: ECs with a green doted cytoplasm; white arrow: ECs without fluorescent calcein AM signal; red arrow: decellularized areas without signals on the Descemet's membrane, forming small areas or large striations. Scale bar: 100 µm.*

The calcein-AM signal was observed mostly in DM-adhered ECs from P1-cryopreserved corneas and, to a lesser extent, in DM-adhered ECs from P2-cryopreserved corneas. The fluorescent calcein-AM signal was visualized as green dots in DM-adhered ECs of P2-, P3-, and P4-cryopreserved corneas. Some cells without any calcein-AM signal were observed in the endothelium-DM complex of P1-cryopreserved corneas.

After applying Masson's trichrome staining and observing EC viability, protocol 1 was selected to study the cryopreservation protocol parameters, as the resulting cryopreserved cornea showed the lowest stromal thickness and the highest proportion of ECs with enzymatic activity and intact cell membranes. To confirm the endothelial status observed by the calcein-AM assay and to further observe small distortions in stromal collagen arrangement at an ultrastructure level, trypan blue-alizarin red staining was performed on endothelium, and the stroma was analyzed by transmission electron microscopy.

1.3. Variations in endothelial integrity following cryopreservation protocol 1

Ten warmed and washed P1-cryopreserved corneas with a mean ECD of 2216 ± 306 cells/mm^2 were stained with alizarin red and trypan blue to visualize the integrity of the endothelium in the cornea. One cornea was discarded due to the absence of the endothelium and DM in approximately 75% of the cornea.

While the hypothermic stored cornea showed a complete and homogeneous endothelium (**Figure 24**, A; **Figure 25**, A), decellularized DM areas of variable sizes were observed mainly in the periphery of all cryopreserved corneas. Five of the nine cryopreserved corneas also showed a denuded region in the central portion of their endothelium (**Figure 24**, B,C,D; **Figure 25**, B,C,D).

In many areas, red artifacts were deposited on the endothelium surface, which prevented the observation of the cells immediately below them. Those artifacts were more numerous in corneas with decellularized DM areas, despite preemptive washing with PBS to remove artifacts before alizarin red staining (**Figure 25**). Folds were also perceptible in all corneas, as red artifacts frequently accumulated on them (**Figure 24**).

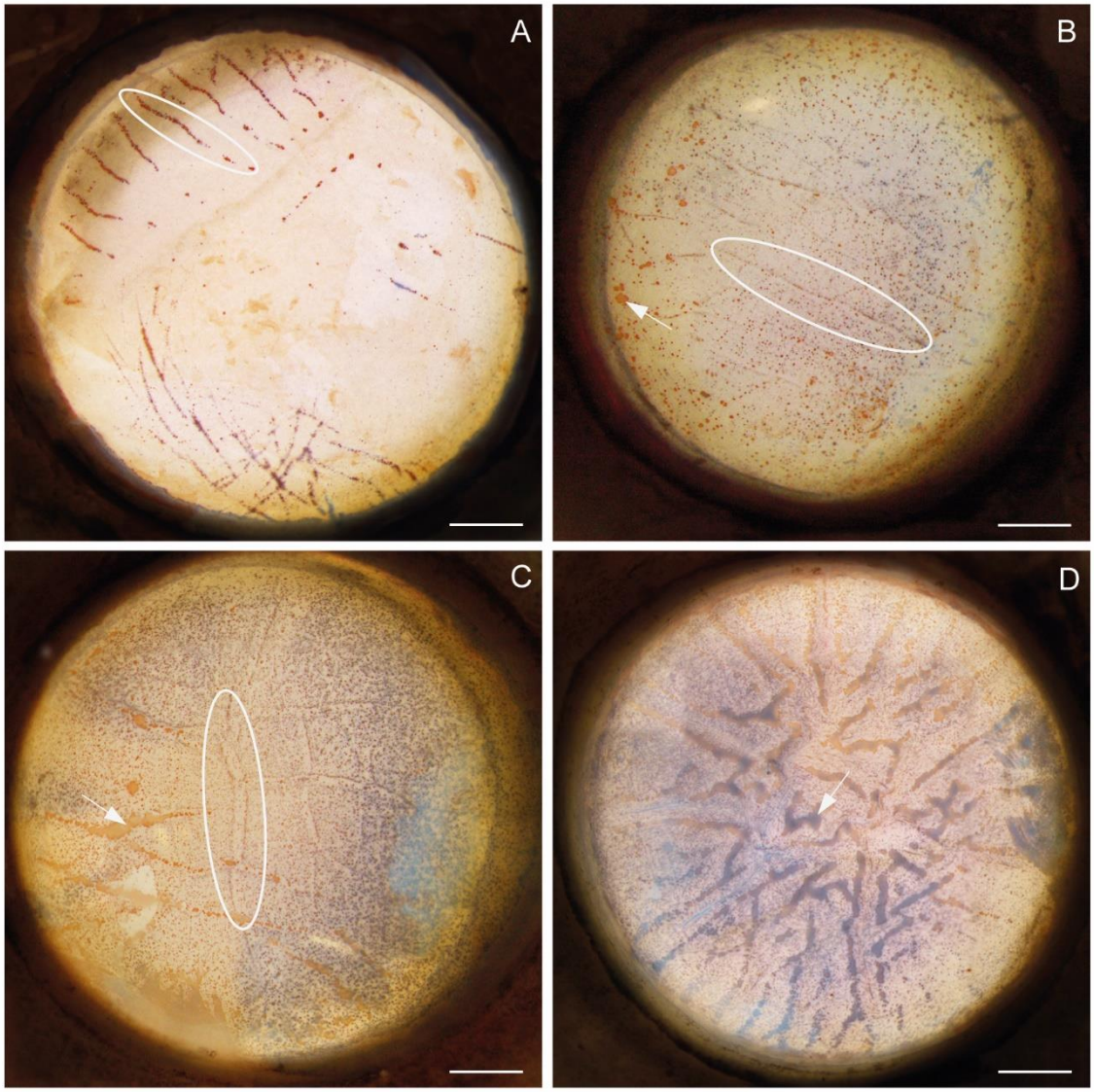

***Figure 24**. Images of endothelia stained with trypan blue and alizarin red on a hypothermic stored cornea (A) and on three P1-cryopreserved corneas (B-D). White arrows: decellularized areas; white ovals: folds. Scale bar: 1 mm.*

Accumulation of cells with blue nuclei, which indicated damage to EC membranes, were observed in all cryopreserved corneas (**Figure 25**, B-F), but in lower numbers and in a single disposition at the center of four cryopreserved corneas (**Figure 25**, E, F). Damaged cells were also found at the periphery of the denuded DM areas (**Figure 25**, D), creating striae in folds where there were accumulations of red artifacts (**Figure 25**, B,C,E), or randomly disposed groups at the periphery and in the central region of the endothelium (**Figure 25**, E). In the hypothermic stored cornea, damaged cells were not observed (**Figure 25**, A).

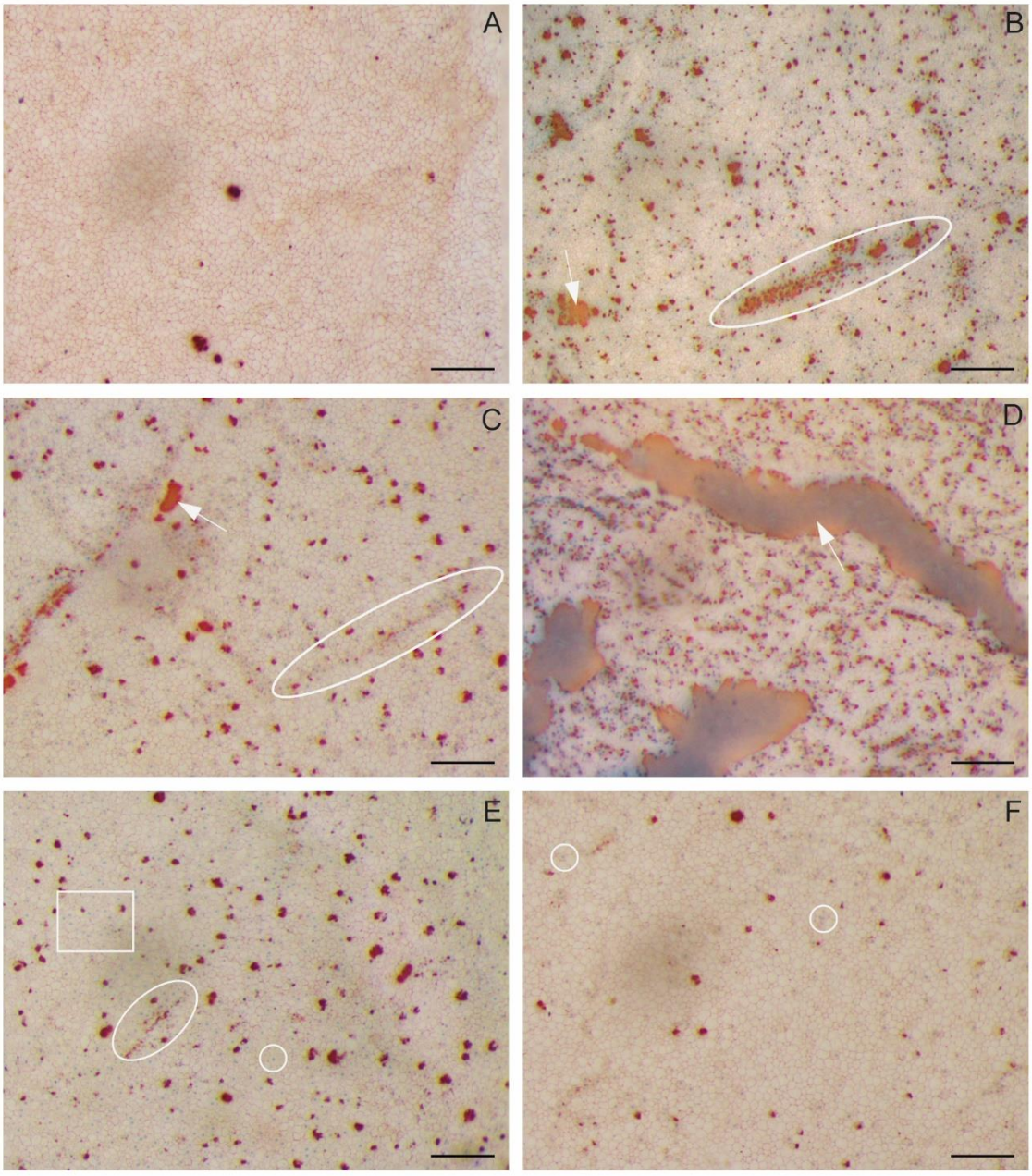

***Figure* 25**. *Details of a hypothermic stored corneal endothelium (A) and P1-cryopreserved corneal endothelia (B-F) stained with trypan blue and alizarin red. White arrow: denuded Descemet's membrane areas stained in red; white oval: cells with blue nuclei creating lines; white square: cells with blue nuclei creating groups; white round: single cells with blue nuclei. Scale bar: 200 µm.*

ECD after cryopreservation, and the percentage of damaged ECs compared to the ECD before cryopreservation were calculated using images where visible adhered cells, with and without damage, could be counted (**Annex IV**). Image regions portraying only denuded areas and regions with red artifacts were omitted in the analysis. Final ECDs and percentage of ECD loss for each cornea are shown in **Table 4**. The percentage of ECD loss ranged from -1 ± 9% to 41 ± 12%, and when the ECDs for the different samples were combined, the ECD difference before and after cryopreservation was significant (p value < 0.05). However, there was no correlation between ECD in the two groups before and after cryopreservation, i.e., ECD loss was highly variable and did not follow any trend.

***Table 4**. Endothelial cell density (ECD) before and after cryopreservation measured using the trypan blue and alizarin red staining. Calculations were performed using only the adhered cells with and without membrane damage.*

		After cryopreservation	
Cornea code	**Previous ECD (cells/mm²)**	**ECD (cells/mm²)**	**ECD loss (%)**
Cryo1	2342	1379 ± 277	41 ± 12
Cryo2	2326	1965 ± 200	16 ± 9
Cryo3	2618	1585 ± 145	39 ± 6
Cryo4	1992	1682 ± 189	16 ± 9
Cryo5	1894	1921 ± 166	-1 ± 9
Cryo6	2217	1710 ± 169	23 ± 8
Cryo7	2488	2053 ± 168	17 ± 7
Cryo8	2451	2327 ± 86	5 ± 4
Cryo9	1608	1521 ± 145	5 ± 9

1.4. Collagen fiber integrity in corneas cryopreserved with protocol 1

TEM images of the posterior stroma of the hypothermic stored (**Figure 26**, A,B) and cryopreserved corneas (**Figure 26**, C,D) showed similar collagen bundles arrangements. Cryopreserved corneas did not show any visible collagen fibers disruption. The average distance between transversal collagen fibers of the posterior stroma in two P1-cryopreserved corneas were 27.1 ± 7.9 nm and 23.2 ± 7.7 nm, which was significantly higher than interfibrillar distance in the hypothermic stored cornea (19.4 ± 6.1 nm; p

value < 0.05 for both cryopreserved corneas). Some keratocytes in P1-cryopreserved corneas showed an extremely dehydrated morphology, as is perceptible in **Figure 26**, C.

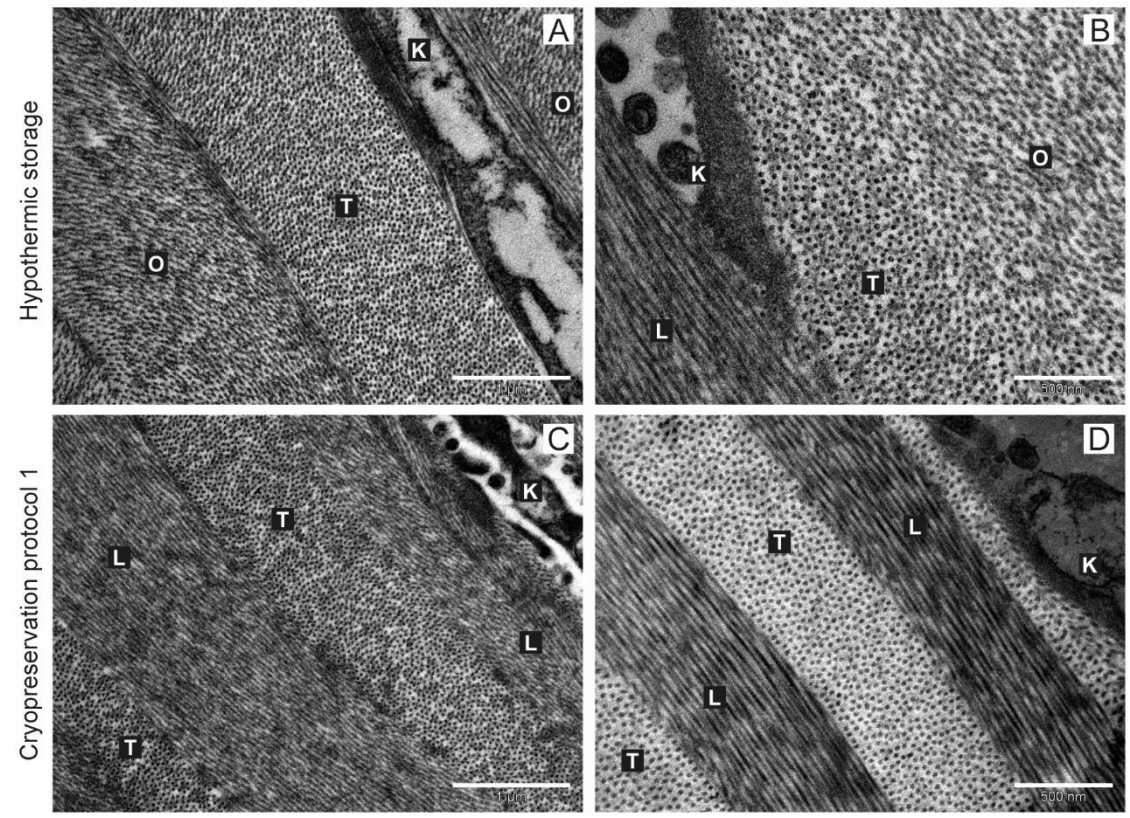

***Figure 26**. Transmission electron microscopy of the posterior stroma of a hypothermic stored cornea (A-B) and of cryopreserved corneas (C-D). Collagen fibers were transversally (T), longitudinally (L), and obliquely (O) sectioned to the cut plane. Keratocytes (K) laid between layers. Scale bar of A and C: 1 µm. Scale bar of B and D: 500 nm.*

1.5. Determination of cryopreservation parameters of protocol 1

Osmolalities in CS1.1, CS1.2, and CS1.3 were 639.0 ± 1.5 mOsm/kg, 1026.7 ± 4.2 mOsm/kg, and 1647.0 ± 7.2 mOsm/kg, respectively. The osmolality of wash solution Human Albumin Grifols® 200 g/L was 274.0 ± 1.0 mOsm/kg, a significantly lower value than that of CS1.3 (p value < 0.05) (**Figure 27**). The pH of all solutions remained at a physiological level of 7.3 (21 °C).

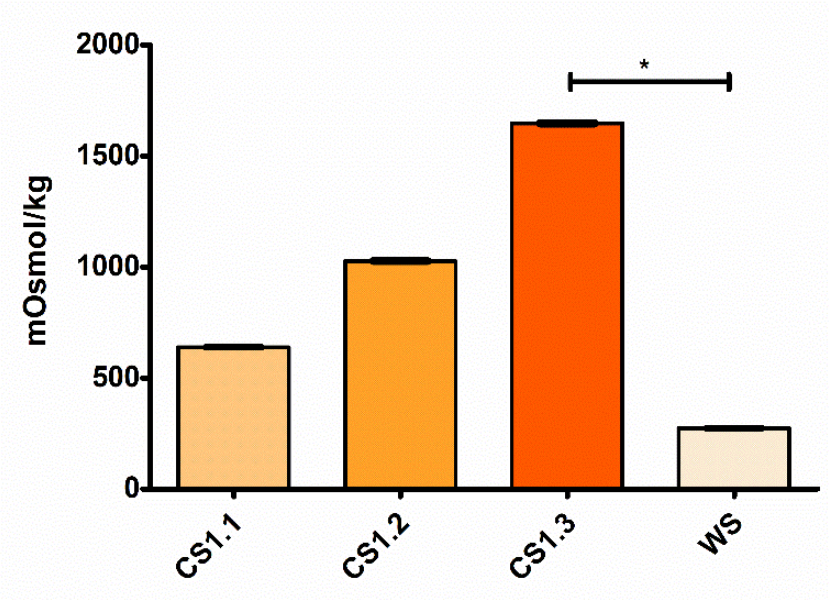

***Figure 27**. Osmolalities of the three protocol 1 cryoprotectant solutions (CSs) and the Human Albumin Grifols® 200 g/L used as wash solution (WS). *: Dunn's post-test p-value ≤ 0.05.*

Samples were frozen using a biological freezer. Sample cooling rates and final temperatures reached at the end of each segment were calculated (**Annex V**) and are plotted in **Figure 28**. Briefly, cooled corneal samples, previously equilibrated in ice with CS1.3 and at an initial temperature of 4.9 °C, were cooled down to 4.2 °C in 15 min. Then, using shock cooling, ice nucleation was forced, with the consequent release of latent heat, raising the sample temperature from −7.9 °C to −2.7 °C in 33 seconds. The equilibrium freezing temperature was reached at this point, forming a plateau between -2.6 °C and -2.7 °C that was maintained for 1 min 10 s (**Figure 29**). This was followed by a slow decrease in temperature (**Figure 29**). The cooling rate of the sample was then programmed to increase progressively from –1.09 °C/min when the sample temperature was at −6 °C to −3.80 °C/min when the sample reached −78 °C.

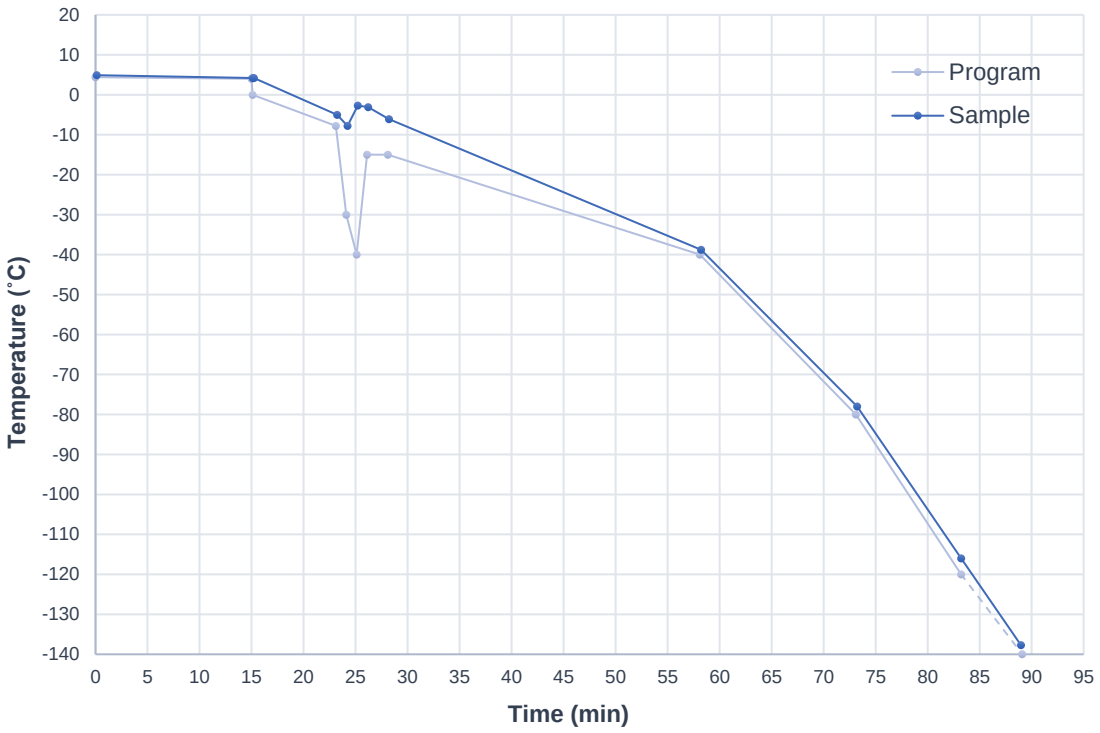

***Figure 28**. Sample cooling rate and programmed cooling rate for the P1-cryopreserved corneas. Each point represents the temperature at the end of a programmed segment. Although the last segment of the programed cooling rate is supposed to finish at -120 °C, the temperature continues to decrease (striped light blue line) until the sample is removed from the biological freezer.*

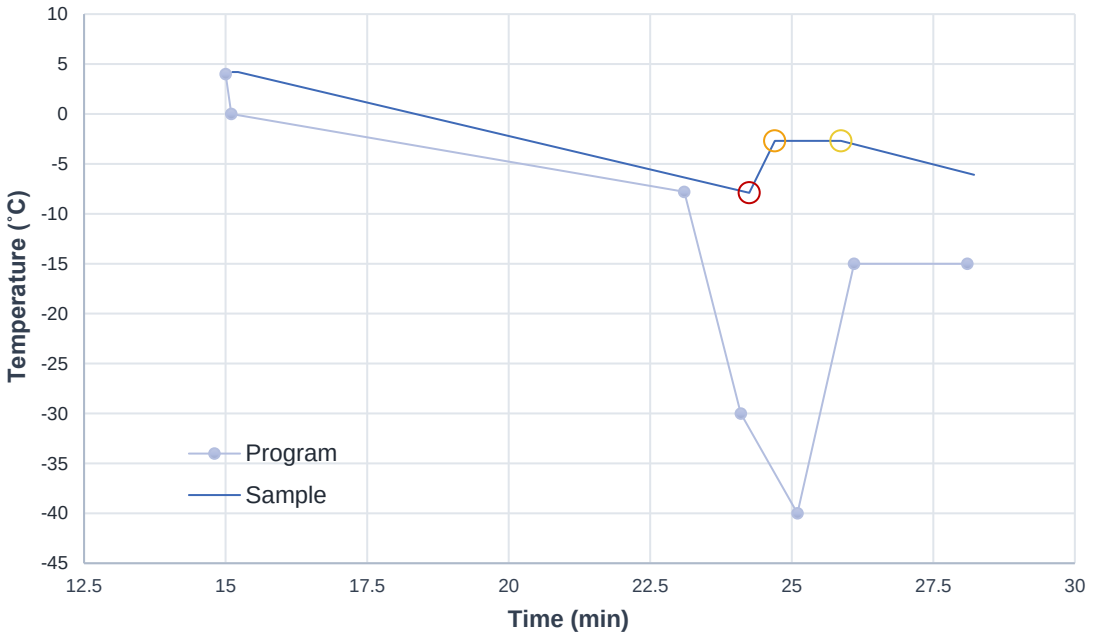

***Figure 29**. Details of the controlled ice nucleation in the P1-corneal samples using a programmed shock cooling. In red, the point where the ice nucleation begins. In orange, the melting temperature of the CS with the sample. In yellow, the point where the sample temperature starts decreasing again. Blue points represent the final temperature at the end of each cooling programed segment.*

The DMSO concentration in unwashed samples was 0.83 ± 0.08 M. A decrease in DMSO concentration was observed after the first (0.31 ± 0.05 M), second (0.14 ± 0.01 M), and third wash (0.10 ± 0.02 M) (**Figure 30**). The difference in DMSO concentration between the third wash and the initial unwashed condition was statistically significant (p value < 0.05).

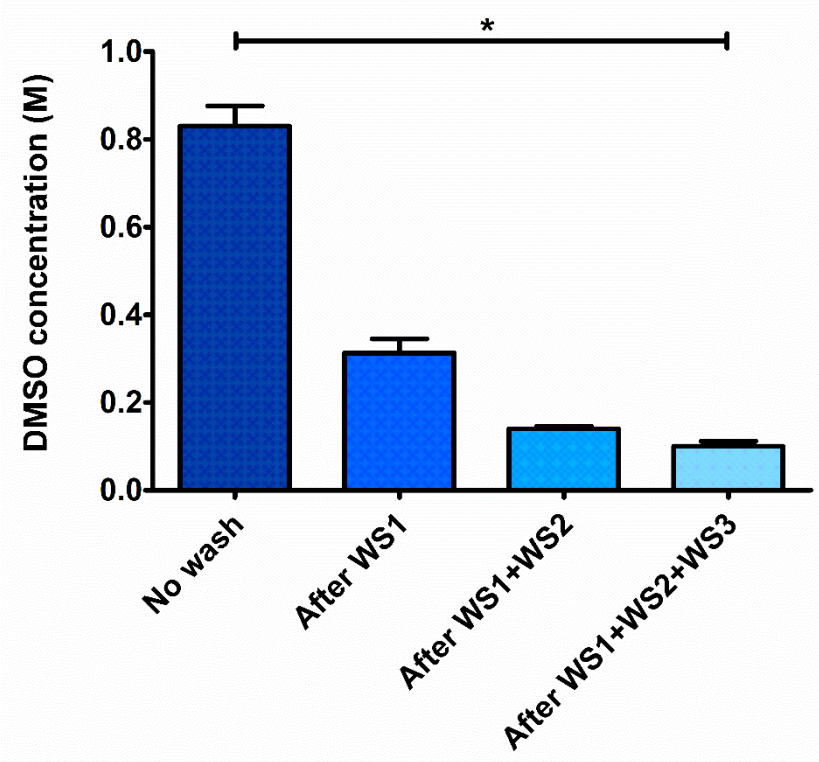

***Figure 30**. Dimethyl sulfoxide (DMSO) tissue concentration during the cryoprotectant agents' removal step of the protocol 1. *: Dunne's post-test p-value ≤ 0.05. M: molarity; WSn: wash solution 1, 2, 3.*

2. Penetrating keratoplasty *in vitro*

The female X cornea and the male Y cornea were successfully transplanted to each other. The X cornea was slightly decentered at the moment of trephination.

During the first three weeks, several changes were observed in the PK models (**Figure 31**). First, the grafted corneal bottom, which at day 0 was transparent, showed a gradual opacification of its stroma, registered at day 7 in the X^Y model and at day 14 in the Y^X model. Then, de-epithelialization was registered at day 14 in the X^Y model and at day 21 in the Y^X model. The latter state was maintained until removal of the model from culture.

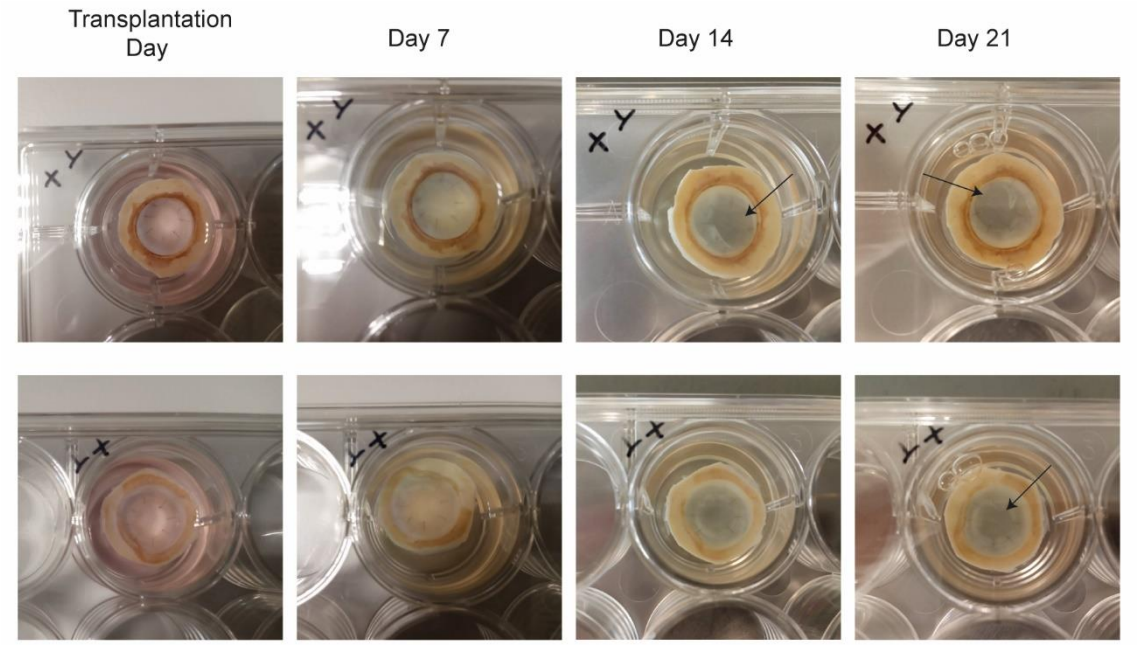

***Figure 31**. X^Y and Y^X PK models' state changes during the first three weeks. The depithelializated area is signaled with an arrow.*

2.1. Identification of graft and receptor endothelium with cell tracers and protein cell analysis

After 4 weeks, the X^Y model was removed from culture. While cutting the sample into 8 pieces, it was observed that the X graft was partially detached from the receptor Y cornea.

Following immunofluorescence analysis on whole pieces, no signal of any of the cell tracers DiO or Dil was observed within the tissues, and no signal of ZO-1, N-cadherin, Ki-67, or p27 was observed in the cells. Phalloidin stained actin in fibroblast-like cells (keratocytes), but there was no presence of hexagonal-like cells (ECs) (**Figure 32**).

In light of the resulting absence of cell tracer, subsequent immunofluorescence assays using whole pieces were discarded, and later immunofluorescence assays were instead performed on cryosections from an OCT-embedded piece of the Y^X model cultured for 9 weeks. Hoechst staining on those sections confirmed that the endothelium, except for an anecdotal number of nuclei, was not conserved during the process (**Figure 33**). Due to the absence of endothelium, immunofluorescence experiments using OCT sections of the Y^X model with ZO-1, N-cadherin, p27, and Ki-67 antibodies were not carried out.

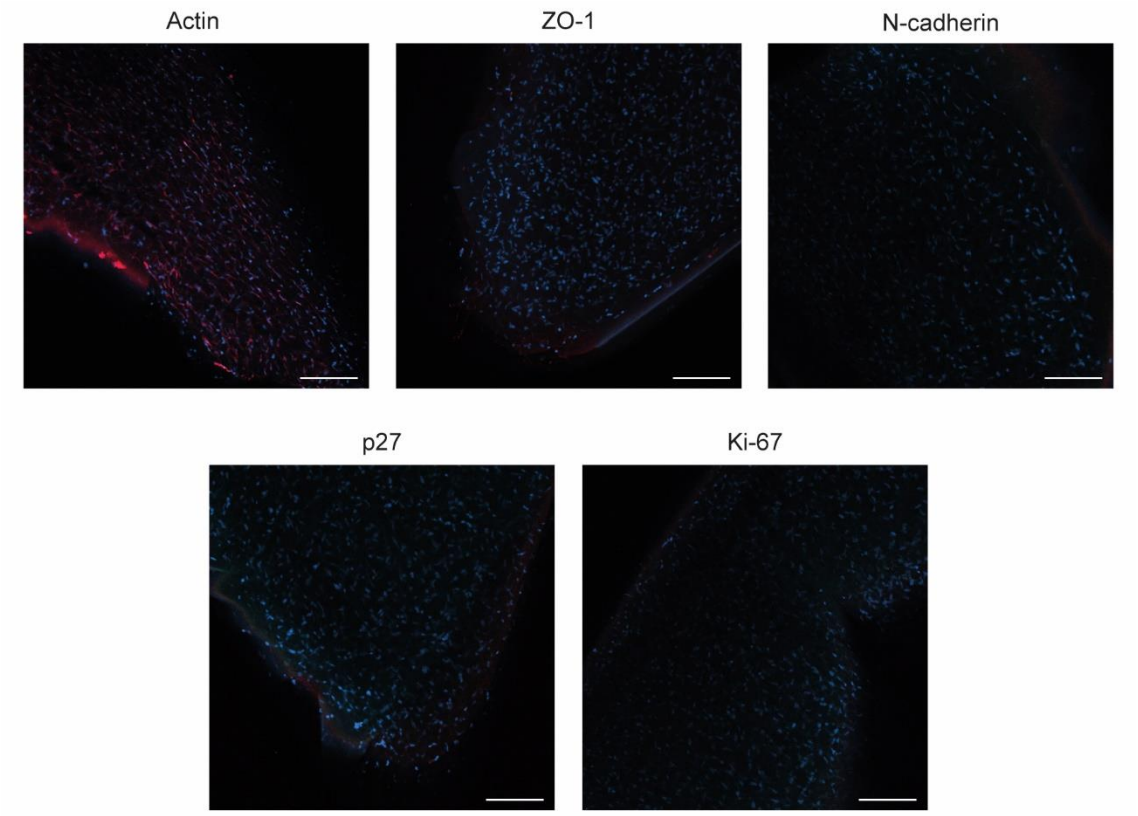

Figure 32. *Merged immunofluorescence images of the X^Y model. Microphotographs were obtained using the corresponding laser to excite phalloidin (red) and the secondary antibody (red), Dil (orange), DiO (green) and Hoechst (blue). ZO-1: zonula occludens 1. Scale bar: 200 μm.*

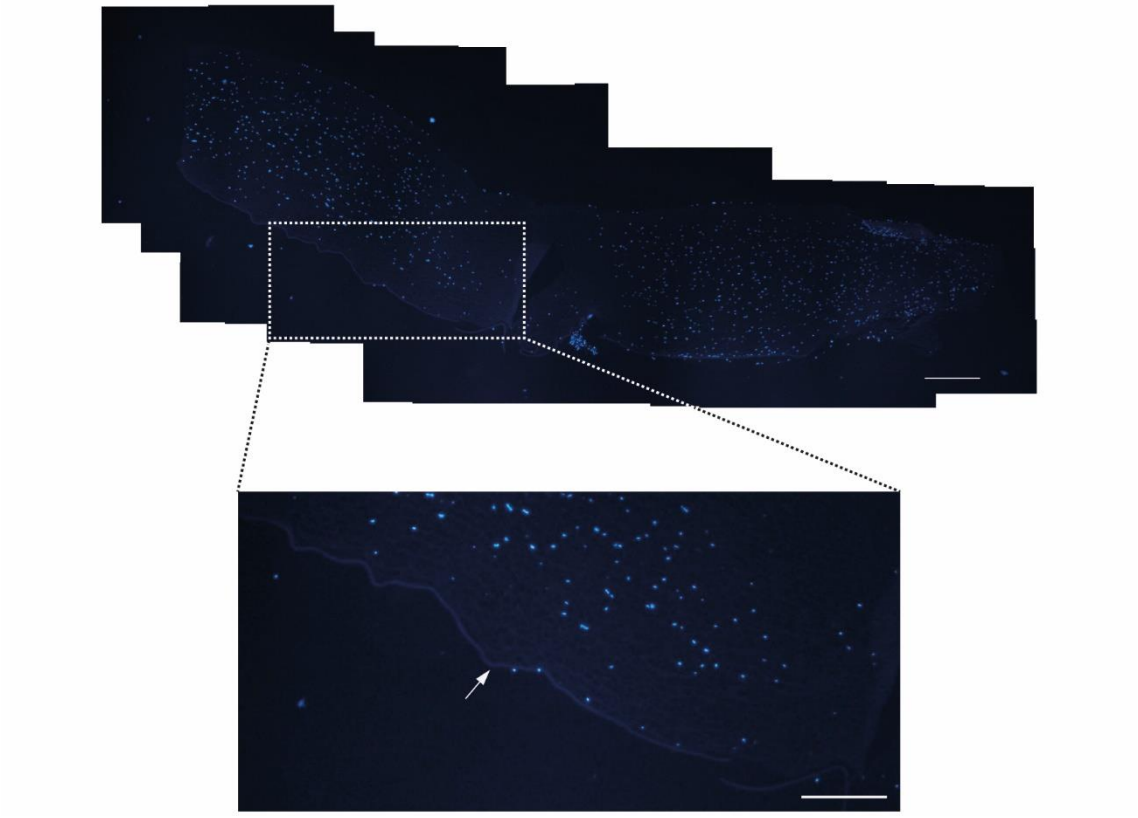

Figure 33. *Hoechst nuclei staining of a Y^X paraffined section (scale bar: 500 μm) and a higher magnification of the posterior stroma where the DM (white arrow) is denuded. Scale bar: 300 μm.*

2.2. Identification of receptor corneal tissue and graft corneal tissue with fluorescence *in situ* hybridization

None of the paraffin-embedded sections from the X^Y and Y^X models showed any endothelium. Nonetheless, FISH was performed to test whether the receptor and host tissues could be identified by using X and Y chromosome probes.

The clinical FISH protocol allowed for the visualization of bright probes (**Figure 34**). However, this protocol did not maintain tissue structure, which was largely disrupted, folded, and/or detached from the slide. As a result, regions of tissues were unidentifiable. In the X^Y model, the X probe signal and the Y probe signal were observed in the same nuclei, with single Y or X signal in some cells. In the Y^X model, only the X probe signal was observed in the same nuclei, with single X signal in some cells.

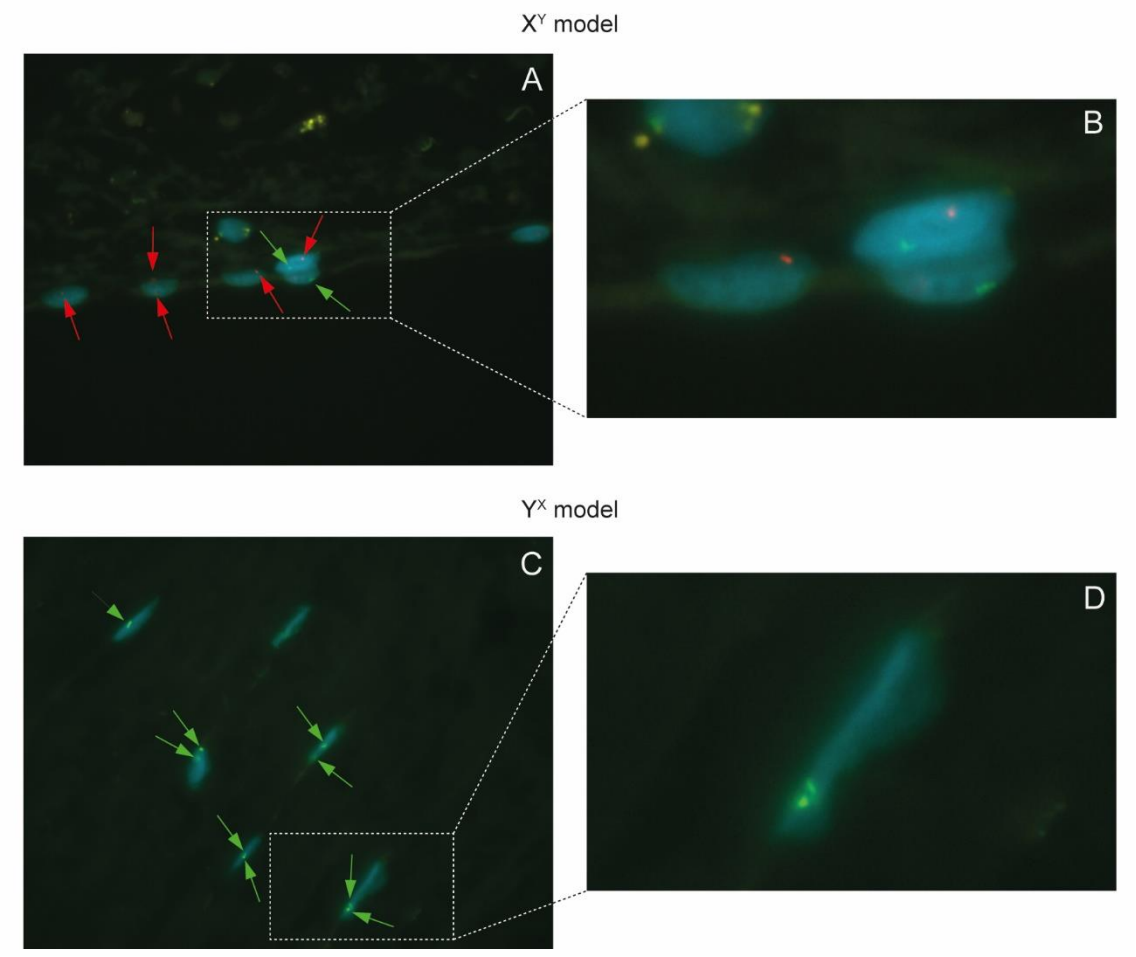

***Figure 34**. Fluorescence in situ hybridization of X^Y (A,B) and Y^X (C,D) model with a 30-min heat pretreatment in a Coplin jar and a 20-min enzymatic treatment. The nuclei detail of B and D was manually zoomed in. In blue, cell nuclei with X probes (green dot, green arrow) and Y probes (red dot; red arrow) hybridization. Magnification: 1000X.*

The FISH protocol included a pretreatment step at 98 °C in a Coplin jar. When this step was omitted, the tissues remained undamaged. To evaluate whether a shorter incubation period at such temperature could reduce tissue disintegration, experiments were performed with increasingly longer incubation periods of 5, 10, and 15 minutes (**Figure 35**). Tissue damage was more extensive in Y^X model sections where tissues were detached, torn, and folded onto themselves. The iris, trabecular meshwork, and sclera remained adhered on the slides. In X^Y sections, the iris, trabecular meshwork, Schlemm's canal, and sclera remained identifiable. However, corneal tissue was markedly damaged. Changing the duration of the incubation period of the heat pretreatment had no impact on the damage observed within each section.

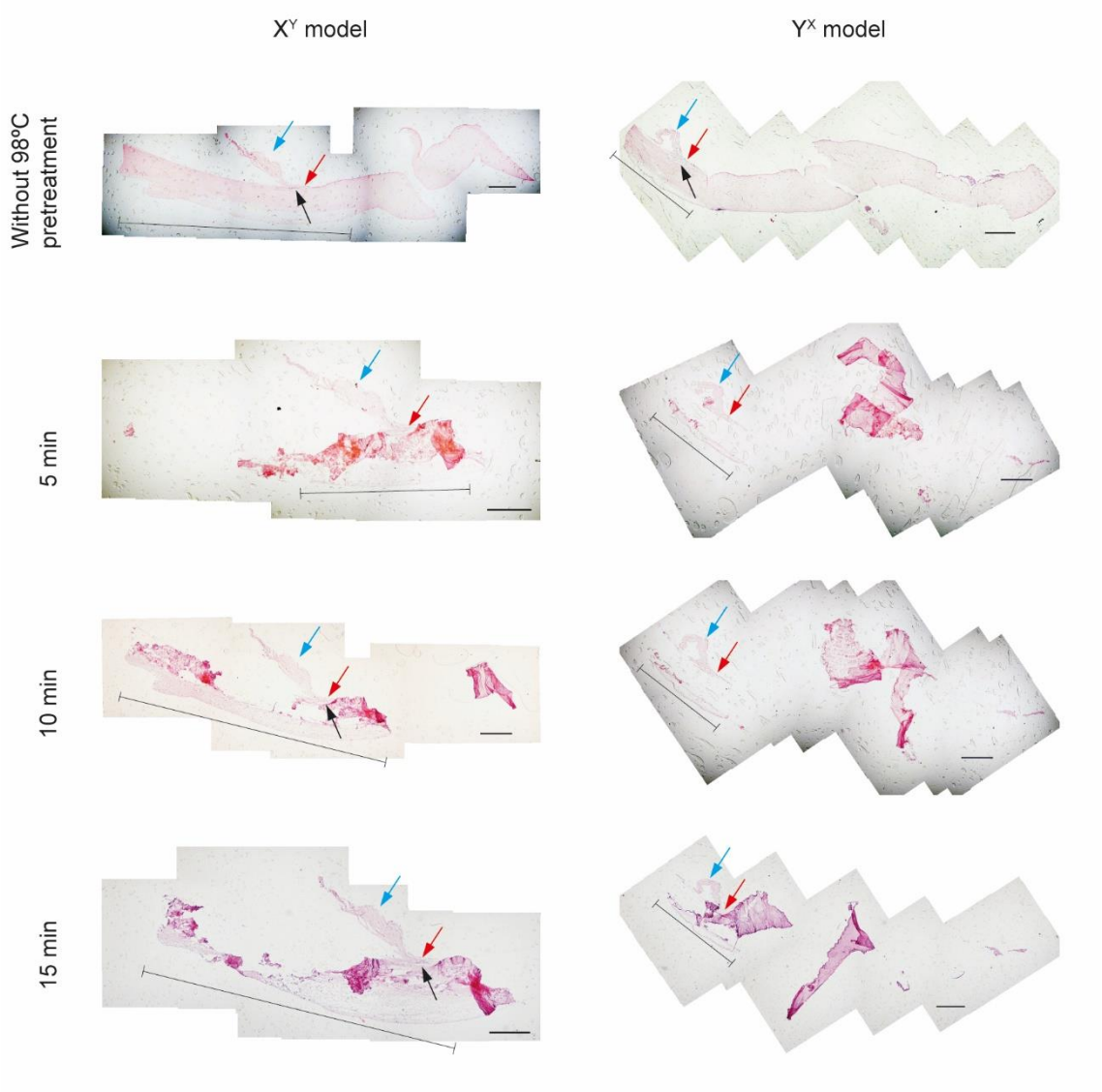

***Figure 35**. Transversal sections of X^Y and Y^X model stained with hematoxylin-eosin after different heat pretreatments times. Red arrow: trabecular meshwork; blue arrow: iris; Black arrow: Schelemm's canal; segment: sclera. Scale bar: 500 μm.*

An enzymatic treatment was consequently applied without disruptive pretreatment incubation at 98 °C (**Figure 36**). This allowed visualizing the probes in the X^Y model at a lower probe signal but on a recognizable iris, trabecular meshwork, sclera, and cornea. The Y and X signals were detected together in the nuclei. As for the Y^X model, tissue was lost following its detachment from the slide at the moment of lifting the coverslip slide after hybridization.

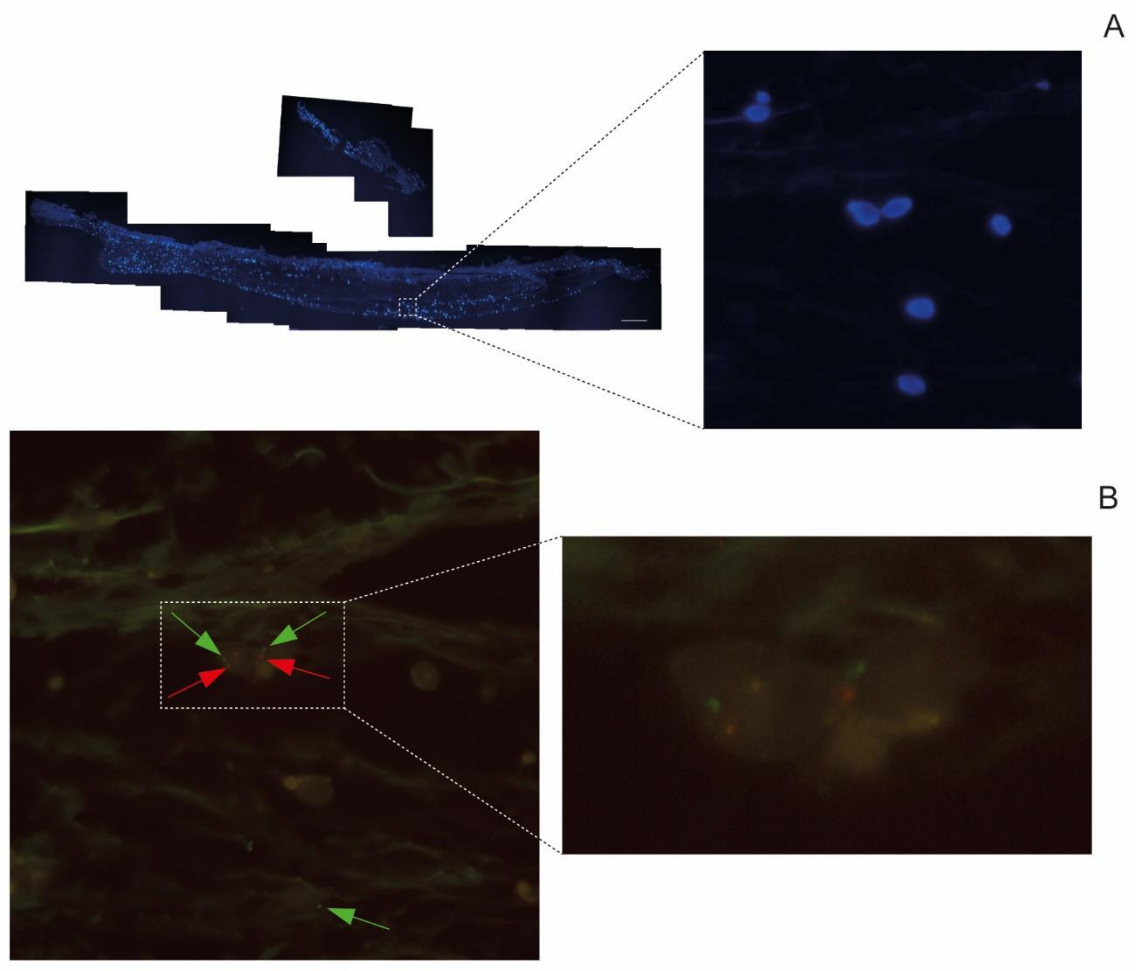

***Figure 36**. Fluorescence in situ hybridization (FISH) analysis of the X^Y model with a 20-min enzymatic treatment and no heat pretreatment. A) Complete section of the tissue following a FISH treatment with the nuclei counterstained in blue using Hoechst (left; scale bar: 200 µm), with a higher resolution of the analyzed nuclei (right; magnification: 1000X). B) Photographed area showing the X probe (green dot, green arrow), and the Y probe (red dot; red arrow) hybridization (magnification: 1000X). The nuclei detail with the X and Y probes at left was manually zoomed in.*

The combination of 10-min pretreatment at 90 °C in the hybridizer with enzymatic treatment resulted in brighter X and Y probe signals compared to when pretreatment was omitted (**Figure 37**). However, it also caused a disruption of the tissue where only the iris, the trabecular meshwork, and the sclera remained attached to the slide.

The Y^X model section was mostly detached from the slide in the last two experiments at the moment of lifting the coverslip slide following the hybridization step.

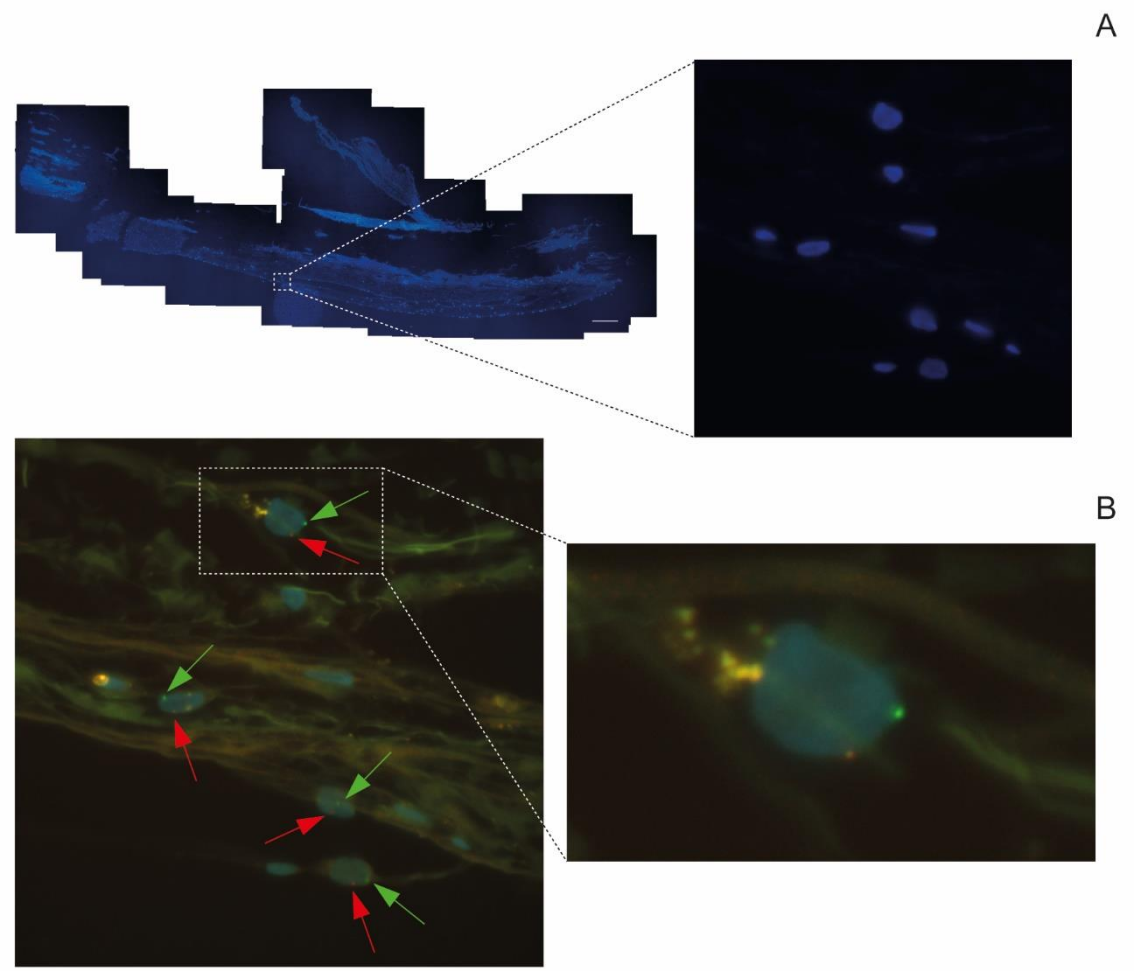

***Figure 37**. Fluorescence in situ hybridization (FISH) analysis of the X^Y model with a 10-min heat pretreatment in the hybridizer and a 20-min enzymatic treatment. A) Complete section of the tissue after FISH treatment with the nuclei counterstained in blue using Hoechst (left; scale bar: 200 μm), with a higher resolution of the analyzed nuclei (right; magnification: 1000X) B) Photographed area showing the X probe (green dot, green arrow), and the Y probe (red dot; red arrow) hybridization (magnification 1000X). The nuclei detail with the X and Y probes at left was manually zoomed in.*

IV. Results:

Objective 2

1. Tissue engineered – endothelial keratoplasty grafts construction

Decellularization of the Descemet's membrane was carried out by subjecting a cornea to three freeze/thawing cycles. During the last washing step to remove cell debris, decellularized DMs (dDM) were peeled from the stroma. The dDM were thinner and more fragile than native ones. Stretching the dDMs onto the Petri dish was more difficult, because they were torn and incomplete and folds persisted (**Figure 38**, A).

1.1. Optimization of tissue engineered – endothelial keratoplasty graft construction with immortalized endothelial cells

ECs of the immortalized cell line HCEnC-21T were seeded at a volume of 200 µL on a moist dDM. The cell suspension did not entirely remain on the dDM, spilling over into the Petri dish during the adhesion step. At day 5, the cells had spread and fully covered the dDM (**Figure 38**, B) and the Petri dish. The constructed HCEnC-21T-TE-EK graft was partly detached from the Petri dish. Folds in the engineered tissue obstructed the visualization of cells under inverted microscope.

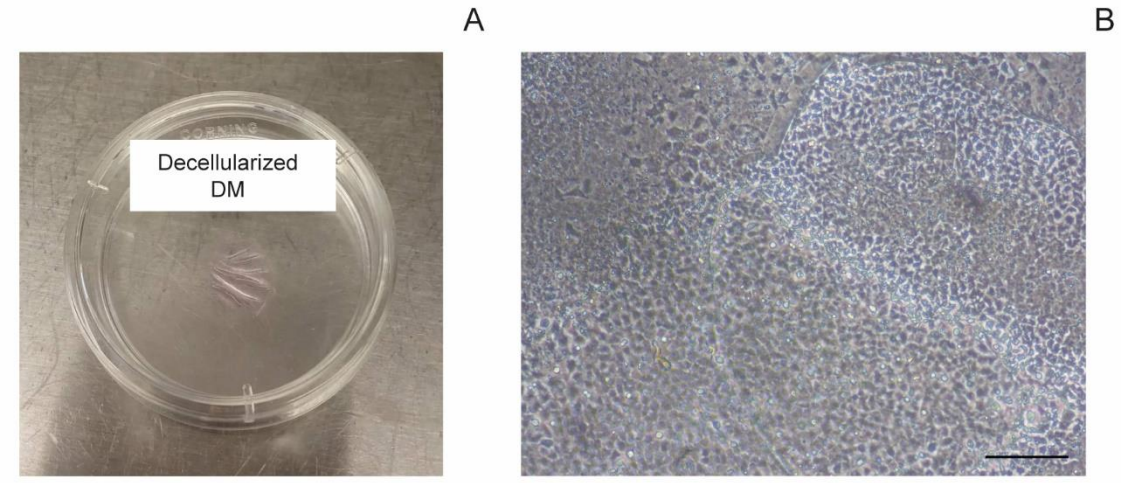

***Figure 38**. Photographs of a decellularized Descemet's membrane (A) and of the HCEnC-21T-TE-EK graft at day 5 (B). Scale bar: 200 µm.*

At day 5, immunofluorescence assays targeting ZO-1, with Hoechst and phalloidin counterstaining, were performed on a native endothelium-DM complex and an HCEnC-21T-TE-EK graft. HCEnC-21T nuclei were larger than primary EC nuclei. Actin filaments revealed a higher pleiomorphism within the HCEnC-21T cells, which were also crowded but maintained a polygonal shape (**Figure 39**). In both samples, ZO-1 was located at the cell membrane level in ECs (**Figure 40**).

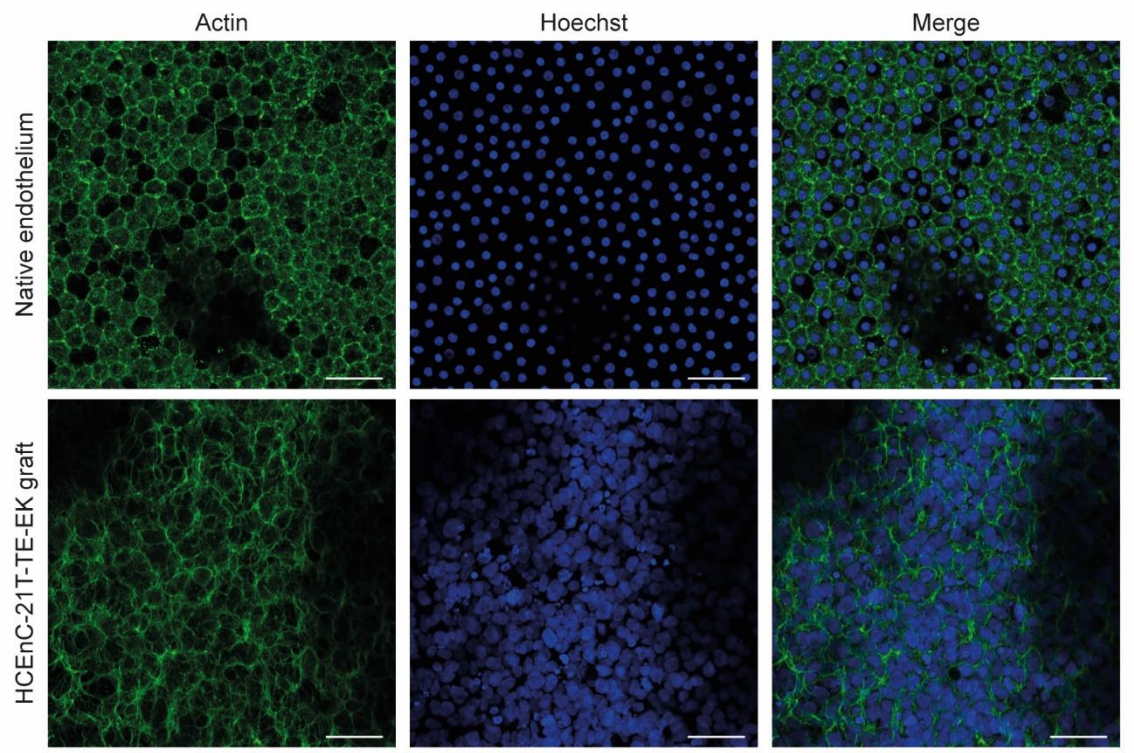

Figure 39. *Actin expression (green) at day 5 in endothelial cells of a native endothelium and a HCEnC-21T-TE-EK graft. Cells were counterstained with Hoechst to stain the nuclei in blue. Scale bar: 50 µm.*

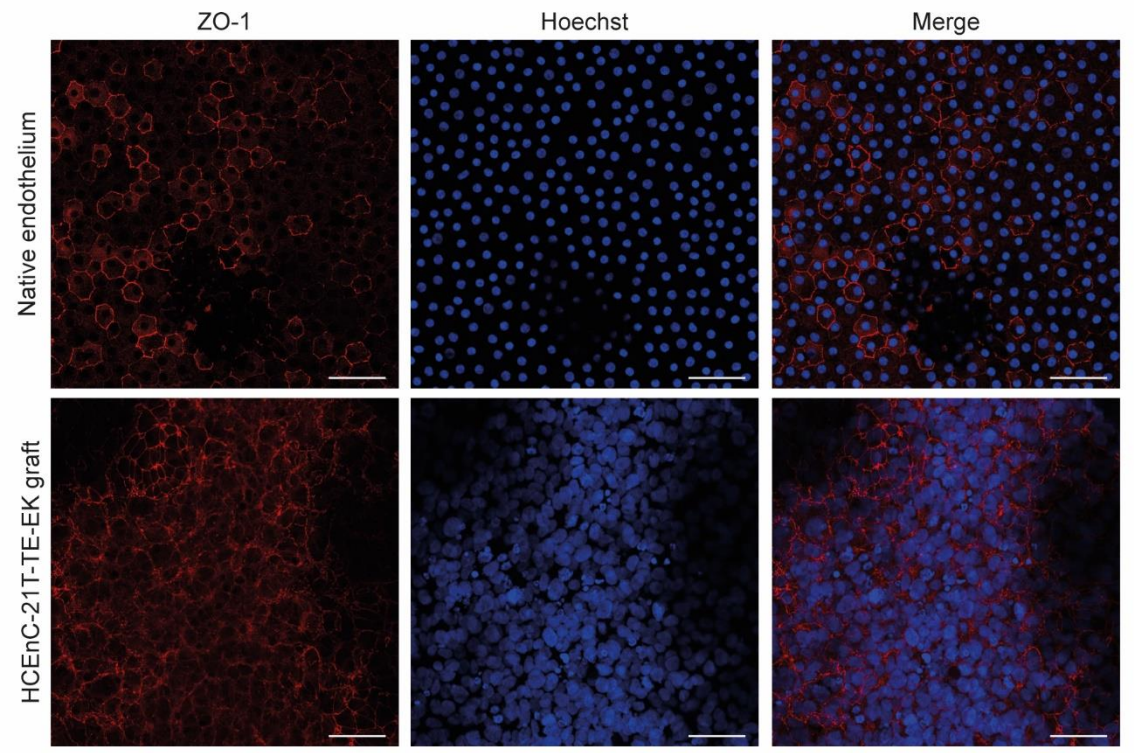

Figure 40. *ZO-1 expression (red) at day 5 in endothelial cells of a native endothelium and a HCEnC-21T-TE-EK graft. Cells were counterstained with Hoechst to stain nuclei in blue. Scale bar: 50 µm.*

1.2. Tissue engineered – endothelial keratoplasty graft construction with primary endothelial cells

Primary ECs at passage 1, which showed some of them an elongated morphology (**Figure 41**, A), were seeded at a volume of 2.35 x 10^5 cells/DM in 100 µL on partially dried dDMs. During the cell adhesion period, the liquid remained on the dDMs without spilling over to the Petri dishes (**Figure 41**, B).

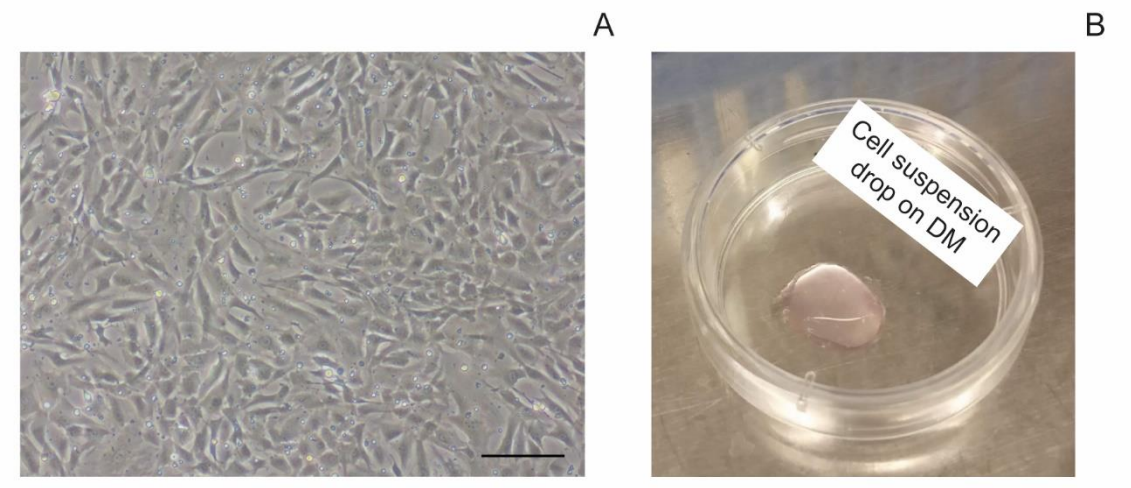

***Figure 41**. A) Photograph of primary endothelial cells at passage 1 used in the four TE-EK grafts (scale bar: 200 µm); B) Cell suspension drop on a decellularized Descemet's membrane.*

After 24 h, ECs were observed to have adhered to the central part of the dDM; however, they did not fully cover the peripheral portions of the dDM. ECs were also observed to have adhered to the Petri dish (**Figure 42**). At day 4, TE-EK grafts 1.2 and 2.1 were slightly detached and rolled up, hindering follow-up observations of cell proliferation and spreading in these areas on a phase-contrast microscope. After 7 days of culture, ECs on the TE-EK grafts had grown and spread onto the empty areas of the dDMs. They had also migrated and proliferated on the plastic dishes (**Figure 42**). TE-EK grafts 1.2 and 2.1 were nearly completely detached and rolled up.

Circularity values for ECs for each of the TE-EK grafts and for cells located on the plastic Petri dish are shown in **Table 5**. Under all conditions, the cells on the plastic dish had lower circularity values compared with the cells on the primary TE-EK grafts.

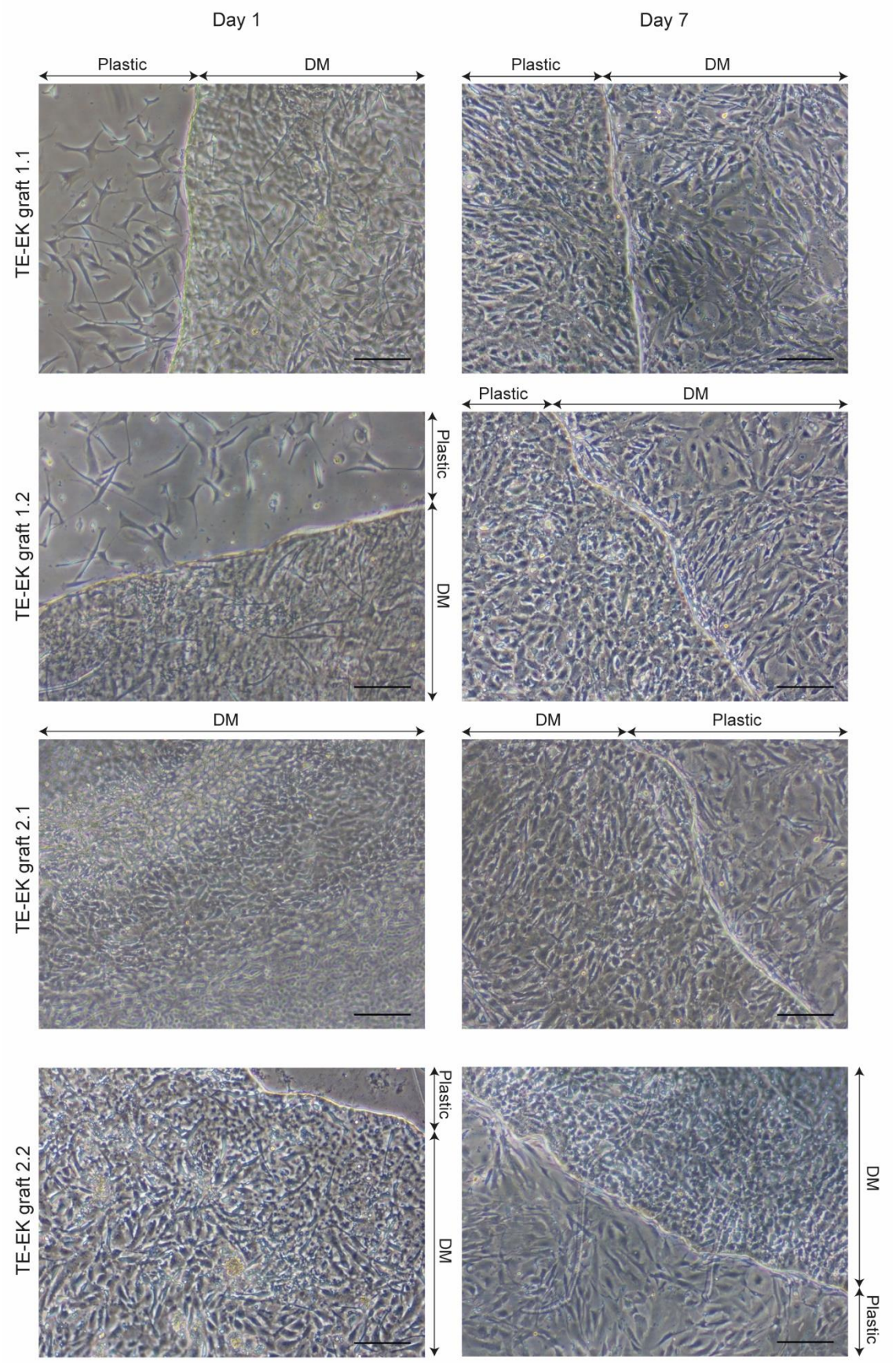

***Figure 42**. Phase contrast microscopy photographs of TE-EK grafts at day 1 and day 7 of culture. DM: Descemet's membrane; Plastic: Petri dish plastic. Scale bar 200 μm.*

***Table 5**. Circularity of endothelial cells on four TE-EK grafts and on the endothelial cells located on the plastic of the Petri dish surrounding the graft.*

	TE-EK graft 1.1	**TE-EK graft 1.2**	**TE-EK graft 2.1**	**TE-EK graft 2.2**
Central	0.61 ± 0.14	–	–	0.69 ± 0.13
Periphery	–	0.66 ± 0.15	0.66 ± 0.13	–
Cells on plastic	0.55 ± 0.20	0.62 ± 0.16	0.54 ± 0.20	0.52 ± 0.20

Counterstaining analysis using phalloidin (actin) revealed that ECs had an enlongated morphology in all TE-EK grafts and on plastic, with cytoplasmic projections overlapping neighboring cells (**Figure 43**). However, some cells in TE-EK grafts 2.1 and 2.2 showed a more defined polygonal shape. In TE-EK grafts, proteins N-cadherin (**Figure 44**) and β-catenin (**Figure 45**) were used as markers for the adherens junctions of the cell monolayer. These proteins were present throughout the cell cytoplasm at day 7. In the native endothelium, N-cadherin and β-catenin were located only at the cell membrane level. The sample TE-EK graft 1.1 for β-catenin immunofluorescence was lost during processing. ZO-1 (**Figure 46**) was observed at the cell membrane level in some cells of TE-EK grafts 2.1 and 2.2, while no expression of ZO-1 was found in TE-EK graft 1. Expression of ZO-1 in the native endothelium was limited to the cell membrane level. No N-cadherin, β-catenin, or ZO-1 proteins were observed in primary ECs grown on plastic at a similar timepoint.

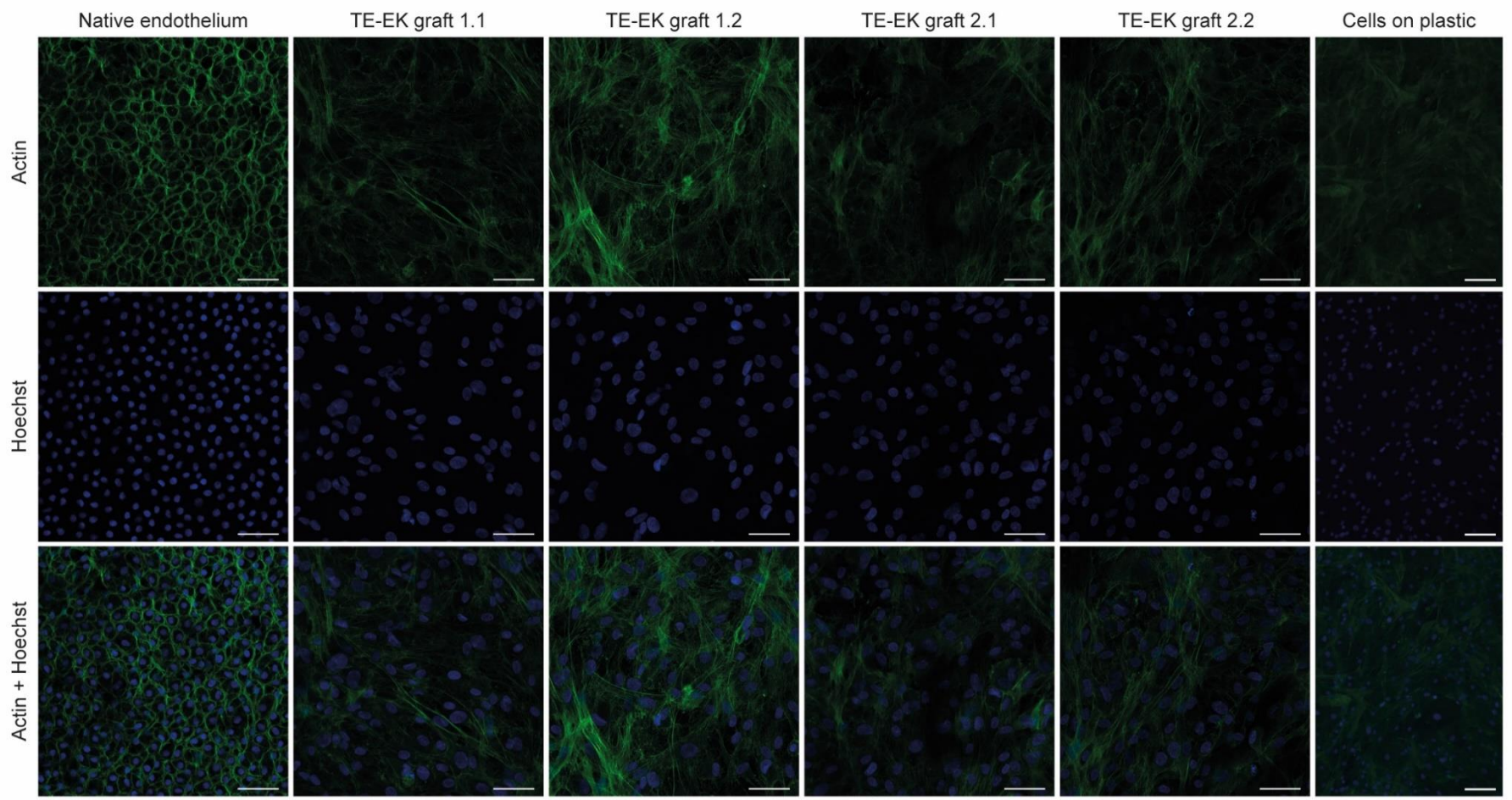

***Figure 43**. Actin expression (green) in primary TE-EK-grafts and in endothelial cells cultured on a plastic Petri dish. In blue, cell nuclei. Scale bar for TE-EK-grafts: 50 μm. Scale bar for the plastic Petri dish: 100 μm.*

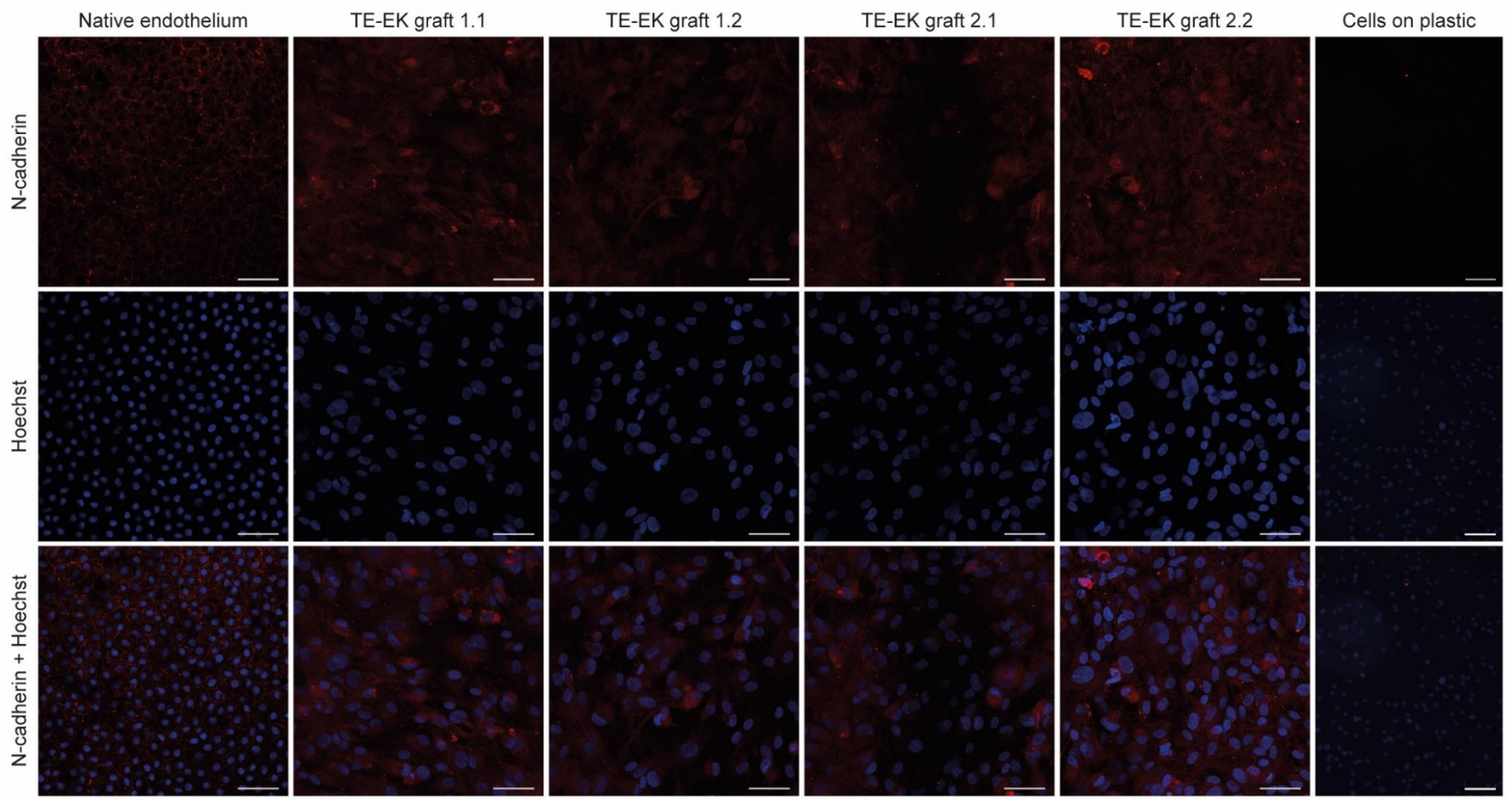

***Figure 44**. N-cadherin expression (red) in endothelial cells of a native endothelium and in primary TE-EK grafts at day 7. Cells were counterstained with Hoechst to visualize nuclei in blue. Scale bar for TE-EK-grafts: 50 µm. Scale bar for the plastic Petri dish: 100 µm.*

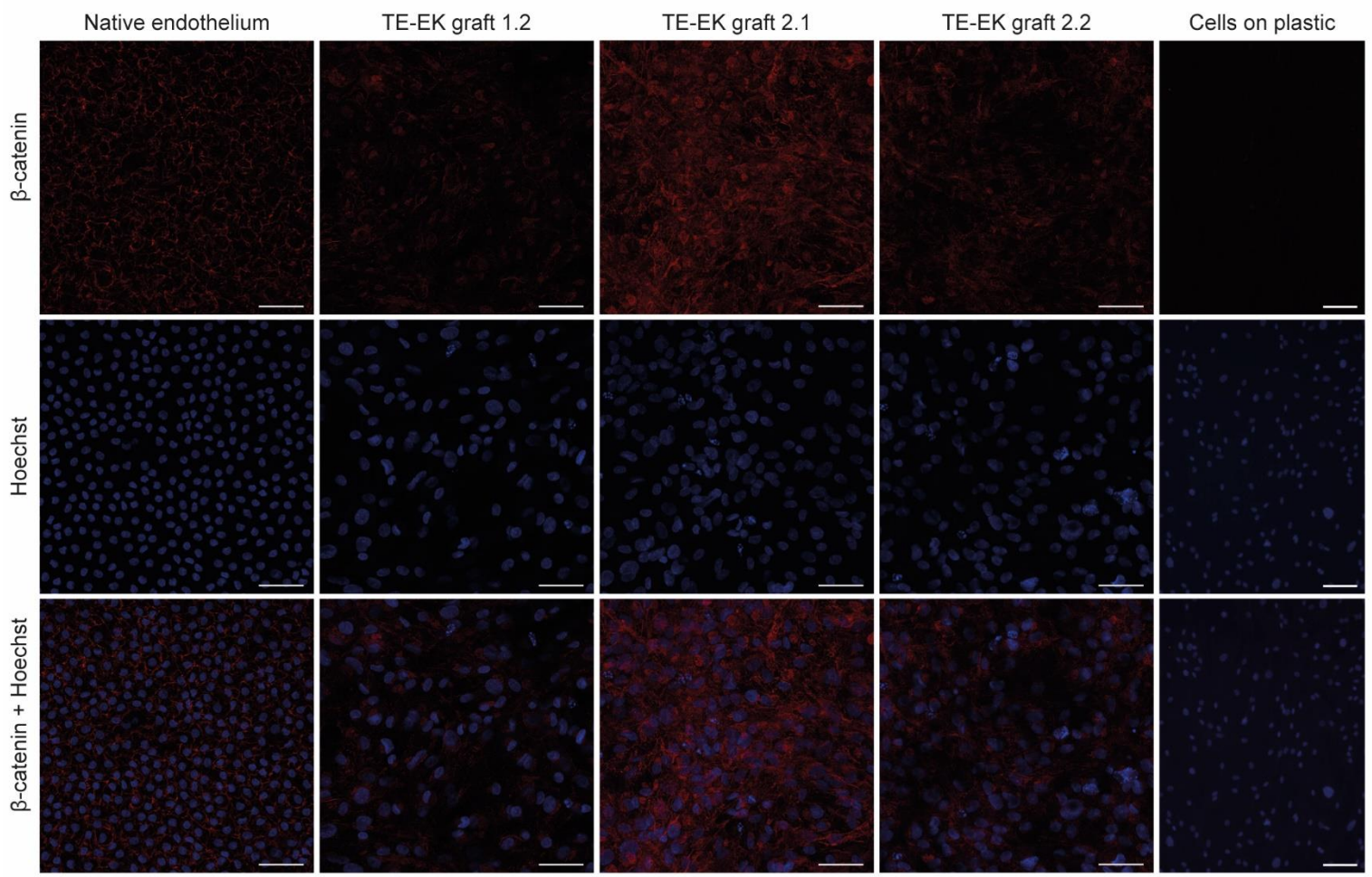

Figure 45. *β-catenin expression (red) in endothelial cells of a native endothelium and in primary TE-EK grafts at day 7. Cells were counterstained with Hoechst to visualize nuclei in blue. Scale bar for TE-EK-grafts: 50 µm. Scale bar for the plastic Petri dish: 100 µm.*

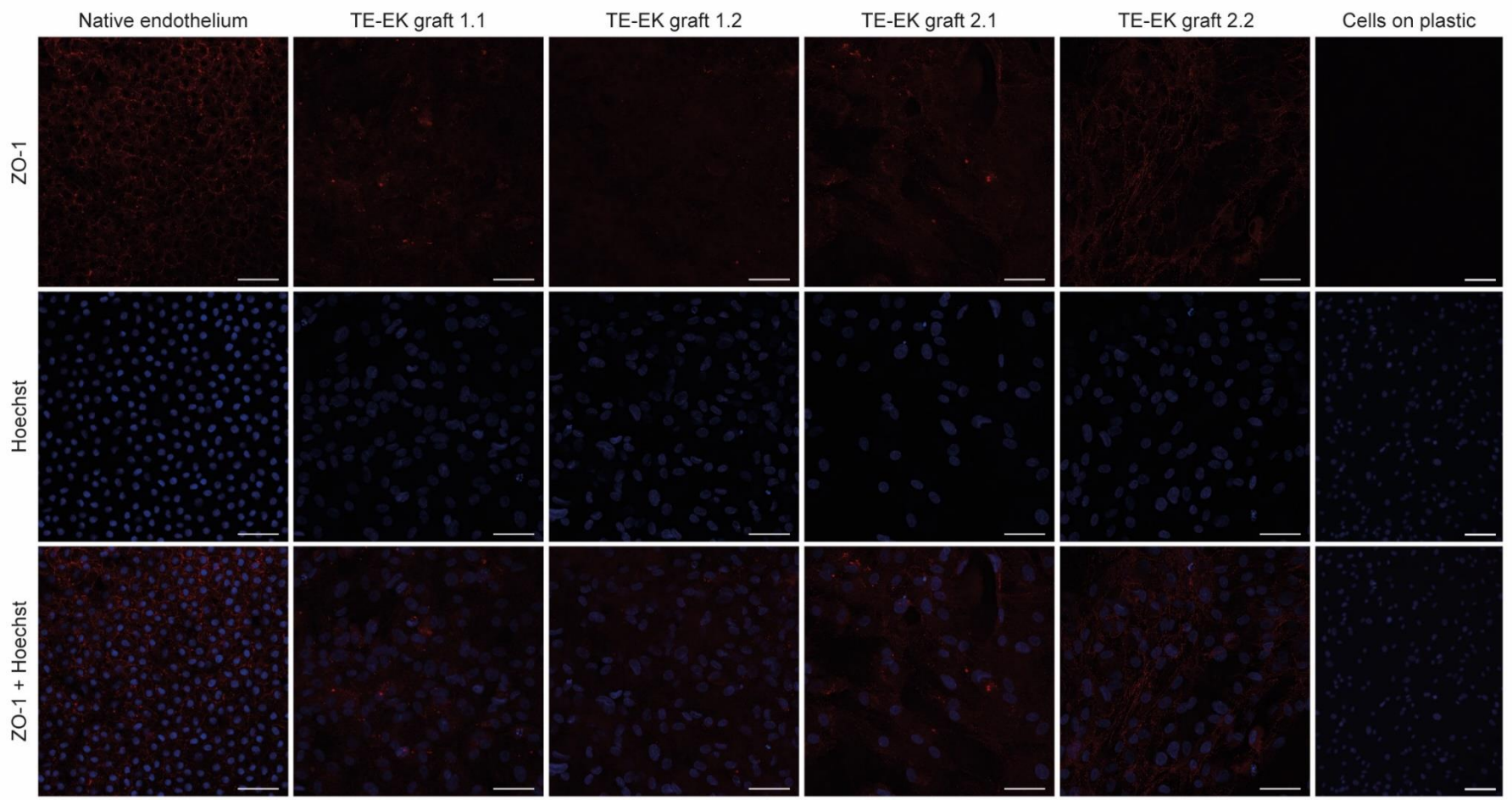

***Figure 46**. ZO-1 expression (red) in endothelial cells of a native endothelium and in primary TE-EK grafts at day 7. Cells were counterstained with Hoechst to visualize nuclei in blue. Scale bar for TE-EK-grafts: 50 µm. Scale bar for the plastic Petri dish: 100 µm.*

V. Discussion

Structural integrity of cryopreserved corneas

Corneal cryopreservation could constitute a long-term storage method that would extend the lifespan of corneas for functional keratoplasties. As such, it could decrease the number of discarded tissues compared with the short-lived hypothermic or organ culture storage methods. Moreover, this preservation technique could simplify surgery logistics planning and thus help surgeons and patients better prepare for corneal transplantation. It could also increase the availability of corneas to be used for emergencies (Brunette *et al.*, 2001). Research in this field started in the mid-20th century with the search for adequate corneal cryopreservation solutions (Brunette *et al.*, 2001; Armitage, 2011). Despite numerous efforts, none of the tested corneal cryopreservation protocols were good enough for corneal functional storage (Bourne and Nelson, 1994; Canals *et al.*, 1996, 1999; Bourne, Nelson and Hodge, 1999; Brunette *et al.*, 2001; Halberstadt *et al.*, 2003). Then, the field of cryopreservation was abandoned for the last two decades, and research was instead focused on hypothermic and organ culture storage, which became the established methods used in clinical practice (Bourne, Nelson and Hodge, 1999). More recently, the interest in corneal cryopreservation was renewed, partly because of the reduced availability of donor corneas as a result of the COVID-19 pandemic (Chaurasia, Das and Roy, 2020; Martínez-Conesa *et al.*, 2022).

In this study, we have tested two conventional cryopreservation and two vitrification protocols. The conventional protocols usually require fewer steps but entail higher risks of ice formation, as it is controlled, but not eliminated. Vitrification protocols work better to prevent ice formation. However, they require longer times and additional steps for tissue equilibration with CSs due to the higher concentration of toxic CPAs, and tissues are at risk of damage by ice during warming if devitrification occurs. Although endothelial integrity and viability are the main features to be evaluated, it is worth remembering that corneal cryopreservation also impacts a complex multilayered tissue whose molecular organization needs to be preserved to ensure corneal transparency.

At the general level, P1 and P2 resulted in better corneal structural integrity, despite the slight increase in stromal thickness. This increase was also observed when measuring the distance between stromal collagen fibers in P1-cryopreserved corneas. Furthermore, with both P1 and P2, the endothelium and epithelium of cryopreserved corneas were for the most part attached to the DM and to the Bowman's layer. Some exceptions were observed

for P2, which could be due to technically generated damages resulting from sectional cutting. The detachment of these two layers—particularly of the endothelium, which cannot regenerate from limbal stem cells like the epithelium—is one of the most recurrent problems following corneal cryopreservation (Madden *et al.*, 1993; Canals *et al.*, 1996, 1999). It can possibly be caused either by ice formation between the cell layer and the membrane or by an osmotic damage mechanism (Walcerz, Taylor and Busza, 1995). Endothelium detachment will be further discussed later.

Conversely, vitrification protocols resulted in cryopreserved corneas with a notable adenomatous stroma. Moreover, in P3- and P4-cryopreserved corneas, neither the epithelium nor the endothelium was conserved in the central portion of the cornea. This is problematic because this is the portion that would normally be excised and used as corneal graft.

The increase in stromal thickness observed in cryopreserved corneas had already been reported (Routledge and Armitage, 2003). Swelling of the stroma and separation of collagen bundles could probably have been caused by excessive tissue water uptake during the cryopreservation process. Corneas have been previously described to maintain a high permeability to water even at 0 °C (Walcerz, Taylor and Busza, 1995). The water influx could distort the normal arrangement of collagen fibers, and such distortion would usually be first observed in the posterior (endothelial) region of the stroma where keratan sulfate, the most hydrophilic stromal GAG, is located (L. Müller, Pels and Vrensen, 2001; Dua and Said, 2019a). This situation could be promoted by several factors. One of them is the decrease in endothelial metabolic activity at the hypothermic temperatures used during tissue equilibration with CPAs and during CPA removal. This would promote the establishment of a detrimental passive osmotic response (Armitage, Hall and Routledge, 2002; Routledge and Armitage, 2003). In addition, a lack or an insufficient concentration of npCPAs could lead to an adenomatous stroma. A npCPA can act as an oncotic or osmotic agent that preserves normal stromal thickness and minimizes osmotic changes that could damage cells, as will be discussed later. This substance can be albumin, chondroitin sulfate, or sugars (Hagenah and Böhnke, 1993; Halberstadt, Athmann and Hagenah, 2001; Armitage, Hall and Routledge, 2002; Halberstadt *et al.*, 2003; Routledge and Armitage, 2003; Wusteman *et al.*, 2008). Sugars are also used in hypothermic corneal storage to prevent excessive stromal hydration (Taylor, 1986; Taylor, Hunt and Madden, 1989; Armitage, 2011).

With respect to the formation of ice crystals, no damage was observed in the TEM images of the posterior stroma of P1-cryopreserved corneas. If a crystal were formed in the anterior or middle stroma, it could damage the collagen structure, reduce its mechanical properties (elasticity and strength), and lead to permanent swelling of the stroma (Fong, Hunt and Pegg, 1987).

Regarding corneal cell morphology of all cryopreserved corneas, several keratocytes were observed to have shrunk, which is indicative of harmful dehydration that could lead to cell death. With respect to epithelial corneal cells, they were smaller and had irregular shapes following cryopreservation. In the epithelium or in the remaining adhered portions of the epithelium, basal cells should have had a columnar shape, but instead showed a round appearance. The epithelial surface also showed an irregular aspect that could be caused by ice. This suggests that the epithelium could act as a surface for ice nucleation that could disturb cell morphology and promote the detachment of squamous epithelial cells. An irregular corneal epithelial surface with variations in thickness was also described by Fong *et al.* (1986) after cryopreservation of rabbit corneas. Similarly to epithelial cells, ECs were irregularly shaped after cryopreservation, and some of them only showed the cytoplasm, which could indicate the loss of cell membrane integrity.

Endothelial integrity and viability

Endothelial viability and integrity are always the first parameters to be evaluated when a cryopreservation protocol is tested, due to the importance of the corneal endothelium for maintaining transparency. Additionally, the low regenerative capacity of these cells makes any damage likely to be irreversible (Canals *et al.*, 1999).

To assess endothelial integrity and EC viability in the four cryopreservation protocols, we selected a cytochemical assay with calcein-AM, a method that is commonly used to evaluate transportation methods for DMEK grafts (Romano *et al.*, 2018). This method is based on the assumption that living cells generate a specific metabolic activity that can be observed using markers (Taylor, 1986). However, several technical problems occurred during sample processing for the calcein-AM assay. The most important one was probably due to the clinical technique used to peel off the complex, which required a high level of manipulation of the endothelium. Manipulation causes damage to the ECs and can thus hide or increase the damages caused by cryopreservation. Furthermore, unrolling and incomplete unfolding the endothelium-DM complex onto the slides caused

visible damage to tissues, as the endothelium-DM complex or the endothelium alone were torn by forceps, especially around their peripheral sections. For this reason, an independently observed qualitative evaluation was performed, and photographs were taken only within unfolded areas. Due to this and taking into account the low number of samples used, the results from the calcein-AM assay should be interpreted with caution. For all these reasons, with the purpose of confirming the results from the calcein-AM assays on P1-cryopreserved corneas, we selected the dye-exclusion assay with trypan blue and alizarin red. This technique, which requires low corneal manipulation, was one of the most commonly used to test endothelial integrity and viability after corneal cryopreservation in a simple and cost-effective manner (Canals *et al.*, 1999, 2000; Halberstadt, Athmann and Hagenah, 2001; Armitage, Hall and Routledge, 2002; Routledge and Armitage, 2003).

Integrity of corneal endothelium

The amounts of DM-attached ECs observed in all calcein-AM stained endothelium-DM complexes of all cryopreserved corneas and in trypan blue-stained P1-cryopreserved corneas were inconsistent with observations on Masson's trichrome-stained slides, where the endothelium was detached following the vitrification protocol. This suggests that the detachment of the endothelium could be caused by sample processing for Masson's trichrome staining during sample slicing and staining instead of resulting from the cryopreservation process itself.

In P1-cryopreserved corneas used for the calcein-AM assay and the trypan blue-alizarin red assay, we observed decellularized areas of different shapes on the DM. The striae-like morphology of some decellularized areas was observed in all cryopreserved corneas and could originate from areas subjected to folding. Corneal tissue folds have been reported to commonly occur in corneas that had suffered swelling during hypothermic storage, which contain dead ECs within the folded areas (Tran *et al.*, 2017). As cryopreserved corneas were initially preserved in hypothermic storage medium, folds could have generated during such storage prior to cryopreservation. An additional cryopreservation process would have likely increased damage to EC with further tissue swelling, promoting cell detachment from the DM.

Cell detachment can also be caused by intracellular ice crystals formed during the cooling or warming steps. The growth of intracellular ice crystals is favored by the presence of

gap junctions between ECs, allowing ice crystals to pass through, grow, and consequently damage groups of ECs at the same time (Ebertz and McGann, 2004; Armitage, 2009; Elliott, 2013). Acker *et al*. (2001) demonstrated that intracellular ice formation was dependent on the cooling rates and, more specifically, on cooling rates higher than the optimal cooling rate needed to prevent the possibility of intracellular ice formation. If the cooling rate was higher but close to the optimal rate, ice crystal formation would randomly start in individual cells within a monolayer, and ice crystals would then propagate among adjacent cells. If the cooling rate was additionally increased, ice crystals would again be formed in one cell but propagated to all adjacent cells following a wave-like pattern, homogeneously affecting an entire area (Acker, Elliott and McGann, 2001). In all cryopreserved corneas, but most notably in P1-cryopreserved corneas, decellularized areas seemed to follow the random pattern described by Acker *et al*. (2001). Otherwise, when performing cryopreservation by vitrification, ice formation could also be generated in a context where the warming step was not quick enough, leading to the growth of ice crystals inside cells in a devitrification process that will be further explained in a later section.

With respect to P1-cryopreserved corneas, a remarkably high inter-individual variability in decellularized areas was observed, despite the fact that all of them had been processed using the same cryopreservation protocol. As the corneas used in this research had been discarded from clinical use for various reasons, this variability could have been the result of defects present within the endothelium or within other corneal layers, which could have somehow interfered in the cryopreservation process. However, Canals *et al.* (1999) observed a high variability in endothelial integrity among human samples, despite all their samples having shown similar characteristics before cryopreservation.

Endothelial cell viability

Viable ECs with intact cell membranes and with esterase activity were mainly observed in P1-cryopreserved corneas and, in fewer proportions, in P2-cryopreserved corneas. Regions with single or grouped cells without any enzymatic activity and/or with damaged membranes where also observed. With the P2, P3, and P4, ECs seemed non-viable, as the calcein-AM fluorescent product was observed in the endothelium as green dots, which is the result of enzyme diffusion out of the cells through injured membranes (Taylor, 1986). Attached but non-viable cells had already been observed by Madden *et al.*

(1993) in conventional cryopreservation and in cryopreservation by vitrification, where EC membranes were extensively perforated after cryopreservation at different rates. With trypan blue-alizarin red staining, the presence of randomly located single or grouped damaged ECs with injured cell membranes was also observed in P1-cryorpeserved corneas. These cells would be equivalent to Hoechst-stained cells without calcein-AM fluorescence signal in the calcein-AM assay. Again, similarly to endothelial integrity, endothelial cell viability in P1-cryopreserved corneas was variable among samples, as was observed when calculating post-cryopreservation ECD, which did not show a homogeneous ECD loss trend. However, the calculated ECD should be interpreted with caution, as it was calculated using the Konan specular microscope software algorithm (which was not developed specifically for this use) and taking into account that only areas with cells were used, while decellularized areas were excluded from ECD calculation. This implies that the actual ECD is most likely lower than estimated.

The classification into viable and non-viable ECs should be interpreted with caution, as this evaluation was performed immediately after warming and CPA removal. It has been observed that ECs need a certain time to recover their biological functions. Some authors performed analyses such as perfusion assays to assess whether the endothelium could still regulate stromal thickness (Bourne, Nelson and Hodge, 1999; Wusteman *et al.*, 1999, 2008; Armitage, Hall and Routledge, 2002; Routledge and Armitage, 2003). Later, they evaluated its viability and integrity. Other authors have placed the corneas in organ culture to allow for EC recovery or detachment of dead cells and, after some time, performed a cell viability assay (Hagenah and Böhnke, 1993). The possible damage to ECs caused by the cryopreservation process, as well as the optimal cryopreservation parameters to preserve endothelial integrity and viability, are discussed below.

Mechanical cell injuries

Mechanical damage caused by ice formation could lead to cell detachment and create acellular areas similar to those observed in cryopreserved corneas, as stated above. Furthermore, intracellular ice crystals could cause membrane damage and result in the non-viable adhered ECs observed in some areas. Areas with such cellular damages seemed to follow the described random pattern in the endothelium of P1- and P2-cryopreserved corneas and a wave-pattern in corneas from the P3 and P4 vitrification protocols. In P3- and P4-cryopreserved corneas, the intracellular nucleation needed for

ice formation could have occurred during the devitrification process as a result of slow warming speeds, which might not have been fast enough to prevent its occurrence. Devitrification is one of the most frequently reported types of damage in cryopreservation through vitrification (Rich and Armitage, 1991), as warming rates need to be extremely rapid and are not usually achieved by conventional corneal warming, which normally consists in removing the vial from a nitrogen tank and introducing it in a water bath at 37 °C, 40 °C, or 60 °C (Rich and Armitage, 1992; Armitage, Hall and Routledge, 2002). To avoid devitrification, the use of CPAs at higher concentrations than those needed (and used) for vitrification has been proposed. Armitage *et al*. (2002) were able to reduce ice crystal formation using 6.8M propylene glycol in vitrified rabbit corneas. However, that implies longer cell exposure times to possibly toxic substances (Rich and Armitage, 1992).

Solution effects

In addition to mechanical injuries caused by ice crystals, EC damage could also be caused by "solution effects", i.e., by excessive exposure to toxic CPAs at inadequately adjusted temperatures or time periods, which could lead to excessive dehydration or intolerable osmotic variations for ECs. All this could be related to the non-stained vacuoles observed in viable ECs from P1- and P2-cryopreserved corneas after the calcein-AM assay. These vacuoles have been reported by several authors after thawing and CPA removal (Bohnke *et al*., 1986). To avoid solution effects, the strategies used throughout the literature have been different, but usually complementary. These strategies are explained below.

Cryoprotectant agent addition and removal steps

The gradual introduction of pCPAs in corneal tissue at low temperatures, as was performed in protocols P1 and P2 with the three CSs, was observed to allow for controlled osmotic changes in cells and controlled cell dehydration without reaching the cell shrinking threshold (Taylor, Hunt and Madden, 1989; Madden *et al*., 1993; Wusteman, Boylan and Pegg, 1997; Wusteman *et al*., 1999). For vitrification protocols P3 and P4, however, the solution was rapidly added dropwise. For cryopreservation by vitrification, full CPA introduction is needed to prevent ice formation, as it requires a high concentration of CPAs inside tissues and cells. For this purpose, the dropwise addition strategy was not optimal because it causes the tissue to be exposed to a single CS in a short time. It was described that, when using a similar vitrification solution called VS41A, composed of 3.1 M DMSO, 3.1 M formamide, and 1.2 M propylene glycol, rabbit corneas

needed about 25 min for tissue equilibration in each of the CS used in series (Bourne and Nelson, 1994). Moreover, it was reported that in rabbit corneas, the CPA addition step of a vitrification solution should always be done in a stepwise manner due to the elevated CS osmolalities caused by high CPA concentrations (Rich and Armitage, 1990, 1991, 1992; Bourne and Nelson, 1994). It is likely that a rapid exposure of ECs and epithelial cells to CS3 and CS4 with high CPA concentrations could cause excessive cell hydration and/or osmotic shock. For P3 and P4, a method using serial CSs with increasing concentrations of CPAs would provide better results. However, that would be time-consuming, as a normal addition step implies multiple different solutions, more than in a conventional cryopreservation procedure, with an extended immersion period for each CS. Additional time is also often required for human corneas, as they are thicker than their rabbit counterparts (Bourne and Nelson, 1994).

In the same way, pCPA removal should also be done gradually, decreasing pCPA concentration in each of the consecutive WSs used. This system was not followed in P1, and the significant difference in osmolality between CS1.3 and albumin wash solution could be responsible for cell osmotic shock or excessive water uptake exceeding the threshold for cell swelling, as the CS was hypertonic compared with the WS (Taylor and Hunt, 1989). Nonetheless, in the case of P1, DMSO removal was effectively managed by the washing steps, leaving only a small concentration of DMSO after washing. pCPAs in P2, P3, and P4 were progressively removed by halving the CPA concentration with the addition of equal volumes of the CS vehicle solution, which was equivalent to the use of a series of WS with decreasing concentrations of the pCPAs (Taylor and Hunt, 1989).

Furthermore, in the introduction and removal steps, temperature and duration of sample immersion in each solution for tissue equilibration are important, as ECs show different pCPA permeation rates depending on the temperature. In this study, we observed that tissue equilibration with the surrounding CS1.3 was incomplete because DMSO tissue concentration immediately after warming was lower than before corneal cooling. The tissue contained 0.8 M DMSO, while CS1.3 contained 1 M DMSO. The importance of pCPA permeation in cryopreservation has been highlighted by several authors, who studied the permeability of pCPAs using NMR spectroscopy, as we did, at different temperatures and in different tissues, such as corneas (Taylor and Busza, 1992; Walcerz, Taylor and Busza, 1995; Wusteman *et al.*, 1999) and arteries (Bateson *et al.*, 1994). By using NMR spectroscopy, we can measure the exact concentration of pCPAs reached at any step

of CPA introduction and the pCPA concentration remaining in the tissue during CPA removal, as long as the previous pCPA concentration achieved is known. As such, we can increase or reduce the duration of each equilibration or removal step or increase or reduce the number of CS or WS to achieve an adequate concentration of pCPAs inside tissues without causing any cell damage. For P1, it became apparent that increasing the duration of each solution addition step was needed to achieve 1 M DMSO inside the cells/tissue.

Cryoprotectant solutions and wash solution composition

CS and WS composition to add and remove CPAs should be controlled to counter "solution effects". For corneal samples, it was observed that the addition of the aforementioned osmotic agents that can control stromal thickness can also control cell volume changes and even reduce concentrations of the pCPAs used. For this reason, npCPAs that can play this role are usually added to CPs and WSs in numerous conventional cryopreservation protocols (Hagenah and Böhnke, 1993; Madden *et al.*, 1993; Routledge and Armitage, 2003) and in vitrification protocols (Armitage, Hall and Routledge, 2002; Wusteman *et al.*, 2008). Among the four protocols tested, only albumin in P1 could act as an osmotic agent, while in P2, P3, and P4 there was no presence of a substance with similar capabilities, as all the CPAs used were pCPAs.

Moreover, the vehicular solution where CPAs are added to create the CS should be considered. Taylor, Hunt and Madden (1989) created a cornea-potassium-NTris(hydroxymethyl)methyl-2-amino ethane sulphonate (CPTES) ionic balance solution to control the ionic balance of ECs at hypothermic temperatures. This solution was then used for many corneal cryopreservation protocols (Fong, Hunt and Pegg, 1987; Madden *et al.*, 1993; Wusteman, Boylan and Pegg, 1997; Wusteman *et al.*, 1999). The use of a commercial culture medium, such as the M199 used in this study for P1 and P2 or the Euro-Collins solution (a solution for hypothermic kidney storage) used for P3 and P4, might not necessarily be well tolerated by corneas under cryopreservation conditions (Taylor, Hunt and Madden, 1989; Bourne and Nelson, 1994). In addition, it should be taken into account that a commercial culture medium offers a range of osmolalities, which can differ among batches. A cryopreservation protocol should therefore always be adjusted for each batch to control the intensity of the osmotic shock, which complicates the application of this type of cryopreservation protocol in clinical practice.

CPA cytotoxicity should always be evaluated at different temperatures and different exposure times during the addition and removal steps. DMSO was proved to be well tolerated by ECs at 0 °C at a 3 M concentration without any remarkable reduction in EC integrity and viability. This concentration was achieved when immersing rabbit corneas in a stepwise manner at 10-min intervals (Taylor and Hunt, 1989). However, the addition and removal of 2.8 M DMSO at 4 °C and at 3-min intervals was observed to be more toxic to porcine corneas (Wusteman *et al.*, 1999) than to rabbit corneas, which showed better tolerance in a similar protocol (Wusteman, Boylan and Pegg, 1997). Thus, interspecies variability in toxicity should be considered when a cryopreservation protocol previously tested in an animal model is assayed on human corneas, as this variability is likely to change the outcome. With respect to CPA concentrations for vitrification, the toxic tolerance of ECs can be improved by decreasing CS temperatures to a range of -5 °C to -15 °C (Rich and Armitage, 1990, 1991, 1992; Armitage, Hall and Routledge, 2002). Consequently, the temperature of CPA addition in P3 and P4 could have been potentially deleterious, as toxicity of CPAs could have been excessive for corneal cells, especially for ECs and epithelial cells, which were the first to be in contact with DP6 or VS55.

Cooling rates

Cooling temperature rates vary according to the CSs and cryopreservation method used. For conventional corneal cryopreservation, the design of a cooling temperature program in a biological freezer is usually the preferred method. Bohnke *et al.* (1986) were among the first authors to use a biological freezer to cryopreserve human corneas at cooling rates of 1 °C/min to -40 °C and -5 °C/min to -80 °C. These and other similar cooling rates (1 °C/min to -60 °C, 1 °C/min to -80 °C) were commonly used to assay conventional corneal cryopreservation protocols (Capella, Kaufman and Robbins, 1965; O'Neill, Mueller and Trevor-Roper, 1967; Taylor, 1986; Hagenah and Böhnke, 1993; Canals *et al.*, 1996, 1999). With this cooling control system, the detection of the ice nucleation starting point and the release of latent heat could be studied to control ice nucleation during cooling, making the protocols more reproducible. However, these temperature rates were not the ones that offered the best results in terms of endothelial integrity and viability. It was observed that for the maintenance of EC viability and endothelial integrity of rabbit corneas, rates slower than 1 °C/min (even of 0.2 °C/min) down to -80 °C using a CS containing propylene glycol were the best (Routledge and Armitage, 2003). This is consistent with the low temperature rates recommended to reduce intracellular ice

formation in cell monolayers (Acker, Elliott and McGann, 2001). These conditions allowed for longer times for water to exit the corneas and for tissue equilibration to be reached at the first steps of the cooling process (Walcerz, Taylor and Busza, 1995). However, Canals *et al.* (1996) reported that the best results in terms of endothelial integrity and viability in human corneas were achieved using a -1 °C/min rate instead of a -0.5 °C/min rate. However, these results were far from convincing for their application in clinical practice due to the loss of endothelial integrity. For P1, which was the only protocol where cooling temperatures were recorded, sample temperature was observed to decrease at a rate of -1 °C/min down to approximately -80 °C. The results achieved by other authors using the same rate of -1 °C/min on human corneas showed similar integrity and result variability to those obtained in this study (Capella, Kaufman and Robbins, 1965; Canals *et al.*, 1996, 1999). Nonetheless, cooling rates are difficult to compare among different cryopreservation protocols where different CS, WS, and animal models were employed. For this reason, following the cooling rates used by other authors was not optimal to validate our method.

With respect to the vitrification process, a biological freezer could also be employed, which allowed recording sample temperature (Bourne and Nelson, 1994). Specific custom-made equipment can also be used to monitor temperature and to cause abrupt temperature drops (Rich and Armitage, 1991). In this study, we used a custom-made system to cryopreserve corneas by vitrification. However, sample cooling temperature was not monitored; therefore, calculating the experimental sample cooling rates was not possible. Additionally, our custom-made method could not provide an accurately reproducible methodology (in contrast with a biological freezer), as it is dependent of inter-technician variability.

***In vitro* penetrating keratoplasty model**

To study EC behavior in P1-cryopreserved corneas when transplanted into a receptor cornea and to enable the translation of our basic research to a preclinical setting, an *in vitro* PK model was proposed. The development of this model could lead to a reduction in the need for animal use. This is the first time that an *in vitro* PK model with human corneas has been assayed. Other similar corneal models have been previously developed: for example, a model developed to monitor epithelial wound healing (Schumann *et al.*, 2021).

Optimization of the PK model was limited, as only two corneas of different sexes with high ECD had been discarded from clinical use in the same week and were available for this experiment. Thus, only one culture method (static organ culture condition), one culture medium condition (specific corneal endothelial medium), two different culture times (4 and 9 weeks), two methods to identify the receptor and graft cells (cell tracers and FISH), and two methods for endothelium immunofluorescence (on the whole cornea or using cryosections) were assayed.

The changes visualized in PK models during the first 21 days, which were corneal opacification and de-epithelialization, could be related to damages during the surgery process and to organ culture conditions. Corneas stored in static conditions in culture medium become adenomatous and lose their transparency. To solve this problem, in the clinical practice, a deswelling medium containing osmotic agents is used after corneal organ culture storage and before transplantation (L. J. Müller, Pels and Vrensen, 2001; Parekh, Elbadawy, *et al.*, 2018). It was observed that dynamic organ culture using bioreactors offered an environment closer to that of a real-life setting. With these bioreactors, it is possible to create an intraocular pressure similar to the one that exists in the eye, helping to maintain the endothelial barrier and corneal transparency (Thériault *et al.*, 2019). Furthermore, it has been reported that in corneal organ culture, de-epithelialization occurs and epithelial cells suffer apoptosis within the first week (Crewe and Armitage, 2001; Raeder *et al.*, 2007). In this study, a medium specifically formulated for the culture and expansion of ECs was used with the aim of better maintaining ECs. However, this medium was not formulated for the culture and preservation of other corneal cell types, and damage to epithelial cells may have occurred as a result (Crewe and Armitage, 2001; L. J. Müller, Pels and Vrensen, 2001; Schumann *et al.*, 2021). For other corneal models, a more generic medium such as DMEM was used. Other available media were the ones used for clinical organ culture. These are routinely used by eye banks and have been developed in order to maintain corneal integrity for weeks. Further experiments would benefit from using DMEM or clinical organ culture media to reduce damage to epithelial and other corneal cells.

The wound dehiscence between the receptor and grafts observed at 4 weeks in the first X^Y model and 5 weeks later in the Y^X model could be due to damage or loss of stromal keratocytes that would have otherwise rebuilt and joined both graft and donor stroma together. It is known that under culture conditions, the number of keratocytes decreases

after 21 days (L. J. Müller, Pels and Vrensen, 2001) and that, immediately after damage to the epithelium, the keratocytes located in the wound undergo apoptosis (Bukowiecki *et al.*, 2017). If the remaining keratocytes are not able to migrate and repair the wound, the dehiscence observed could be a likely result. Furthermore, it is worth noting that the remodeling process for wound healing in the cornea could take a longer or shorter time depending on wound depth and donor age. In a clinical setting, to ensure optimal healing following PK, the sutures are sometimes removed up to a year post-surgery (Pagano *et al.*, 2022). It could therefore be hypothesized that periods longer than 4 and 9 weeks are needed for optimal wound healing and restoration of corneal integrity.

As for the endothelium, none of the PK models maintained this layer. It was therefore impossible to visualize the results using either immunofluorescence or cell tracers. This made cell tracking for corneal endothelium evaluation impossible using the two different cell tracers, which were excited and emitted at different wavelengths to differentiate the ECs from the graft and from the donor. Observation of protein expression using secondary antibodies emitting at complementary wavelengths to those of cell tracers was also impossible. Although the reason why the endothelium detached is not clear, several causes can be identified as possible culprits. For example, manipulation damage could have occurred during surgery. Immediately after PK, endothelium has been reported to undergo severe ECs loss, especially at the periphery of the graft and around the sutures (Alqudah *et al.*, 2013). The PK models were also manipulated after culture and cut in pieces for fixation. This could have been an additional source of endothelial damage. When ECs are lost, the remaining cells migrate and cover the emptied area to maintain the barrier function. If EC detachment was important, the remaining cells could have migrated and enlarged to a point where they became fragile and were ultimately lost during subsequent damages (Bukowiecki *et al.*, 2017). Moreover, to restore the endothelium barrier function, IOP has been demonstrated to play an important role in enhancing the expression of endothelial barrier proteins, especially in ECs with fibroblastic morphology, an appearance that can be adopted by ECs when they are migrating (Anney, Thériault and Proulx, 2021). An absence of IOP may have made the interaction of those cells with the DM more fragile, thus favoring detachment. For this reason, the use of a corneal bioreactor after *in vitro* PK could probably help to maintain the endothelium attached.

Since tracking the origin of EC cells with tracers was not possible, we used keratocytes to test whether it was possible to perform FISH using the distinctive sex between the donor and the graft as a way to differentiate them. This cytology technique has been used in the past to identify ECs in transplanted corneas of patients after death (Wollensak, Perlman and Green, 2001; Lavy *et al.*, 2017). For this study, we used the clinical protocol routinely applied by the *Centro Oncológico de Galicia*. However, while correct hybridization with the X and Y probes was achieved, samples did not remain properly fixed to the slides, yielding poor results. Interestingly, X and Y probing revealed that only the receptor side remained on the slides. Moreover, heat seemed to interfere in the adhesion of tissues onto the slide. However, Wollensak *et al.* (2001) and Lavy *et al.*, (2017) performed FISH protocols in corneas including boiling pretreatments and did not observe section detachment. Charged slides were used in this study to enhance tissue adhesion. The use of coated slides, such as polylisine (Lavy *et al.*, 2017) or silenized slides (Wollensak, Perlman and Green, 2001), could have resulted in better sample adhesion. In any case, as long as sample adhesion can be properly achieved, the FISH technique could be used as an efficient method to identify donor and receptor cells.

Tissue engineered-endothelial keratoplasty graft

In addition to searching for a long-term storage method for donor corneas, other alternatives to reduce the waiting list for corneal transplantations and to increase corneal tissue availability for keratoplasties were investigated. Thus, the possibility of creating an engineered EK graft made from discarded corneas containing healthy DMs and healthy endothelia was evaluated. This way, discarded corneas could be recycled, therefore reducing the loss of resources used to obtain donor corneas. For this project, we used research-grade discarded corneas to test a TE-EK graft model using human DMs and primary cultures of hECs.

Decellularization of DMs was carried out by physical freeze-thaw cycles. Compared with an unprocessed DM, the dDM was more prone to tearing when detached from the stroma. This could be the result of changes in ECM protein in the DM and the stroma during the freeze-thaw cycles. Alternative methods for decellularization are either chemically based, e.g. using Triton-X100, or enzymatic, e.g. using trypsin. However, these methods can also damage ECM proteins and alter their properties. The freeze-thaw cycles method does not damage the ECM to the same extent, as its effects are mainly targeted toward cells where

intracellular ice crystals are formed and disrupt cell membranes (Lynch and Ahearne, 2013; Gilpin and Yang, 2017). As a result, this physical decellularization method should be optimal to preserve the mechanical and optic properties of the DM. Such preservation of the DM's characteristics could make it easier to use with the current surgical instruments used for DMEK and could reduce or eliminate graft detachment issues. Moreover, as DM shows a concave shape, it could generate a compatible format for its optimal adhesion to the stroma (Rodríguez-Fernández *et al.*, 2021).

Before experimenting with primary cells, optimization with immortalized hECs (hCEnT-21T) was performed. This cell line was characterized by forming a monolayer, which showed similar characteristics in culture to those of the native endothelium, with cell markers such as ZO-1 or Na^+/K^+ ATPase, but with larger nuclei than those of native cells (Schmedt *et al.*, 2012). After placing and unrolling the dDMs on the Petri dish, it was observed that a volume of 100 µL of cell suspension was needed to cover the entire dDM. Higher volumes generated leaks and spreading of the cells not only onto the dDM, but onto the Petri dish as well. As the cell line divided quickly, ECs completely covered the dDM and started to form a confluent endothelium even in folds, where cells were attached to each other via ZO-1.

Regarding with the primary TE-EK graft, cells in passage 1 were used to reduce the occurrence of the endothelial-mesenchymal transition observed at higher passages (Peh *et al.*, 2013; Roy *et al.*, 2015). This transition is problematic because one of the requirements to qualify as a graft is to have an endothelium with hexagonal morphology. Nevertheless, this requirement limits the choice of cells that can be used to engineer a corneal endothelium to the same hexagonal morphology standard (Rodríguez-Fernández *et al.*, 2021; Català *et al.*, 2022). Despite all these precautions, the primary ECs adopted an elongated morphology when they were in culture. Nevertheless, we continued with the experiment, seeding cells at a high density to obtain an ECD of 3×10^3 cells/mm^2. Folds and partial TE-EK graft detachment from the Petri dish made it impossible to perform full follow up on cells during culture using a phase contrast microscope. Nonetheless, it was possible to observe that cells covered not only the folds of the dDM in the attached TE-EK grafts, but also the Petri dish. One way to prevent these cells from moving out of the dDM could be to use non-adherent plastic. Additionally, to prevent folds, the use of a concave biocompatible device imitating the shape of the endothelium could provide better scaffolding during culture.

At day 7, circularity values were higher in cells on plastic than in cells on DM. This can be partly explained because ECs were seeded directly on the dDM, which favored a quicker cell adhesion to the DM and cell-cell contact in confluent areas, reversing the endothelial-mesenchymal transition. Conversely, cells had to migrate to cover the plastic areas, which explains the elongated morphology. This has been observed in other studies, where cells on plastic continued to migrate and showed a more marked fibroblast-like shape with more actin stress fibers, typical of migrating cells (Ljubimov and Saghizadeh, 2015; Roy *et al.*, 2015). Moreover, in TE-EK graft 2.1, it was possible to observe an actin disposition in some cells lining the inside of the cell membrane, which potentially indicates a readjustment toward a native hexagonal EC morphology.

Expression of endothelial structural proteins was also investigated. This included ZO-1, a marker of tight junctions between ECs, and β-catenin and N-cadherin, which are part of the adherens junctions. Results showed that at day 7, ZO-1 started to be observed at the membrane level only in the two TE-EK 2 grafts. This suggests the initial formation of a cell-cell interaction. It is likely that ZO-1 would have appeared in other ECs if the TE-EK graft had been cultured for 21 or 28 days. This limited presence of ZO-1 at week 1 was also observed by Spinozzi *et al.* (2020) in a human dDM, but their primary hECs offered a spread morphology instead of being polygonal. In addition, after 5 days of culture, Lu *et al.*, (2020) only observed a light ZO-1 marking at the membrane level of hECs seeded and cultured on a porcine dDM. With respect to the β-catenin and N-cadherin proteins, none of them were detected at the membrane level. Instead, they were observed in the cytoplasm, suggesting that adherens junctions had not been formed at this point. Consequently, longer culture periods would be needed to obtain an endothelium with well-established cell-cell junctions. It has been reported that hydrodynamic conditions is beneficial to enhance the transcription of ZO-1, especially for fibroblast-like ECs, which may help to restore the polygonal morphology of ECs (Anney, Thériault and Proulx, 2021). For this reason, the construction and culture of the engineered graft would provide better results if hydrodynamic conditions and IOP were included, using a corneal bioreactor. That was confirmed by Li *et al.* (2017), who used a perfusion device to create an endothelium on a curved collagen sheet, cultured for one week, with a remarkable expression of endothelial-related proteins and a correct maintenance of EC morphology.

Undoubtedly, corneal cryopreservation is far from established in clinical practice despite the promising results of P1. Further analyses should be performed to improve the statistical power of the results and the cryopreservation parameters described in this discussion. For example, additional human corneal samples would be necessary to test several different cryopreservation conditions and to further assess the functionality of cryopreserved corneal endothelium. For *in vitro* PK modeling, additional human samples would also be required to establish the optimal conditions for corneal culture media, which should be the first parameters to be controlled in order to maintain all the corneal layers in an optimal state. Finally, to engineer TE-EK grafts compatible with clinical practice, it would be necessary to establish a standardized protocol for EC isolation and culture and to improve the methodology used to create the engineered grafts in order to obtain a healthy and functional endothelium.

In summary, although none of the cryopreservation protocols tested can be used in the clinical practice, cryopreservation P1 showed great potential to become an effective corneal cryopreservation protocol, provided that some cryopreservation-related variables are modified. In addition, the TE-EK alternative proposed in this study could be effective to alleviate the shortage of donor corneal tissue.

VI. Conclusions

The main conclusion related to the Objective 1 is that any of the cryopreservation protocols provided a good conservation of the general corneal state for a use in the clinical practice.

1.1. The two conventional cryopreservation P1 and P2 and the two vitrification P3 and P4 were developed to preserve corneal tissue.

1.2. Cryopreservation P1 was the best of the four cryopreservation protocols in terms of corneal endothelial viability and integrity and at general corneal structural level.

1.3. P1-cryopreserevd corneas showed partial endothelial integrity and viability, and a slightly distorted stroma.

1.4. CS1s and WSs composition, the CPA addition and removals steps, and the cooling rate were the main observed parameters affecting the corneal integrity and the endothelial viability when cryopreserving corneas using P1.

1.5. In vitro PK model did not allow to preserve the endothelium; therefore, ECs behavior could not be studied.

The main conclusion related to the Objective 2 is that dDM and primary hECs from discarded corneas are useful for the development of an EK graft by tissue engineering.

2.1. The freeze-thaw method for DM decellularization and the extraction of the endothelium-DM complex for hECs isolation and culture was suitable.

2.2. TE-EK graft was successfully constructed using primary hECs and dDMs as scaffolds.

2.3. TE-EK grafts did not show a functional endothelium, but hECs on the dDM scaffold tended to an EC-like morphology

VII. References

Acker, J. P., Elliott, J. A. W. and McGann, L. E. (2001) 'Intercellular ice propagation: experimental evidence for ice growth through membrane pores', *Biophysical Journal*, 81(3), pp. 1389–1397. doi: 10.1016/S0006-3495(01)75794-3.

Akhoondi, M. *et al.* (2012) 'Freezing-induced cellular and membrane dehydration in the presence of cryoprotective agents', *Molecular Membrane Biology*, 29(6), pp. 197–206. doi: 10.3109/09687688.2012.699106.

Al-Aqaba, M. A. *et al.* (2019) 'Corneal nerves in health and disease', *Progress in Retinal and Eye Research*, 73, p. 100762. doi: 10.1016/j.preteyeres.2019.05.003.

Ali, M. *et al.* (2016) 'Biomechanical relationships between the corneal endothelium and Descemet's membrane', *Experimental Eye Research*, 152, pp. 57–70. doi: 10.1016/j.exer.2016.09.004.

Alqudah, A. A. *et al.* (2013) 'Immediate endothelial cell loss after penetrating keratoplasty', *Cornea*. Cornea, 32(12), pp. 1587–1590. doi: 10.1097/ICO.0b013e3182a73822.

Anney, P., Thériault, M. and Proulx, S. (2021) 'Hydrodynamic forces influence the gene transcription of mechanosensitive intercellular junction associated genes in corneal endothelial cells', *Experimental Eye Research*, 206, p. 108532. doi: 10.1016/j.exer.2021.108532.

Armitage, W. J. (1989) 'Survival of corneal endothelium following exposure to a vitrification solution', *Cryobiology*, 26(4), pp. 318–327. doi: 10.1016/0011-2240(89)90055-2.

Armitage, W. J. (2009) 'Cryopreservation for Corneal Storage', *Developments in Ophthalmology*, 43, pp. 63–69. doi: 10.1159/000223839.

Armitage, W. J. (2011) 'Preservation of Human Cornea', *Transfusion Medicine and Hemotherapy*, 38(2), pp. 143–147. doi: 10.1159/000326632.

Armitage, W. J., Hall, S. C. and Routledge, C. (2002) 'Recovery of endothelial function after vitrification of cornea at - 110°C', *Investigative Ophthalmology and Visual Science*, 43(7), pp. 2160–2164.

Armitage, W. J. and Rich, S. J. (1990) 'Vitrification of organized tissues', *Cryobiology*. Cryobiology, 27(5), pp. 483–491. doi: 10.1016/0011-2240(90)90037-5.

Bakhach, J. (2009) 'The cryopreservation of composite tissues: Principles and recent advancement on cryopreservation of different type of tissues', *Organogenesis*, 5(3), pp.

119–126. doi: 10.4161/org.5.3.9583.

Bashir, H., Seykora, J. and Lee, V. (2017) 'Invisible shield: Review of the corneal epithelium as a barrier to UV radiation, pathogens, and other environmental stimuli', *Journal of Ophthalmic and Vision Research*, 12(3), pp. 305–311. doi: 10.4103/jovr.jovr_114_17.

Bateson, E. A. J. *et al.* (1994) 'Permeation of rabbit common carotid arteries with dimethyl sulfoxide', *Cryobiology*, 31(4), pp. 393–397. doi: 10.1006/cryo.1994.1047.

Baust, J. G., Gao, D. and Baust, J. M. (2009) 'Cryopreservation: An emerging paradigm change', *Organogenesis*, 5(3), pp. 90–96. doi: 10.4161/org.5.3.10021.

Best, B. P. (2015) 'Cryoprotectant Toxicity: Facts, Issues, and Questions', *Rejuvenation Research*, 18(5), pp. 422–436. doi: 10.1089/rej.2014.1656.

Van den Bogerd, B. *et al.* (2019) 'Corneal endothelial cells over the past decade: Are we missing the mark(er)?', *Translational Vision Science and Technology*, 8(6), p. 13. doi: 10.1167/tvst.8.6.13.

Van den Bogerd, B., Ní Dhubhghaill, S. and Zakaria, N. (2018) 'Characterizing human decellularized crystalline lens capsules as a scaffold for corneal endothelial tissue engineering', *Journal of Tissue Engineering and Regenerative Medicine*, 12(4), pp. e2020–e2028. doi: 10.1002/term.2633.

Bohnke, M. *et al.* (1986) 'A simple method for controlled freezing of human donor corneae', *Ophthalmic research*, 18(6), pp. 327–331. doi: 10.1159/000265458.

Bojic, S. *et al.* (2021) 'Winter is coming: the future of cryopreservation', *BMC Biology*. BioMed Central, 19(1), p. 56. doi: 10.1186/S12915-021-00976-8.

Bonanno, J. A. (2012) 'Molecular mechanisms underlying the corneal endothelial pump', *Experimental Eye Research*, 95(1), pp. 2–7. doi: 10.1016/j.exer.2011.06.004.

Bourne, W. M., Nelson, L. I. L. and Hodge, D. O. (1997) 'Central corneal endothelial cell changes over a ten-year period', *Investigative Ophthalmology and Visual Science*, 38(3), pp. 779–782. doi: 10.1016/s0002-9394(14)70810-4.

Bourne, W. M. and Nelson, L. R. (1994) 'Human corneal studies with a vitrification solution containing dimethyl sulfoxide, formamide, and 1,2-propanediol', *Cryobiology*, 31(6), pp. 522–530. doi: 10.1006/cryo.1994.1063.

Bourne, W. M., Nelson, L. R. and Hodge, D. O. (1999) 'Comparison of three methods for human corneal cryopreservation that utilize dimethyl sulfoxide', *Cryobiology*, 39(1), pp. 47–57. doi: 10.1006/CRYO.1999.2182.

Brockbank, K. G. M. *et al.* (2015) 'Vitrification of Heart Valve Tissues', *Methods in Molecular Biology*, 1257, pp. 399–421. doi: 10.1007/978-1-4939-2193-5_20.

Brockbank, K. G. M., Chen, Z. Z. and Song, Y. C. (2010) 'Vitrification of porcine articular cartilage', *Cryobiology*, 60(2), pp. 217–221. doi: 10.1016/j.cryobiol.2009.12.003.

Brunette, I. *et al.* (2001) 'Corneal Transplant Tolerance of Cryopreservation', *Cornea*, 20(6), pp. 590–596. doi: 10.1097/00003226-200108000-00007.

Bukowiecki, A. *et al.* (2017) 'Wound-Healing Studies in Cornea and Skin: Parallels, Differences and Opportunities', *International Journal of Molecular Sciences*, 18(6), p. 1257. doi: 10.3390/IJMS18061257.

Canals, M. *et al.* (1996) 'Long-term cryopreservation of human donor corneas - PubMed', *Eur J Opthalmol*.

Canals, M. *et al.* (1999) 'Morphological study of cryopreserved human corneal endothelium', *Cells Tissues Organs*, 164(1), pp. 37–45. doi: 10.1159/000016641.

Canals, M. *et al.* (2000) 'Optimization of a method for the cryopreservation of rabbit corneas: Attempted application to human corneas', *Cell and Tissue Banking*, 1(4), pp. 271–278. doi: 10.1023/A:1010115623379.

Capella, J. A., Kaufman, H. E. and Robbins, J. E. (1965) 'Preservation of viable corneal tissue', *Cryobiology*, 2(3), pp. 116–121. doi: 10.1016/S0011-2240(65)80096-7.

Català, P. *et al.* (2022) 'Approaches for corneal endothelium regenerative medicine', *Progress in Retinal and Eye Research*, 87, p. 100987. doi: 10.1016/J.PRETEYERES.2021.100987.

Chaurasia, S., Das, S. and Roy, A. (2020) 'A review of long-term corneal preservation techniques: Relevance and renewed interests in the COVID-19 era', *Indian Journal of Ophthalmology*, 68(7), pp. 1357–1363. doi: 10.4103/IJO.IJO_1505_20.

Chen, S. *et al.* (2019) 'Advances in culture, expansion and mechanistic studies of corneal endothelial cells: a systematic review', *Journal of Biomedical Science*, 26(1), p. 2. doi: 10.1186/s12929-018-0492-7.

Crewe, J. M. and Armitage, W. J. (2001) 'Integrity of epithelium and endothelium in organ-cultured human corneas', *Investigative Ophthalmology and Visual Science*, 42(8), pp. 1757–1761.

Cui, Y.-B. and Wu, J. (2012) 'Research progress on the negative factors of corneal endothelial cells proliferation', *International Journal of Ophthalmology*, 5(5), pp. 614–619. doi: 10.3980/J.ISSN.2222-3959.2012.05.14.

DelMonte, D. W. and Kim, T. (2011) 'Anatomy and physiology of the cornea', *Journal of Cataract and Refractive Surgery*, 37(3), pp. 588–598. doi: 10.1016/j.jcrs.2010.12.037.

Dickman, M. M. *et al.* (2016) 'Changing Practice Patterns and Long-term Outcomes of Endothelial Versus Penetrating Keratoplasty: A Prospective Dutch Registry Study', *American Journal of Ophthalmology*, 170, pp. 133–142. doi: 10.1016/j.ajo.2016.07.024.

Dua, H. S. *et al.* (2005) 'Limbal epithelial crypts: a novel anatomical structure and a putative limbal stem cell niche', *British Journal of Ophthalmology*, 89(5), pp. 529–532. doi: 10.1136/BJO.2004.049742.

Dua, H. S. and Said, D. G. (2019a) 'Applied Anatomy of the Corneal Stroma', in Alió, J. L., Alió del Barrio, J. L., and Arnalich-Montiel, F. (eds) *Corneal Regeneration. Therapy and Surgery*. Springer Cham, pp. 349–362. doi: 10.1007/978-3-030-01304-2_23.

Dua, H. S. and Said, D. G. (2019b) 'Ocular Surface Epithelium: Applied Anatomy', in Alio, J. L., Alió del Barrio, J. L., and Arnalich-Montiel, F. (eds) *Corneal Regeneration. Therapy and Surgery*. Springer, Cham, pp. 175–190. doi: 10.1007/978-3-030-01304-2_12.

EBAA Eye banking statistical report 2019 (2020) *Eye Bank Assoc Am.* Available at: www.restoresight.org.

Ebertz, S. L. and McGann, L. E. (2004) 'Cryoinjury in endothelial cell monolayers', *Cryobiology*, 49(1), pp. 37–44. doi: 10.1016/j.cryobiol.2004.04.003.

Eghrari, A. O., Riazuddin, S. A. and Gottsch, J. D. (2015) 'Overview of the Cornea: Structure, Function, and Development', *Progress in Molecular Biology and Translational Science*, 134, pp. 7–23. doi: 10.1016/BS.PMBTS.2015.04.001.

Eisenberg, D. P. *et al.* (2014) 'Thermal expansion of vitrified blood vessels permeated with DP6 and synthetic ice modulators', *Cryobiology*, 68(3), pp. 318–326. doi: 10.1016/J.CRYOBIOL.2014.04.010.

Eisenberg, D. P., Taylor, M. J. and Rabin, Y. (2012) 'Thermal expansion of the cryoprotectant cocktail DP6 combined with synthetic ice modulators in presence and absence of biological tissues', *Cryobiology*, 65(2), pp. 117–125. doi: 10.1016/J.CRYOBIOL.2012.04.011.

Elliott, G. D., Wang, S. and Fuller, B. J. (2017) 'Cryoprotectants: A review of the actions and applications of cryoprotective solutes that modulate cell recovery from ultra-low temperatures', *Cryobiology*, pp. 74–91. doi: 10.1016/j.cryobiol.2017.04.004.

Elliott, J. A. W. (2013) 'Intracellular ice formation: The enigmatic role of cell-cell junctions', *Biophysical Journal*, 105(9), pp. 1935–1936. doi: 10.1016/j.bpj.2013.10.001.

Engelmann, K., Böhnke, M. and Friedl, P. (1988) 'Isolation and long-term cultivation of human corneal endothelial cells', *Investigative Opthalmology & Visual Science*, 29(11), pp. 1656–1662.

Enomoto, K. *et al.* (2006) 'Age differences in cyclin-dependent kinase inhibitor expression and rb hyperphosphorylation in human corneal endothelial cells', *Investigative ophthalmology & visual science*, 47(10), pp. 4330–4340. doi: 10.1167/IOVS.05-1581.

European Directorate for the Quality of Medicines and Healthcare (ed.) (2017) 'Chapter 16. Ocular tissue', in *Guide to the Quality and Safety of Tissues and Cells for Human Application*. 3rd edn. Strasbourg: Council of Europe, pp. 185–195.

Fahy, G. M. and Wowk, B. (2021) 'Principles of Ice-Free Cryopreservation by Vitrification', in Wolkers, W. F. and Oldenhof, H. (eds) *Cryopreservation and Freeze- Drying Protocols*. 4th edn. Humana, New York, NY, pp. 27–97. doi: 10.1007/978-1-0716-0783-1_2.

Feizi, S. (2018) 'Corneal endothelial cell dysfunction: etiologies and management', *Therapeutic Advances in Ophthalmology*, 10, p. 251584141881580. doi: 10.1177/2515841418815802.

Figueiredo, G. S. *et al.* (2019) 'Corneal Epithelial Stem Cells: Methods for Ex Vivo Expansion', in Alió, J. L., Alió del barrio, J. L., and Arnalich-Montiel, F. (eds) *Corneal Regeneration. Therapy and Surgery*. Springer, Cham, pp. 77–97. doi: 10.1007/978-3-030-01304-2_6.

Flockerzi, E. *et al.* (2018) 'Trends in Corneal Transplantation from 2001 to 2016 in Germany: A Report of the DOG–Section Cornea and its Keratoplasty Registry', *American*

Journal of Ophthalmology, 188, pp. 91–98. doi: 10.1016/j.ajo.2018.01.018.

Fong, L. P. *et al.* (1986) 'Cryopreservation of rabbit corneas: Assessment by microscopy and transplantation', *British Journal of Ophthalmology*, 70(10), pp. 751–760. doi: 10.1136/bjo.70.10.751.

Fong, L. P., Hunt, C. J. and Pegg, D. E. (1987) 'Cryopreservation of the rabbit cornea: freezing with dimethyl sulphoxide in air or in medium', *Current eye research*, 6(4), pp. 569–577. doi: 10.3109/02713688709025215.

Frausto, R. F. *et al.* (2020) 'Phenotypic and functional characterization of corneal endothelial cells during in vitro expansion', *Scientific reports*, 10(1), p. 7402. doi: 10.1038/S41598-020-64311-X.

Frausto, R. F., Le, D. J. and Aldave, A. J. (2016) 'Transcriptomic analysis of cultured corneal endothelial cells as a validation for their use in cell replacement therapy', *Cell Transplantation*, 25(6), pp. 1159–1176. doi: 10.3727/096368915X688948.

Gain, P. *et al.* (2016) 'Global survey of corneal transplantation and eye banking', *JAMA Ophthalmology*, 134(2), pp. 167–173. doi: 10.1001/jamaophthalmol.2015.4776.

Gilpin, A. and Yang, Y. (2017) 'Decellularization Strategies for Regenerative Medicine: From Processing Techniques to Applications', *BioMed Research International*, 2017, p. 9831534. doi: 10.1155/2017/9831534.

Hagenah, M. and Böhnke, M. (1993) 'Corneal cryopreservation with chondroitin surfate', *Cryobiology*, 30(4), pp. 396–406. doi: 10.1006/cryo.1993.1039.

Halberstadt, M. *et al.* (2003) 'Cryopreservation of Human Donor Corneas with Dextran', *Investigative Ophthalmology and Visual Science*, 44(12), pp. 5110–5115. doi: 10.1167/iovs.03-0370.

Halberstadt, M., Athmann, S. and Hagenah, M. (2001) 'Corneal cryopreservation with dextran', *Cryobiology*, 43(1), pp. 71–80. doi: 10.1006/CRYO.2001.2342.

He, Z., Forest, F., Gain, P., *et al.* (2016) '3D map of the human corneal endothelial cell', *Scientific Reports*, 6(1), p. 29047. doi: 10.1038/srep29047.

He, Z., Forest, F., Bernard, A., *et al.* (2016) 'Cutting and decellularization of multiple corneal stromal lamellae for the bioengineering of endothelial grafts', *Investigative*

Ophthalmology and Visual Science, 57(15), pp. 6639–6651. doi: 10.1167/iovs.16-20256.

Van Horn, D. L. *et al.* (1977) 'Regenerative capacity of the corneal endothelium in rabbit and cat', *Investigative Ophthalmology and Visual Science*, 16(7), pp. 597–613.

Hos, D. *et al.* (2019) 'Immune reactions after modern lamellar (DALK, DSAEK, DMEK) versus conventional penetrating corneal transplantation', *Progress in Retinal and Eye Research*, 73, p. 100768. doi: 10.1016/j.preteyeres.2019.07.001.

Jang, T. H. *et al.* (2017) 'Cryopreservation and its clinical applications', *Integrative Medicine Research*, 6(1), pp. 12–18. doi: 10.1016/j.imr.2016.12.001.

Jeang, L. J., Margo, C. E. and Espana, E. M. (2021) 'Diseases of the corneal endothelium', *Experimental eye research*, 205, p. 108495. doi: 10.1016/J.EXER.2021.108495.

John Morris, G. and Acton, E. (2013) 'Controlled ice nucleation in cryopreservation--a review', *Cryobiology*, 66(2), pp. 85–92. doi: 10.1016/J.CRYOBIOL.2012.11.007.

Joyce, N. C. *et al.* (1996) 'Cell cycle protein expression and proliferative status in human corneal cells', *Investigative Ophthalmology and Visual Science*, 37(4), pp. 645–655.

Joyce, N. C. (2003) 'Proliferative capacity of the corneal endothelium', *Progress in Retinal and Eye Research*, 22(3), pp. 359–389. doi: 10.1016/S1350-9462(02)00065-4.

Joyce, N. C. (2012) 'Proliferative capacity of corneal endothelial cells', *Experimental Eye Research*, 95(1), pp. 16–23. doi: 10.1016/j.exer.2011.08.014.

Joyce, N. C., Harris, D. L. and Mello, D. M. (2002) 'Mechanisms of mitotic inhibition in corneal endothelium: Contact inhibition and TGF-β2', *Investigative Ophthalmology and Visual Science*, 43(7), pp. 2152–2159.

Kabosova, A. *et al.* (2007) 'Compositional differences between infant and adult human corneal basement membranes', *Investigative Ophthalmology and Visual Science*, 48(11), pp. 4989–4999. doi: 10.1167/iovs.07-0654.

Kim, D. K. *et al.* (2018) 'Functionalized silk fibroin film scaffold using β-Carotene for cornea endothelial cell regeneration', *Colloids and Surfaces B: Biointerfaces*, 164, pp. 340–346. doi: 10.1016/j.colsurfb.2017.11.052.

Kim, T. Y. *et al.* (2001) 'Differential activity of TGF-beta2 on the expression of p27Kip1 and Cdk4 in actively cycling and contact inhibited rabbit corneal endothelial cells', *Molceular*

Vision, 20(7), pp. 261–270.

Klyce, S. D. (2020) '12. Endothelial pump and barrier function', *Experimental Eye Research*, 198, p. 108068. doi: 10.1016/J.EXER.2020.108068.

Konomi, K. *et al.* (2005) 'Comparison of the Proliferative Capacity of Human Corneal Endothelial Cells from the Central and Peripheral Areas', *Investigative Ophthalmology & Visual Science*, 46(11), pp. 4086–4091. doi: 10.1167/IOVS.05-0245.

Kruse, M. *et al.* (2018) 'Electro-spun Membranes as Scaffolds for Human Corneal Endothelial Cells', *Current Eye Research*, 43(1), pp. 1–11. doi: 10.1080/02713683.2017.1377258.

Lambert, N. and Chamberlain, W. (2017) 'The structure and evolution of eye banking: a review on eye banks' historical, present, and future contribution to corneal transplantation', *Journal of Biorepository Science for Applied Medicine*, (5), pp. 23–40. doi: 10.2147/bsam.s114197.

Lavy, I. *et al.* (2017) 'Sex Chromosome Analysis of Postmortem Corneal Endothelium after Sex-Mismatch Descemet Membrane Endothelial Keratoplasty', *Cornea*, 36(1), pp. 11–16. doi: 10.1097/ICO.0000000000001019.

Lewis, P. N. *et al.* (2010) 'Structural Interactions between Collagen and Proteoglycans Are Elucidated by Three-Dimensional Electron Tomography of Bovine Cornea', *Structure*, 18(2), pp. 239–245. doi: 10.1016/J.STR.2009.11.013.

Li, S. *et al.* (2017) 'In vitro biomimetic platforms featuring a perfusion system and 3D spheroid culture promote the construction of tissue-engineered corneal endothelial layers', *Scientific Reports*, 7(1). doi: 10.1038/s41598-017-00914-1.

Li, S., Shyam, R., *et al.* (2020) 'Bicarbonate activates glycolysis and lactate production in corneal endothelial cells by increased pHi', *Experimental Eye Research*, 199, p. 108193. doi: 10.1016/J.EXER.2020.108193.

Li, S., Kim, E., *et al.* (2020) 'Corneal Endothelial Pump Coupling to Lactic Acid Efflux in the Rabbit and Mouse', *Investigative ophthalmology & visual science*, 61(2), p. 7. doi: 10.1167/IOVS.61.2.7.

Li, S., Kim, E. and Bonanno, J. A. (2016) 'Fluid transport by the cornea endothelium is dependent on buffering lactic acid efflux', *American Journal of Physiology - Cell Physiology*,

311(1), pp. C116–C126. doi: 10.1152/AJPCELL.00095.2016.

Liu, C. *et al.* (2019) 'Ex vivo construction of rabbit corneal endothelial cell sheets on a porcine descemet membrane graft', *Experimental and Therapeutic Medicine*, 18(1), pp. 242–252. doi: 10.3892/etm.2019.7573.

Liu, S., Wong, Y. L. and Walkden, A. (2022) 'Current Perspectives on Corneal Transplantation', *Clinical Ophthalmology*, 16, pp. 631–646. doi: 10.2147/OPTH.S289359.

Ljubimov, A. V. and Saghizadeh, M. (2015) 'Progress in corneal wound healing', *Progress in retinal and eye research*, 49, pp. 17–45. doi: 10.1016/J.PRETEYERES.2015.07.002.

Lu, Q. *et al.* (2020) 'Evaluation of reconstructed human corneal endothelium sheets made with porcine Descemet's membrane in vitro and in vivo', *Experimental eye research*, 197, p. 108125. doi: 10.1016/J.EXER.2020.108125.

Lynch, A. P. and Ahearne, M. (2013) 'Strategies for developing decellularized corneal scaffolds', *Experimental eye research*, 108, pp. 42–47. doi: 10.1016/J.EXER.2012.12.012.

Madden, P. W. (1989) 'The assessment of endothelial integrity by scanning electron microscopy and fluorescein diacetate staining following treatment with cryoprotective additives', *Current Eye Research*, 8(1), pp. 17–36. doi: 10.3109/02713688909013891.

Madden, P. W. *et al.* (1993) 'The Effect of Polyvinylpyrrolidone and the Cooling Rate during Corneal Cryopreservation', *Cryobiology*, 30(2), pp. 135–157. doi: 10.1006/cryo.1993.1013.

Maharana, P. *et al.* (2017) 'Component corneal surgery: An update', *Indian Journal of Ophthalmology*, 65(8), pp. 658–672. doi: 10.4103/ijo.IJO_582_17.

Martínez-Conesa, E. M. *et al.* (2022) 'Estrategias adoptadas en el bando de tejido ocular y membrana amniótica tras el impacto de la pandemia por COVID 19', in *XVII congreso de la AEBT*. León (Spain): Asociación Española de Bancos de Tejidos.

Masahito, Y. *et al.* (2015) 'Discovery of molecular markers to discriminate corneal endothelial cells in the human body', *PloS one*, 10(3), p. e0117581. doi: 10.1371/JOURNAL.PONE.0117581.

Massoudi, D., Malecaze, F. and Galiacy, S. (2016) 'Collagens and proteoglycans of the cornea: importance in transparency and visual disorders', *Cell and Tissue Research*, 363(2),

pp. 337–349. doi: 10.1007/s00441-015-2233-5.

Maurice, D. M. (1972) 'The location of the fluid pump in the cornea', *The Journal of Physiology*, 221(1), pp. 43–54. doi: 10.1113/JPHYSIOL.1972.SP009737.

Mazur, P., Leibo, S. P. and Chu, E. H. Y. (1972) 'A two-factor hypothesis of freezing injury. Evidence from Chinese hamster tissue-culture cells', *Experimental cell research*, 71(2), pp. 345–355. doi: 10.1016/0014-4827(72)90303-5.

Meek, K. M. and Knupp, C. (2015) 'Corneal structure and transparency', *Progress in Retinal and Eye Research*, 49, pp. 1–16. doi: 10.1016/j.preteyeres.2015.07.001.

Mimura, T. and Joyce, N. C. (2006) 'Replication competence and senescence in central and peripheral human corneal endothelium', *Investigative Ophthalmology and Visual Science*, 47(4), pp. 1387–1396. doi: 10.1167/iovs.05-1199.

Mishima, S. (1982) 'Clinical Investigations on the Corneal Endothelium', *Ophthalmology*, 89(6), pp. 525–530. doi: 10.1016/S0161-6420(82)34755-7.

Moshirfar, M. *et al.* (2021) 'Corneal Donation: Current Guidelines and Future Direction', *Clinical Ophthalmology*, 15, pp. 2963–2973. doi: 10.2147/OPTH.S284617.

Muhammad, R. *et al.* (2015) 'Micro- and nano-topography to enhance proliferation and sustain functional markers of donor-derived primary human corneal endothelial cells', *Acta Biomaterialia*, 19, pp. 138–148. doi: 10.1016/j.actbio.2015.03.016.

Müller, L. J. *et al.* (2004) 'A new three-dimensional model of the organization of proteoglycans and collagen fibrils in the human corneal stroma', *Experimental Eye Research*, 78(3), pp. 493–501. doi: 10.1016/S0014-4835(03)00206-9.

Müller, L. J., Pels, E. and Vrensen, G. F. J. M. (2001) 'The effects of organ-culture on the density of keratocytes and collagen fibers in human corneas', *Cornea*, 20(1), pp. 86–95. doi: 10.1097/00003226-200101000-00017.

Müller, L., Pels, E. and Vrensen, G. (2001) 'The specific architecture of the anterior stroma accounts for maintenance of corneal curvature', *The British Journal of Ophthalmology*, 85(4), pp. 437–443. doi: 10.1136/BJO.85.4.437.

Müller, T. M. *et al.* (2016) 'Histopathologic Features of Descemet Membrane Endothelial Keratoplasty Graft Remnants, Folds, and Detachments', *Ophthalmology*, 123(12), pp. 2489–

2497. doi: 10.1016/j.ophtha.2016.08.014.

Murphy, C., Alvarado, J. and Juster, R. (1984) 'Prenatal and postnatal growth of the human Descemet's membrane', *Investigative Ophthalmology and Visual Science*, 25(12), pp. 1402–1415.

Myrna, K. E., Pot, S. A. and Murphy, C. J. (2009) 'Meet the Corneal Myofibroblast: the role of myofibroblast transformation in corneal wound healing and pathology', *Veterinary Ophthalmology*, 12(Suppl 1), pp. 25–27. doi: 10.1111/J.1463-5224.2009.00742.X.

Nagy, Z. P., Shapiro, D. and Chang, C. C. (2020) 'Vitrification of the human embryo: a more efficient and safer in vitro fertilization treatment', *Fertility and sterility*, 113(2), pp. 241–247. doi: 10.1016/J.FERTNSTERT.2019.12.009.

Nguyen, T. T. and Bonanno, J. A. (2012) 'Lactate-H+ Transport Is a Significant Component of the In Vivo Corneal Endothelial Pump', *Investigative Ophthalmology & Visual Science*, 53(4), pp. 2020–2029. doi: 10.1167/IOVS.12-9475.

Nishino, T. *et al.* (2019) 'Changing indications and surgical techniques for keratoplasty during a 16-year period (2003–2018) at a tertiary referral hospital in Japan', *Clinical Ophthalmology*, 13, pp. 1499–1509. doi: 10.2147/OPTH.S214515.

Nucci, P. *et al.* (1990) 'Normal endothelial cell density range in childhood', *Archives of ophthalmology*, 108(2), pp. 247–248. doi: 10.1001/ARCHOPHT.1990.01070040099039.

O'Neill, P., Mueller, F. O. and Trevor-Roper, P. D. (1967) 'On the preservation of corneae at -196 degrees C. for full-thickness homografts in man and dog.', *The British journal of ophthalmology*, 51(1), pp. 13–30. doi: 10.1136/bjo.51.1.13.

Okumura, N. *et al.* (2014) 'Cell surface markers of functional phenotypic corneal endothelial cells', *Investigative ophthalmology & visual science*, 55(11), pp. 7610–7618. doi: 10.1167/IOVS.14-14980.

de Oliveira, R. C. and Wilson, S. E. (2020) 'Descemet's membrane development, structure, function and regeneration', *Experimental eye research*, 197, p. 108090. doi: 10.1016/J.EXER.2020.108090.

Pagano, L. *et al.* (2022) 'Clinical Medicine Update on Suture Techniques in Corneal Transplantation: A Systematic Review', *J. Clin. Med*, 2022, p. 1078. doi: 10.3390/jcm11041078.

Palma-Carvajal, F. *et al.* (2020) 'Trends in corneal transplantation in a single center in Barcelona, Spain. Transitioning to DMEK', *Journal Francais d'Ophtalmologie*, 43(1), pp. 1–6. doi: 10.1016/j.jfo.2019.06.026.

Parekh, M., Ahmad, S., *et al.* (2017) 'Human Corneal Endothelial Cell Cultivation From Old Donor Corneas With Forced Attachment', *Scientific Reports*, 7(1), p. 142. doi: 10.1038/s41598-017-00209-5.

Parekh, M., Baruzzo, M., *et al.* (2017) 'Standardizing Descemet Membrane Endothelial Keratoplasty Graft Preparation Method in the Eye Bank—Experience of 527 Descemet Membrane Endothelial Keratoplasty Tissues', *Cornea*, 36(12), pp. 1458–1466. doi: 10.1097/ICO.0000000000001349.

Parekh, M., Borroni, D., *et al.* (2018) 'A comparative study on different Descemet membrane endothelial keratoplasty graft preparation techniques', *Acta Ophthalmologica*, 96(6), pp. e718–e726. doi: 10.1111/AOS.13746.

Parekh, M., Leon, P., *et al.* (2018) 'Graft detachment and rebubbling rate in Descemet membrane endothelial keratoplasty', *Survey of Ophthalmology*, 63(2), pp. 245–250. doi: 10.1016/j.survophthal.2017.07.003.

Parekh, M., Elbadawy, H., *et al.* (2018) 'Recombinant human serum albumin for corneal preservation', *Acta Ophthalmologica*, 96(1), pp. e79–e86. doi: 10.1111/aos.13498.

Pegg, D. E. (2010) 'The relevance of ice crystal formation for the cryopreservation of tissues and organs', *Cryobiology*, 60(3 SUPPL.). doi: 10.1016/j.cryobiol.2010.02.003.

Pegg, D. E. (2015) 'Principles of Cryopreservation', in Wolkers, W. F. and Oldenhof, H. (eds) *Cryopreservation and Freeze-Drying Protocols*. Springer, New York, NY, pp. 3–19. doi: 10.1007/978-1-4939-2193-5_1.

Peh, G. S. *et al.* (2013) 'Optimization of human corneal endothelial cell culture: density dependency of successful cultures in vitro', *BMC Research Notes*, 6(1), p. 176. doi: 10.1186/1756-0500-6-176.

Peh, G. S. L. *et al.* (2011) 'Cultivation of Human Corneal Endothelial Cells Isolated from Paired Donor Corneas', *PLoS ONE*. Edited by R. R. Mohan, 6(12), p. e28310. doi: 10.1371/journal.pone.0028310.

Peh, G. S. L. *et al.* (2015) 'Propagation of Human Corneal Endothelial Cells: A Novel Dual

Media Approach', *Cell Transplantation*, 24(2), pp. 287–304. doi: 10.3727/096368913X675719.

Peh, G. S. L. *et al.* (2017) 'Regulatory Compliant Tissue-Engineered Human Corneal Endothelial Grafts Restore Corneal Function of Rabbits with Bullous Keratopathy', *Scientific Reports*, 7(1), pp. 1–17. doi: 10.1038/s41598-017-14723-z.

'Plan Nacional de Córneas. 2016' (2016). Organización Nacional de Trasplantes, pp. 1–40. Available at: http://www.ont.es/infesp/DocumentosDeConsenso/DOCUMENTO PLAN NACIONAL DE CORNEAS 2016.pdf.

Price, M. O. *et al.* (2017) 'EK (DLEK, DSEK, DMEK): New Frontier in Cornea Surgery', *Annual Review of Vision Science*, 3(1), pp. 69–90. doi: 10.1146/annurev-vision-102016-061400.

Proulx, S. *et al.* (2009) 'Tissue engineering of feline corneal endothelium using a devitalized human cornea as carrier.', *Tissue engineering. Part A*, 15(7), pp. 1709–18. doi: 10.1089/ten.tea.2008.0208.

Radner, W. *et al.* (1998) 'Interlacing and cross-angle distribution of collagen lamellae in the human cornea', *Cornea*, 17(5), pp. 537–543. doi: 10.1097/00003226-199809000-00012.

Raeder, S. *et al.* (2007) 'Effects of Organ Culture and Optisol-GS Storage on Structural Integrity, Phenotypes, and Apoptosis in Cultured Corneal Epithelium', *Investigative Ophthalmology & Visual Science*, 48(12), pp. 5484–5493. doi: 10.1167/IOVS.07-0494.

Raju, R. *et al.* (2021) 'The need for novel cryoprotectants and cryopreservation protocols: Insights into the importance of biophysical investigation and cell permeability', *Biochimica et biophysica acta. General subjects*, 1865(1), p. 129749. doi: 10.1016/J.BBAGEN.2020.129749.

Ramachandran, C. *et al.* (2020) 'In Vitro Culture of Human Corneal Endothelium on Non-Mulberry Silk Fibroin Films for Tissue Regeneration', *Translational Vision Science & Technology*, 9(4), pp. 12–12. doi: 10.1167/TVST.9.4.12.

Rich, S. J. and Armitage, W. J. (1990) 'Propane-1,2-diol as a potential component of a vitrification solution for corneas', *Cryobiology*, 27(1), pp. 42–54. doi: 10.1016/0011-2240(90)90051-5.

Rich, S. J. and Armitage, W. J. (1991) 'Corneal tolerance of vitrifiable concentrations of propane-1,2-diol', *Cryobiology*, 28(2), pp. 159–170. doi: 10.1016/0011-2240(91)90018-J.

Rich, S. J. and Armitage, W. J. (1992) 'Corneal tolerance of vitrifiable concentrations of glycerol', *Cryobiology*, 29(2), pp. 153–164. doi: 10.1016/0011-2240(92)90016-U.

Rizwan, M. *et al.* (2017) 'Sequentially-crosslinked bioactive hydrogels as nano-patterned substrates with customizable stiffness and degradation for corneal tissue engineering applications', *Biomaterials*, 120, pp. 139–154. doi: 10.1016/j.biomaterials.2016.12.026.

Röck, T., Bartz-Schmidt, K. U. and Röck, D. (2018) 'Trends in corneal transplantation at the University eye hospital in Tübingen, Germany over the last 12 years: 2004 – 2015', *PLoS ONE*, 13(6), pp. 2004–2015. doi: 10.1371/journal.pone.0198793.

Rodríguez-Fernández, S. *et al.* (2021) 'Current development of alternative treatments for endothelial decompensation: Cell-based therapy', *Experimental eye research*, 207. doi: 10.1016/J.EXER.2021.108560.

Romano, V. *et al.* (2018) 'Comparison of preservation and transportation protocols for preloaded Descemet membrane endothelial keratoplasty', *British Journal of Ophthalmology*, 102(4), pp. 549–555. doi: 10.1136/bjophthalmol-2017-310906.

Routledge, C. and Armitage, W. J. (2003) 'Cryopreservation of cornea: A low cooling rate improves functional survival of endothelium after freezing and thawing', *Cryobiology*, 46(3), pp. 277–283. doi: 10.1016/S0011-2240(03)00044-0.

Roy, O. *et al.* (2015) 'Understanding the Process of Corneal Endothelial Morphological Change In Vitro', *Investigative Ophthalmology & Visual Science*, 56(2), pp. 1228–1237. doi: 10.1167/iovs.14-16166.

Schindelin, J. *et al.* (2012) 'Fiji: An open-source platform for biological-image analysis', *Nature Methods*, 9(7), pp. 676–682. doi: 10.1038/nmeth.2019.

Schmedt, T. *et al.* (2012) 'Telomerase Immortalization of Human Corneal Endothelial Cells Yields Functional Hexagonal Monolayers', *PLOS ONE*, 7(12), p. e51427. doi: 10.1371/JOURNAL.PONE.0051427.

Schumann, S. *et al.* (2021) 'Establishment of a Robust and Simple Corneal Organ Culture Model to Monitor Wound Healing', *Journal of clinical medicine*, 10(16), p. 3486. doi: 10.3390/JCM10163486.

Senoo, T. and Joyce, N. C. (2000) 'Cell cycle kinetics in corneal endothelium from old and young donors', *Investigative Ophthalmology and Visual Science*, 41(3), pp. 660–667.

Senoo, T., Obara, Y. and Joyce, N. C. (2000) 'EDTA: A promoter of proliferation in human corneal endothelium', *Investigative Ophthalmology and Visual Science*, 41(10), pp. 2930–2935.

Seow, W. Y. *et al.* (2019) 'Ultrathin, Strong, and Cell-Adhesive Agarose-Based Membranes Engineered as Substrates for Corneal Endothelial Cells', *ACS biomaterials science & engineering*, 5(8), pp. 4067–4076. doi: 10.1021/ACSBIOMATERIALS.9B00610.

Singh, N., Said, D. and Dua, H. (2018) 'Lamellar keratoplasty techniques', *Indian Journal of Ophthalmology*, pp. 1239–1250. doi: 10.4103/ijo.IJO_95_18.

Soh, Y., Peh, G. S. . and Mehta, J. (2016) 'Translational issues for human corneal endothelial tissue engineering', *J Tissue Eng Regen Med*, 11(9), pp. 2425–2442. doi: 10.1002/term.2131.

Soma, T. *et al.* (2019) 'Clinical evaluation of a newly developed graft inserter (NS endo-inserter) for descemet stripping automated endothelial keratoplasty', *Clinical Ophthalmology*, 13, pp. 43–48. doi: 10.2147/OPTH.S182628.

Song, J. E. *et al.* (2019) 'Characterization of surface modified glycerol/silk fibroin film for application to corneal endothelial cell regeneration', *Journal of biomaterials science. Polymer edition*, 30(4), pp. 263–275. doi: 10.1080/09205063.2018.1535819.

Song, Z. *et al.* (2008) 'Expression of senescence-related genes in human corneal endothelial cells', *Molecular Vision*, 14, pp. 161–170. Available at: /pmc/articles/PMC2254959/ (Accessed: 31 October 2021).

Spinozzi, D. *et al.* (2020) 'In Vitro Evaluation and Transplantation of Human Corneal Endothelial Cells Cultured on Biocompatible Carriers', *Cell Transplantation*, 29, p. 963689720923577. doi: 10.1177/0963689720923577.

Taylor, M. J. (1986) 'Clinical cryobiology of tissues: Preservation of corneas', *Cryobiology*, 23(4), pp. 323–353. doi: 10.1016/0011-2240(86)90038-6.

Taylor, M. J. *et al.* (2019) 'New Approaches to Cryopreservation of Cells, Tissues, and Organs', *Transfusion Medicine and Hemotherapy*, 46(3), pp. 197–215. doi: 10.1159/000499453.

Taylor, M. J. and Busza, A. L. (1992) 'A convenient, non-invasive method for measuring the kinetics of permeation of dimethyl sulphoxide into isolated corneas using NMR spectroscopy', *Cryo-Letters*, 13, pp. 273–282.

Taylor, M. J. and Hunt, C. J. (1981) 'Dual staining of corneal endothelium with trypan blue and alizarin red S: Importance of pH for the dye-lake reaction', *British Journal of Ophthalmology*, 65(12), pp. 815–819. doi: 10.1136/bjo.65.12.815.

Taylor, M. J. and Hunt, C. J. (1989) 'Tolerance of corneas to multimolar dimethyl sulfoxide at 0 degrees C. Implications for cryopreservation', *Investigative Ophthalmology & Visual Science*, 30(3), pp. 400–412.

Taylor, M. J., Hunt, C. J. and Madden, P. W. (1989) 'Hypothermic preservation of corneas in a hyperkalaemic solution (CPTES): II. Extended storage in the presence of chondroitin sulphate', *The British Journal of Ophthalmology*, 73(10), p. 792. doi: 10.1136/BJO.73.10.792.

Taylor, M. J., Song, Y. C. and Brockbank, K. G. M. (2004) 'Vitrification in Tissue Preservation: New Developments', in Fuller, B. J., Lane, N., and Benson, E. E. (eds) *Life in the Frozen State*. 1st edn. CRC Press, pp. 603–641. doi: doi:10.1201/9780203647073.ch22.

Thériault, M. *et al.* (2019) 'Physiological pressure enhances the formation of tight junctions in engineered and native corneal endothelium', *Experimental Eye Research*, 179, pp. 102–105. doi: 10.1016/j.exer.2018.11.004.

Tran, K. D. *et al.* (2017) 'Rapid warming of donor corneas is safe and improves specular image quality', *Cornea*, 36(5), pp. 581–587. doi: 10.1097/ICO.0000000000001166.

Vázquez, N. *et al.* (2016) 'Human bone derived collagen for the development of an artificial corneal endothelial graft. in Vivo results in a rabbit model', *PLoS ONE*, 11(12), pp. 1–18. doi: 10.1371/journal.pone.0167578.

Vázquez, N. *et al.* (2017) 'Silk fibroin films for corneal endothelial regeneration: Transplant in a rabbit descemet membrane endothelial keratoplasty', *Investigative Ophthalmology and Visual Science*, 58(9), pp. 3357–3365. doi: 10.1167/iovs.17-21797.

Walcerz, D. B., Taylor, M. J. and Busza, A. L. (1995) 'Determination of the kinetics of permeation of dimethyl sulfoxide in isolated corneas', *Cell Biophysics*, 26(2), pp. 79–102. doi: 10.1007/BF02796236.

Winkler, M. *et al.* (2013) 'Three-Dimensional Distribution of Transverse Collagen Fibers in the Anterior Human Corneal Stroma', *Investigative Ophthalmology & Visual Science*, 54(12), pp. 7293–7301. doi: 10.1167/IOVS.13-13150.

Wolkers, W. F. and Oldenhof, H. (2021) 'Principles Underlying Cryopreservation and

Freeze-Drying of Cells and Tissues', in Wolkers, W. F. and Oldenhof, H. (eds) *Methods in Molecular Biology. Cryopreservation and Freeze-Drying Protocols*. 4th edn. Springer US, pp. 3–25. doi: 10.1007/978-1-0716-0783-1_1.

Wollensak, G., Perlman, E. J. and Green, W. R. (2001) 'Interphase fluorescence in situ hybridisation of the X and Y chromosomes in the human eye', *The British journal of ophthalmology*, 85(10), pp. 1244–1247. doi: 10.1136/BJO.85.10.1244.

Woo, J. H. *et al.* (2019) 'Descemet Membrane Endothelial Keratoplasty Versus Descemet Stripping Automated Endothelial Keratoplasty and Penetrating Keratoplasty', *American Journal of Ophthalmology*, 207, pp. 288–303. doi: 10.1016/j.ajo.2019.06.012.

Wowk, B. (2010) 'Thermodynamic aspects of vitrification', *Cryobiology*, 60(1), pp. 11–22. doi: 10.1016/j.cryobiol.2009.05.007.

Wusteman, M. C. *et al.* (1999) 'Cryopreservation studies with porcine corneas', *Current eye research*, 19(3), pp. 228–233. doi: 10.1076/ceyr.19.3.228.5310.

Wusteman, M. C. *et al.* (2008) 'Vitrification of Rabbit Tissues with Propylene Glycol and Trehalose', *Cryobiology*, 56(1), pp. 62–71. doi: 10.1016/j.cryobiol.2007.10.177.

Wusteman, M. C., Boylan, S. and Pegg, D. E. (1997) 'Cryopreservation of rabbit corneas in dimethyl sulfoxide', *Investigative Ophthalmology and Visual Science*, 38(10), pp. 1934–1943.

Yoshida, J. *et al.* (2017) 'Transplantation of Human Corneal Endothelial Cells Cultured on Bio-Engineered Collagen Vitrigel in a Rabbit Model of Corneal Endothelial Dysfunction', *Current Eye Research*, 42(11), pp. 1420–1425. doi: 10.1080/02713683.2017.1351568.

Yoshida, K. *et al.* (2004) 'Involvement of p27KIP1 in the proliferation of the developing corneal endothelium', *Investigative Ophthalmology and Visual Science*, 45(7), pp. 2163–2167. doi: 10.1167/iovs.03-1238.

di Zazzo, A. *et al.* (2021) 'Corneal angiogenic privilege and its failure', *Experimental eye research*, 204, p. 108457. doi: 10.1016/J.EXER.2021.108457.

VIII. Annexes

Annex I – Ethics committee approval

XUNTA DE GALICIA
CONSELLERÍA DE SANIDADE
Secretaría Xeral Técnica

Secretaria Técnica
Comité Autonómico de Ética da Investigación de Galicia
Secretaria Xeral. Consellería de Sanidade
Edificio Administrativo San Lázaro
15703 SANTIAGO DE COMPOSTELA
Tel: 881 546425; ceic@sergas.es

galicia

DICTAMEN DEL COMITÉ DE ÉTICA DE LA INVESTIGACIÓN DE A CORUÑA-FERROL

Carlos Rodríguez Moreno, Secretario del Comité de Ética de la Investigación de A Coruña-Ferrol

CERTIFICA:

Que este Comité evaluó en su reunión del día 12/19/2017 el estudio:

Título: Regeneración endotelial corneal: células madre endoteliales y proliferación celular endotelial
Promotor: Silvia M.ª Díaz Prado
Tipo de estudio: Outros
Version:
Código del Promotor:
Código de Registro: 2017/594

Y, tomando en consideración las siguientes cuestiones:

- La pertinencia del estudio, teniendo en cuenta el conocimiento disponible, así como los requisitos legales aplicables, y en particular la Ley 14/2007, de investigación biomédica, el Real Decreto 1716/2011, de 18 de noviembre, por el que se establecen los requisitos básicos de autorización y funcionamiento de los biobancos con fines de investigación biomédica y del tratamiento de las muestras biológicas de origen humano, y se regula el funcionamiento y organización del Registro Nacional de Biobancos para investigación biomédica, la ORDEN SAS/3470/2009, de 16 de diciembre, por la que se publican las Directrices sobre estudios Posautorización de Tipo Observacional para medicamentos de uso humano, y el la Circular nº 07 / 2004, investigaciones clínicas con productos sanitarios.
- La idoneidad del protocolo en relación con los objetivos del estudio, justificación de los riesgos y molestias previsibles para el sujeto, así como los beneficios esperados.
- Los principios éticos de la Declaración de Helsinki vigente.
- Los Procedimientos Normalizados de Trabajo del Comité.

Emite un **INFORME FAVORABLE** para la realización del estudio **por el/la investigador/a del centro:**

Centros	Investigadores Principales
INIBIC-C.H. Universitario de A Coruña	Silvia M.ª Díaz Prado

Firmado digitalmente por: RODRIGUEZ MORENO CARLOS - 05614327G
Fecha: 2017.12.20 13:57:56 +02'00'

XUNTA DE GALICIA
CONSELLERÍA DE SANIDADE
Secretaría Xeral Técnica

Secretaria Técnica
Comité Autonómico de Ética da Investigación de Galicia
Secretaria Xeral. Consellería de Sanidade
Edificio Administrativo San Lázaro
15703 SANTIAGO DE COMPOSTELA
Tel: 881 546425; ceic@sergas.es

galicia

Y hace constar que:

1.- El Comité Territorial de Ética de la Investigación de A Coruña-Ferrol cumple los requisitos legales vigentes (Ley 14/2007 de Investigación Biomédica y el Decreto 63/2013 por el que se regulan los comités de ética de investigación en Galicia).

2.- La composición actual del Comité Territorial de Ética de la Investigación de A Coruña-Ferrol es:

Salvador Pita Fernández (Presidente). Médico especialista en Medicina Familiar y Comunitaria. Área de Gestión Integrada A Coruña.
Lucía Fuster Sanjurjo (Vicepresidenta). Farmacéutica. Especialista en Farmacia Hospitalaria. Área de Gestión Integrada Ferrol
Carlos Rodríguez Moreno (Secretario). Médico especialista en Farmacología Clínica. Área de Gestión Integrada Santiago
Natalia Cal Purriños (Vicesecretaria). Licenciada en derecho. Fundación "Profesor Nóvoa Santos". A Coruña
Juana Mª Cruz del Rio. Trabajadora social. Consellería de Sanidad
Begoña Graña Suárez. Médica especialista en Oncología Médica. Área de Gestión Integrada A Coruña
Angel Lopez-Silvarrey Varela. Médico especialista en Pediatría. Área de Gestión Integrada A Coruña
Alejandro Pazos Sierra. Médico. Universidad de A Coruña
Gonzalo Peña Pérez. Médico especialista en Cardiología. Hospital de San Rafael. A Coruña
José Mª Rumbo Prieto. Diplomado en enfermería. Área de Gestión Integrada Ferrol
María Isabel Sastre Gervás. Farmacéutica Atención Primaria. Área de Gestión Integrada A Coruña

Para que conste donde proceda, y a petición del promotor / investigador, en Santiago de Compostela,

El secretario

XUNTA DE GALICIA SECRETARÍA XERAL TÉCNICA SECRETARÍA DO COMITÉS DE ÉTICA DA INVESTIGACIÓN CONSELLERÍA DE SANIDADE

Firmado digitalmente por: RODRIGUEZ MORENO CARLOS - 05614327G
Fecha: 2017.12.20 13:58:02 +02'00'

XUNTA DE GALICIA
CONSELLERÍA DE SANIDADE
Secretaría Xeral Técnica

Secretaría Técnica
Comité Autonómico de Ética da Investigación de Galicia
Secretaría Xeral. Consellería de Sanidade
Edificio Administrativo San Lázaro
15703 SANTIAGO DE COMPOSTELA
Tel: 881 546425; ceic@sergas.es

galicia

DICTAMEN DEL COMITÉ DE ÉTICA DE LA INVESTIGACIÓN DE A CORUÑA-FERROL

Sonia Pértega Díaz, Vicesecretaria del Comité de Ética de Investigación de A Coruña-Ferrol

CERTIFICA:

Que este Comité evaluó en su reunión del día 17/04/18 el estudio:

Título: Regeneración endotelial corneal: células madre endoteliales y proliferación celular endotelial.
Promotor: Silvia M.ª Díaz Prado
Enmienda:enmienda nº1
Código del Promotor:
Código de Registro: 2017/594

Y que este Comité emite un **INFORME FAVORABLE** de conformidad con sus procedimientos normalizados de trabajo y tomando en cuenta los requisitos éticos, metodológicos y legales exigibles a los estudios de investigación con seres humanos, sus muestras o registros, que dicha enmienda sea incorporada al estudio de investigación que se está realizando en los centros aprobados.

Y HACE CONSTAR QUE:

1. El Comité Territorial de Ética de la Investigación de A Coruña-Ferrol cumple los requisitos legales vigentes (Ley 14/2007 de Investigación Biomédica y el Decreto 63/2013 por el que se regulan los comités de ética de investigación en Galicia).

2. La composición actual del Comité Territorial de Ética de la Investigación de A Coruña-Ferrol es:

Lucía Fuster Sanjurjo (Presidenta). Farmacéutica. Especialista en Farmacia Hospitalaria. Área de Gestión Integrada Ferrol
Angel Lopez-Silvarrey Varela. **(Vicepresidente)**.Médico especialista en Pediatría. Área de Gestión Integrada A Coruña
Natalia Cal Purriños. (Secretaria). Licenciada en Derecho. Fundación "Profesor Novoa Santos". A Coruña
Sonia Pértega Díaz. (Vicesecretaria). Matemática. Área de Gestión Integrada A Coruña
Juana Mª Cruz del Rio. Trabajadora social. Consellería de Sanidad
Portal González Lorenzo. Médica especialista en Medicina Familiar y Comunitaria. Área de Gestión Integrada Ferrol
Begoña Graña Suárez. Médica especialista en Oncología Médica. Área de Gestión Integrada A Coruña
Carmen Mella Pérez. Médica especialista en Medicina Interna. Área de Gestión Integrada Ferrol
Alejandro Pazos Sierra. Médico. Universidad de A Coruña
Gonzalo Peña Pérez. Médico especialista en Cardiología. Hospital de San Rafael. A Coruña
Carlos Rodríguez Moreno. Médico especialista en Farmacología Clínica. Área de Gestión Integrada Santiago
José Mª Rumbo Prieto. Diplomado en Enfermería. Área de Gestión Integrada Ferrol
María Isabel Sastre Gervás. Farmacéutica Atención Primaria. Área de Gestión Integrada A Coruña

Para que conste donde proceda y a petición del promotor / investigador, en A Coruña

La Vicesecretaria

PERTEGA DIAZ, SONIA (AUTENTICACIÓN)

Firmado digitalmente por PERTEGA DIAZ, SONIA (AUTENTICACIÓN)
Nombre de reconocimiento (DN): c=ES, serialNumber=77596773V, sn=PERTEGA, givenName=SONIA, cn=PERTEGA DIAZ, SONIA (AUTENTICACIÓN)
Fecha: 2018.04.26 11:49:55 +02'00'

Annex II – Research authorization of Xerencia de Xestión Integrada da Coruña

XUNTA DE GALICIA
CONSELLERÍA DE SANIDADE

SERVIZO GALEGO de SAÚDE

CONFORMIDAD DE LA DIRECCIÓN DEL CENTRO

D. José Manuel Vázquez Rodríguez, Coordinador de Docencia e I+D+i de la Xerencia de Xestión Integrada de A Coruña

C E R T I F I C A

Que conoce la propuesta realizada por la Promotora e Investigadora Principal, Dª. SILVIA Mª DÍAZ PRADO, del Grupo de Investigación de Terapia Celular y Medicina Regenerativa del INIBIC, para que sea realizado en este Centro el estudio clínico titulado **"REGENERACIÓN ENDOTELIAL CORNEAL: CÉLULAS MADRE ENDOTELIALES Y PROLIFERACIÓN CELULAR ENDOTELIAL"**.

Que acepta la realización de dicho estudio clínico en este Centro, el cual no comenzará a ejecutarse hasta que se disponga de las autorizaciones por parte de Comité/s de Ética de la Investigación correspondiente/s y, si procede, de Agencia Española del Medicamento y Productos Sanitarios.

Lo que firma en A Coruña, a 21 Diciembre 2017

Xerencia de Xestión Integrada
Coordinador de Docencia, I+D+i

Fdo.: D. José Manuel Vázquez Rodríguez
Coordinador de Docencia e I+D+i

Xerencia de Xestión Integrada
A Coruña

www.galiciasaude.es
Tel. 981 178 000
Xubias de Arriba, 84
15006 A Coruña

056618
J.C. 47

Annex III – Certificate of the internship at the Centre de Recherche du CHU de Québec – Université Laval

IMPRÍMASE EN PAPEL OFICIAL DO CENTRO RECEPTOR DO/A SOLICITANTE DA AXUDA
PRINT IT ON THE OFFICIAL PAPER OF THE INSTITUTION RECEIVING THE APPLICANT
À IMPRIMER SUR LE PAPIER OFFICIEL DU CENTRE DU/DE LA DEMANDEUR/EUSE DE LA 'AIDE

CERTIFICADO DE INCORPORACIÓN_- FINALIZACIÓN DA ESTADÍA
CERTIFICATE OF INCORPORATION AND END OF STAY
CERTIFICAT DE INCORPORATION-FIN DU STAGE

A CUMPLIMENTAR POLO/LA RESPONSABLE DO CENTRO RECEPTOR
TO BE COMPLETED BY THE HEAD OF THE WELCOMING INSTITUTION
A REMPLIR PAR LE RESPONSABLE DU CENTRE DE RECHERCHE D' ACCUEIL

CENTRO RECEPTOR: *Welcoming institution* Centre d'accueil	Centre de Recherche du CHU de Québec – Université Laval, axe médecine régénératrice
APELIDOS E NOME DO/A RESPONSABLE DO CENTRO: *Surnames and name of the head of the institution* Nom et prénom du directeur du centre de recherche	Proulx, Stephanie
O/A abaixo asinante, certifica que o/a investigador/a D./Dª. *The undersigned certifies that the researcher Mr./Ms.* Je soussigné certifie que le chercheur M./Mme.	Silvia Rodríguez Fernández
incorporouse a este centro de investigación o (dd/mm/aaaa). joined the institution on (day/month/year). a rejoint le centre de recherche le (jour/mois/année).	03/09/2019
e finalizou a súa estadía o (dd/mm/aaaa). and finished his/her stay on (day/month/year). et termina son stage le (jour/mois/année).	03/12/2019

En / *In* / A Québec, QC, Canada a / *on* / le 25/11/2020

Stéphanie Proulx
2020.11.25 15:49:32 -05'00'

Fdo. / *Signed* / Signé: Stéphanie Proulx, PhD, Codirectrice de l'Axe médecine régénératrice du Centre de Recherche du CHU de Québec-Université Laval
O/A RESPONSABLE DO CENTRO
(*Head of the welcoming institution* / Directeur du centre d'accueil)

Annex IV – Endothelial cell density (ECD) analysis for each measured endothelial area

Cornea code	Previous ECD (cells/mm²)	Area1 (µm²)	n total cells	n damaged adhered cells	ECD (cells/mm²)	lost ECD (%)	Area2 (µm²)	n total cells	n damaged adhered cells	ECD (cells/mm²)	lost ECD (%)
Cryo1	2342	42615.625	75	14	1431	38.9	43357.812	77	26	1176	49.8
Cryo2	2326	47457.812	115	11	2191	5.8	47339.062	107	9	2070	11.0
Cryo3	2618	32634.375	70	17	1624	38.0	34329.688	73	22	1486	43.3
Cryo4	1992	50217.188	106	10	1912	4.0	50315.625	99	26	1451	27.2
Cryo5	1894	47837.500	95	3	1923	-1.5	49796.875	112	5	2149	-13.4
Cryo6	2217	39943.750	74	14	1502	32.2	36493.75	78	9	1891	14.7
Cryo7	2488	31234.375	78	20	1857	25.4	32979.688	92	18	2244	9.8
Cryo8	2451	18339.062	43	2	2236	8.8	11462.500	28	0	2443	0.3
Cryo9	1608	31744.056	45	0	1418	11.8	35945.659	56	0	1558	3.1

Cornea code	Previous ECD (cells/mm²)	Area3 (µm²)	n total cells	n damaged adhered cells	ECD (cells/mm²)	lost ECD (%)	Area4 (µm²)	n cell (total)	n damaged adhered cells	ECD (cells/mm²)	lost ECD (%)
Cryo1	2342	37942.188	58	14	1160	50.5	19425.000	37	3	1750	25.3
Cryo2	2326	45853.125	92	8	1832	21.2	47029.688	100	17	1765	24.1
Cryo3	2618	27065.625	68	20	1773	32.3	26089.062	62	24	1457	44.4
Cryo4	1992	52898.438	99	11	1664	16.5	49320.312	96	12	1703	14.5
Cryo5	1894	50181.250	100	7	1853	2.1	52823.438	104	11	1761	7.0
Cryo6	2217	40676.562	83	10	1795	19.1	39300.000	79	14	1654	25.4
Cryo7	2488	29690.625	74	15	1987	20.1	25412.500	63	9	2125	14.6
Cryo8	2451	9040.625	22	1	2323	5.2	13865.625	37	5	2308	5.8
Cryo9	1608	39380.067	55	0	1397	13.1	35667.531	61	0	1710	-6.4

Annex V – Sample temperature rates for each programed segment

Segments	Initial temperature (°C)	Final temperature (°C)	Temperature change (°C)	Time (min)	Rate (°C/min)
Seg 1 + 2	4.9	4.2	-0.7	15.08	-0.05
Seg 3	4.2	-5.0	-9.2	7.98	-1.15
Seg 4	-5.0	-7.7	-2.7	0.98	-2.75
Seg 5	-7.8	-2.7	+5.1	0.98	+5.20
Seg 6	-2.7	-3.0	-0.3	0.98	-0.31
Seg 7	-3.1	-6.0	-2.9	1.98	-1.46
Seg 8	-6.1	-38.8	-32.7	29.98	-1.09
Seg 9	-38.8	-78.0	-39.2	14.98	-2.62
Seg 10	-78.0	-116.0	-38.0	10.00	-3.80

Annex VI – Pre-doctoral Scientific Production

Scientific Papers

Rodríguez-Fernández S, Piñeiro-Ramil M, Castro-Viñuelas R, Sanjurjo-Rodríguez C, Alvarez-Portela M, Fuentes-Boquete IM, Rendal-Vázquez E, Díaz-Prado SM. Current development of alternative treatments for endothelial decompensation: Cell-based therapy. Exp. Eye Res. 2021;207:108560. doi: 10.1016/j.exer.2021.108560.

Piñeiro-Ramil M, Sanjurjo-Rodríguez C, Rodríguez-Fernández S, Castro-Viñuelas R, Hermida-Gomez T, Blanco-Garcia FJ, Fuentes-Boquete I, Díaz-Prado SM. Generation of Mesenchymal Cell Lines Derived from Aged Donors. Int. J. Mol. Sci. 2021;22(19). doi: 10.3390/ijms221910667.

Castro-Viñuelas R, Sanjurjo-Rodríguez C, Piñeiro-Ramil M, Rodríguez-Fernández S, Lopez-Baltar I, Fuentes-Boquete I, Blanco FJ, Díaz-Prado SM. Tips and tricks for successfully culturing and adapting human induced pluripotent stem cells. Mol. Ther. Methods Clin. Dev. 2021;23:569-81. doi: 10.1016/j.omtm.2021.10.013.

Rodríguez-Fernández S, Alvarez-Portela M, Rendal-Vazquez E, Piñeiro-Ramil M, Sanjurjo-Rodríguez C, Castro-Viñuelas R, Sánchez-Ibáñez J, Fuentes-Boquete I, Díaz-Prado SM. Analysis of Cryopreservation Protocols and Their Harmful Effects on the Endothelial Integrity of Human Corneas. Int. J. Mol. Sci. 2021;22(22). doi: 10.3390/ijms222212564.

Castro-Viñuelas R, Sanjurjo-Rodríguez C, Piñeiro-Ramil M, Hermida-Gomez T, Rodríguez-Fernández S, Oreiro N, de Toro J, Fuentes I, Blanco FJ, Díaz-Prado SM. Generation and characterization of human induced pluripotent stem cells (iPSCs) from hand osteoarthritis patient-derived fibroblasts. Sci. Rep. 2020;10(1):4272. doi: 10.1038/s41598-020-61071-6.

Piñeiro-Ramil M, Castro-Viñuelas R, Sanjurjo-Rodríguez C, Rodríguez-Fernández S, Hermida-Gomez T, Blanco-Garcia FJ, Fuentes-Boquete I, Díaz-Prado SM. Immortalizing Mesenchymal Stromal Cells from Aged Donors While Keeping Their Essential Features. Stem. Cells. Int. 2020;2020:5726947. doi: 10.1155/2020/5726947.

Sanjurjo-Rodríguez C, Castro-Viñuelas R, Piñeiro-Ramil M, Rodríguez-Fernández S, Fuentes-Boquete I, Blanco FJ, Díaz-Prado SM. Versatility of Induced Pluripotent Stem Cells (iPSCs) for Improving the Knowledge on Musculoskeletal Diseases. Int. J. Mol. Sci. 2020;21(17). doi: 10.3390/ijms21176124.

Castro-Viñuelas R, Sanjurjo-Rodríguez C, Piñeiro-Ramil M, Rodríguez-Fernández S, Fuentes-Boquete IM, Blanco FJ, Díaz-Prado SM. Generation of a human control iPS cell line (ESi080-A) from a donor with no rheumatic diseases. Stem. Cell. Res. 2020;43:101683. doi: 10.1016/j.scr.2019.101683.

Piñeiro-Ramil M, Sanjurjo-Rodríguez C, Castro-Viñuelas R, Rodríguez-Fernández S, Fuentes-Boquete IM, Blanco FJ, Díaz-Prado SM. Usefulness of Mesenchymal Cell Lines for Bone and Cartilage Regeneration Research. Int. J. Mol. Sci. 2019;20(24). doi: 10.3390/ijms20246286.

Poster Presentations

Sanjurjo-Rodríguez C, Fraga-Lodeiro M, Fernández-Abeledo I, Rodríguez-Fernández S, Hermida-Gómez T, Piñeiro-Ramil M, Fuentes-Boquete I; Blanco FJ; Díaz-Prado S; de Toro FJ. Aislamiento y caracterización de exosomas obtenidos de diferentes tipos celulares provenientes de pacientes sin artrosis. Exhibited at: XLVIII Congreso Nacional de la Sociedad Española de Reumatología. 2022 May 10-13. Granada, Spain.

Piñeiro-Ramil M, Sanjurjo-Rodríguez C, Rodríguez-Fernández S, Rocío Castro-Viñuelas R, Hermida-Gómez T, De Toro-Santos J, Blanco-García F, Fuentes-Boquete I, Díaz-Prado S. Inmortalización de condrocitos articulares para investigación en artrosis. Exhibited at: XLVII congreso nacional de la Sociedad Española de Reumatología. 2021 Oct 19-22. Palma de Mallorca, Spain.

C. Sanjurjo-Rodríguez C, Montoto-Fernández A, Hermida-Gómez T; Piñeiro-Ramil M, Rodríguez-Fernández S, Fuentes-Boquete IM, de Toro FJ, Blanco FJ, Díaz-Prado SM. Aislamiento y caracterización de exosomas obtenidos de células madre pluripotentes inducidas provenientes de pacientes sin artrosis [poster]. Exhibited at: XLVII congreso nacional de la Sociedad Española de Reumatología. 2021 Oct 19-22. Palma de Mallorca, Spain.

Piñeiro-Ramil M, Sanjurjo-Rodríguez C, Rodríguez-Fernández S, Rocío Castro-Viñuelas R, Hermida-Gómez T, Blanco-García F, Fuentes-Boquete I, Díaz-Prado S. Generation of an immortalized chondrocyte cell line from osteoarthritis articular cartilage. Exhibited at: 2021 OARSI Virtual World Congress. 2021 Apr 29-May 1.

Castro-Viñuelas R, Sanjurjo-Rodríguez C, Piñeiro-Ramil M, Rodríguez-Fernández S, Fuentes-Boquete IM, Blanco-García FJ, Díaz-Prado SM. Comparison of three different chondrogenic differentiation protocols to obtain chondrocyte-like cells from induced pluripotent stem cells. Exhibited at: 2020 OARSI World Congress on Osteoarthritis. 2020 Apr 30-May 3. Vienna, Austria. doi: 10.1016/j.joca.2020.02.056.

Rodríguez-Fernández S, Thériault M, Proulx S; Díaz-Prado S. Tissue-engineered graft for a Descemet Membrane Endothelial Keratoplasty. Exhibited at: 11 Journée Annuelle de ThéCell (Réseau de thérapie cellulaire, tissulaire et génique du Québec). 2019 Nov 26. Québec, Canada.

Rodríguez-Fernández S, Álvarez-Portela M, Rendal-Vázquez ME, Montero-Salinas A, Piñeiro-Ramil M, Castro-Viñuelas R, de Rojas MV, Sánchez-Ibáñez J, Fuentes-Boquete IM, Díaz-Prado S. Corneal cryopreservation: an endothelial cell viability and histomorphological study of the cornea. Ehbitied at : III Annual Meeting CINBIO. 2019 Jul 1-2. Vigo, España.

Piñeiro-Ramil M, Castro-Viñuelas R, Sanjurjo-Rodríguez C, Rodríguez-Fernández S, Hermida-Gómez T, de-Toro-Santos FJ, Blanco-García FJ, Fuentes-Boquete IM, Díaz-Prado SM. Generation of osteoarthritic mesenchymal stromal cell lines. Annals of the Rheumatic Diseases. Exhibited at: Annual European Congress of Rheumatology (EULAR). 2019. 2019 Jun 12-15. Madrid, Spain. doi: 10.1136/annrheumdis-2019-eular.6717.

Oral Presentations

Rodríguez-Fernández S, Rendal-Vázquez E, Álvarez-Portela M, Piñeiro-Ramil M, Rodríguez-Sanjurjo C, Sánchez-Ibáñez J, Fuentes-Boquete I, Díaz-Prado S. Análisis de un protocolo de criopreservación de córneas y del estado final de las córneas criopreservadas. XVII Congreso de la AEBT (Asociación Española de Bancos de Tejidos). 2022. León, Spain.

Castro-Viñuelas R, Sanjurjo-Rodríguez C, Piñeiro-Ramil M, Rodríguez-Fernández S, Hermida-Gómez T, de Toro-Santos J, Blanco-García, F, Fuentes-Boquete I, Díaz-Prado S.

Establishment of human induced pluripotent stem cell-lines (iPSc) as a tool for studying hand osteoarthritis. Fifth E.S.T.R.O.T. (European Society of Tissue Regeneration in Orthopedics and Traumatology). 2019. Málaga, Spain.

Piñeiro Ramil M, Castro-Viñuelas R, Sanjurjo-Rodríguez C, Rodríguez-Fernández S, Hermida-Gómez T, de Toro-Santos J, Blanco-García F, Fuentes-Boquete I, Díaz-Prado, S. Generation of mesenchymal stromal cell lines from osteoarthritic patients. Fifth E.S.T.R.O.T. (European Society of Tissue Regeneration in Orthopedics and Traumatology) Congress. 2019. Málaga, Spain.

Piñeiro-Ramil M, Castro-Viñuelas R, Sanjurjo-Rodríguez C, Rodríguez-Fernández S, Hermida-Gómez T, Blanco-García F, Fuentes-Boquete I, Díaz-Prado S. Generación y caracterización de líneas celulares mesenquimales "artrósicas" y "sanas" (Generation and characterization of "arthritic" and "health" mensenchymal cell lines). XLV Congreso Nacional de la Sociedad Española de Reumatología. 2019. Valencia, Spain.

Rodríguez-Fernández S. Conservación y regeneración de la córnea para aloimplante. 14ª Happy Hour CICA-INIBIC (Centro de Investigaciones Avanzadas de la Universidade da Coruña – Instituto de Investigación Biomédica de A Coruña). 2019. A Coruña, Spain.

Sánchez-Ibáñez J, Rodríguez-Fernández S, Álvarez-Portela M, Rendal-Vázquez ME, Montero-Salinas A, Piñeiro-Ramil M, Castro-Viñuelas R, de Rojas MV, Fuentes-Boquete IM, Díaz-Prado S. Corneal cryopreservation: an enndotelial cell viability and histomorphology study of the cornea. 27th Annual Congress of the European Association of Cells and Tissue Bank. 2018. Lille, France.

Annex VII – Extended abstract in Galician

O transplante de córnea ou queratoplastia é en moitas ocasións o único tratamento dispoñible para tratar as enfermidades endoteliais corneais e traumas graves neste tecido. Porén, o número de córneas doadas é inferior ao número de persoas que precisan un transplante de córnea actualmente. O número de pacientes con problemas corneais increméntase ano a ano debido, por un lado, ao aumento da esperanza de vida da poboación e, por outro lado, á seguridade que ofrecen os transplantes a nivel poscirúrxico, que fai que se propoña unha queratoplastia como tratamento para certas enfermidades corneais que se atopan en estadios iniciais. Así, a enfermidade non chega a avanzar máis e a danar máis tecido. Por estas razóns, o número de pacientes en lista de espera para realizar unha queratoplastia non deixa de medrar.

Actualmente, os métodos de conservación de tecidos corneais só permiten un almacenamento en óptimas condicións de ata 14 días, se as córneas se almacenan en hipotermia, ou ata un máximo de catro semanas, se estas son postas en cultivo. Se non son transplantadas nese intervalo de tempo, as córneas son automaticamente descartadas. O que marca este límite de almacenamento é a deterioración do endotelio corneal no medio de preservación utilizado. O endotelio corneal é unha monocapa de células que mantén o tecido transparente e que non ten capacidade rexenerativa. Nacemos cunhas densidade celular endotelial de 3.000 células/mm^2 e vaise perdendo ao redor dun 0,6 % de células por ano. Unha enfermidade ou un trauma que afecten directa ou indirectamente á córnea poden acelerar a perda das células endoteliais e, se se chega ao límite de, aproximadamente, 500 células/mm^2, o endotelio deixa de funcionar correctamente, polo que a córnea se volvería translúcida e mesmo se produciría a cegueira.

Por outra banda, certos transplantes de córneas, como as queratoplastias endoteliais que se realizan cando é unicamente o endotelio corneal o que está danado, esixen unha calidade alta en canto a densidade celular endotelial. Debido a que é sabido que co paso dos anos se perden células endoteliais, que estas non se repoñen de forma natural e que os doantes de córneas son de idades avanzadas, é difícil acadar estes requisitos de calidade nas córneas doadas. Por todo o exposto, é preciso buscar alternativas para aumentar o tempo de almacenamento de córneas viables ou buscar outras fontes de tecidos corneais.

A criopreservación é un método de conservación de materias biolóxicos a baixas temperaturas, normalmente a -196 °C, co que se paraliza a actividade encimática das células e que, en condicións ideais, conservaría a viabilidade do material biolóxico criopreservado unha vez desconxelado. Para isto, utilízanse solucións de criopreservación que conteñen axentes crioprotectores, como o dimtelil sulfóxido (DMSO), a formamida ou o polietilenglicol, en que se embebe o material biolóxico. Os axentes crioprotectores axudan a controlar a formación de xeo durante o proceso de arrefriamento e quentamento da mostra, ou mesmo a evitalo se a temperatura de arrefriamento é moi rápida. Neste último caso a criopreservación chámase vitrificación. Con todo, os axentes crioprotectores adoitan ser tóxicos e a súa introdución e retirada do tecido debe ser controlada e feita a baixas temperaturas. Deste xeito, evitaríase a citotoxicidade e os problemas relacionados con desequilibrios na osmose que poden danar as células ou os tecidos.

A idea de aumentar o tempo de conservación de córneas utilizando a criopreservación xurdiu no século pasado. Tras diversos intentos, ningún protocolo testado puido ser aplicado na práctica clínica, pois os resultados mostraban que o endotelio corneal perdía a súa viabilidade e integridade. Por mor disto, e tamén pola gran variabilidade de resultados que se observaron en diferentes estudos clínicos onde se transplantaban córneas criopreservadas en humanos, este método de almacenamento recoméndase, a día de hoxe, só para queratoplastia tectónica. Este tipo de queratoplastia só se utiliza en emerxencias para manter a integridade do globo ocular en caso de que a córnea fose, por exemplo, perforada. O paciente, con este parche de emerxencia que non necesita ser viable, agardaría ata que se lle transplantase unha córnea funcional.

A enxeñaría de tecidos é unha disciplina médica que se podería aplicar para aumentar o número de córneas ou directamente, de enxertos corneais específicos para tipos concretos de transplantes de córnea. Dende hai anos, véñense probando diferentes formas de construír un enxerto para unha queratoplastia endotelial utilizando estruturas naturais ou sintéticas que substitúan o complexo endotelio-membrana de Descemet danado. As estruturas naturais que proceden do corpo humano, como as lamelas estromais corneais ou as membranas que rodean o cristalino, con características físicas semellantes á da membrana de Descemet, son quizais os mellores andamios que se poderían utilizar, xa que serían biocompatibles e posuirían proteínas extracelulares a que se poderían ancorar as células endoteliais para formar un endotelio. A mellor fonte de células para construír

o endotelio, a día de hoxe, serían as células endoteliais humanas primarias, illadas e expandidas en cultivo. Non obstante, aínda se ten que desenvolver un protocolo normalizado de traballo para poder illar, caracterizar e cultivar estas células para clínica, co que se cumprirían as boas prácticas clínicas.

Os obxectivos desta tese foron dous. O primeiro, consistiu en testar catro protocolos diferentes de criopreservación en córneas e avaliar as córneas criopreservadas, facendo fincapé no endotelio corneal para saber se algún deles se poderían aplicar na práctica clínica. O segundo obxectivo consistiu en elaborar un enxerto para queratoplastia endotelial utilizando a membrana de Descemet descelularizada e as células endoteliais de córneas que foron descartadas para seren usadas na clínica.

Para o primeiro obxectivo, partiuse de catro protocolos diferentes: dous de tipo convencional en que a temperatura baixaba de forma controlada para o que se utilizaron como os axentes crioprotectores DMSO e albumina (Protocolo 1, P1) ou só DMSO (Protocolo 2, P2) e dous protocolos de criopreservación mediante vitrificación para os que se utilizaron DMSO, propilenglicol (Protocolo 3, P3) e, a maiores, formamida no Protocolo 4 (P4). Unha vez criopreservadas as córneas con cada un dos protocolos, avaliouse o estado xeral das córneas e das súas capas utilizando a tinguidura de tricrómico de Masson e analizouse a viabilidade e integridade do endotelio cun ensaio de Calceina AM.

A estrutura do estroma corneal viuse deformada tras aplicar todos os protocolos de criopreservación, e o seu grosor tras a criopreservación con P1 (616,8 μm), P2 (617,2 μm), P3 (695,6 μm) e P4 (807,3 μm) foi maior con respecto ao dunha córnea almacenada en hipotermia (452,5 μm). O epitelio corneal só se mantivo adherido nas córneas criopreservadas cos P1 e P2, aínda que non tiña todas as capas celulares e mostraba unha superficie irregular e células máis pequenas do normal. De todos os protocolos, só o P1 proporcionou células endoteliais viables con membranas intactas e actividade encimática, mentres que cos P2, P3 e P4, as células adheridas á membrana de Descemet das córneas criopreservadas non resultaron viables. Por isto, decidiuse seguir analizando as córneas criopreservadas co P1 e analizar os parámetros relacionados coa criopreservación.

Continuouse tinguindo as córneas criopreservadas co P1 coa tinguidura de azul tripán e vermello de alizarina para analizar de novo o endotelio, e con microscopía electrónica de transmisión para estudar o estroma das córneas criopreservadas máis en detalle.

Observouse que a integridade do endotelio e a viabilidade das córneas criopreservadas co P1 semellaba a observada co ensaio de Calceina AM. Apreciouse que había moita variabilidade respecto da integridade dos endotelios. Nalgunhas córneas víronse estrías sen células na membrana de Descemet e áreas acelulares que representarían unha célula ou un grupo de células. O número de células adheridas danadas tamén foi moi variable entre as mostras utilizadas; comunmente aparecían sobre engurras do tecido, aos arredores das áreas sen células, ou de forma illada por todo o endotelio. A porcentaxe de densidade celular endotelial perdida tras a criopreservación, calculada tendo só en conta as células endoteliais adheridas, variou nun rango de entre -1 ± 9 % e 41 ± 12 %. Seguindo co estroma, a distancia media entre as fibras de coláxeno das córneas criopreservadas co P1 foi superior á distancia media dunha córnea almacenada en hipotermia, mais non se viron roturas causadas polo xeo no estroma posterior, aínda que si queratocitos deshidratados.

Para explicar estes resultados, recolléronse distintas variables relacionadas co protocolo de criopreservación. A osmolalidade nas solucións de criopreservación do P1 foi crecendo conforme aumentaba a concentración de DMSO. Porén, a osmolalidade da solución de lavado utilizada para retirar os crioprotectores foi significativamente hipotónica (274.0 ± 1.0 mOsm/kg) con respecto da última solución de criopreservación utilizada (1647.0 ± 7.2 mOsm/kg). Continuando coas solucións de lavado do P1 apreciouse, utilizando espectroscopía de resonancia magnética nuclear, que estas solucións foron efectivas á hora de retirar o DMSO, xa que, tras os tres lavados, quedaba un 0,1 M do 0,8 M de DMSO que contiñan as córneas no seu interior antes da retirada co axente crioprotector. Canto á temperatura de arrefriamento das córneas criopreservadas, esta baixou rapidamente de -1 °C/min ata aproximadamente os -80 °C e -3,8 °C/min ata aproximadamente os -120 °C.

Para continuar co estudo das córenas criopreservadas, propúxose crear un modelo de transplante penetrante *in vitro* co que poder estudar o comportamento das córneas criopreservadas. Para iso, primeiro buscouse optimizar o transplante *in vitro* con dúas córneas almacenadas en hipotermia, procedentes dun home e dunha muller. Así, probáronse as condicións de cultivo (medio e tempo de cultivo), os métodos de identificación das células do donante e receptor (*cell tracers* ou hibridación fluorescente *in situ* (*FISH*; *fluorescence in situ hybridization*)) e o método para detectar as proteínas do endotelio (inmunofluorescencia sobre o endotelio do transplante enteiro ou sobre unha criosección do transplante penetrante). Os dous modelos de transplantes xerados *in vitro*

mantivéronse en cultivo durante 4 e 9 semanas. Con todo, non se puido realizar o seguimento das células endoteliais xa que este se perdeu durante o cultivo, igual que o epitelio, utilizando unha forma de cultivo estática e cun medio específico para a expansión de células endoteliais. Por mor diso, tampouco se puido verificar se os *cell tracers* garantían a identificación das células endoteliais do receptor e do doante. Porén, o *FISH* si foi unha forma efectiva de identificar o sexo dos tecidos, aínda que non se logrou manter a adhesión da sección do modelo no portaobxectos, por se perder sempre a parte do doante.

Para o segundo obxectivo, desvitalizáronse córneas humanas descartadas para o seu uso en clínica. Retiráronse de forma efectiva as células endoteliais da membrana de Descemet das córneas utilizando o método físico de conxelación-desconxelación. Logo, extraéronse as membranas de Descemet descelularizadas para seren utilizadas como andamios. As células endoteliais corneais foron illadas de córneas descartadas para o seu uso en clínica, extraendo primeiro o complexo endotelio-membrana de Descemet, e logo, as células endoteliais deste complexo. Estas células foron cultivadas cun medio de expansión para células endoteliais corneais.

Antes de comezar a crear os enxertos coas células endoteliais primarias, optimizouse o volume de medio para sementar as células utilizando a liña de células endoteliais humanas inmortalizadas HCEnC-21T. Ao crear un enxerto con estas liñas inmortalizadas, observouse que un volume de 200 µl de suspensión celular non se mantiña sobre a membrana de Descemet descelularizada, senón que se expandía na placa de cultivo reducindo o número de células inicial desexado sobre a membrana de Descemet. Tras cinco días de cultivo, as células inmortalizadas cubriran completamente a membrana de Descemet descelularizada. O enxerto creado con células inmortalizadas analizouse mediante inmunofluorescencia para ver se se formara unha monocapa, utilizando a proteína das unións estreitas zonula ocludens-1 (ZO-1) como marcador, e contratinguindo con faloidina para ver as fibras de actina. As células expresaron ZO-1 a nivel de membrana e mostraron unha forma poligonal.

Para crear catro enxertos para queratoplastia endotelial, as células endoteliais primarias en pase 1, e xa sen a súa morfoloxía hexagonal característica, foron sementadas sobre catro membranas de Descemet descelularizadas nunha densidade suficiente como para ter unha densidade celular endotelial de 3 000 células/mm^2 (superior á requirida para unha

queratoplastia endotelial) e nun volume de 100 µl que permitiu que se adherisen principalmente na membrana de Descemet descelularizada. O cultivo dos catro enxertos creados realizouse nunha placa de cultivo adherente durante sete días e cambiábaselles o medio en días alternos. Realizouse un seguimento do crecemento e a expansión celular co microscopio de contraste de fases e apreciouse que dous enxertos dos catro se desadheriron do plástico de cultivo e se enrolaron dificultando a visualización das células. Tamén se observou que, do día un ao sete, os ocos baleiros que tiña a membrana de Descemet descelularizada se foron cubrindo con células primarias, as cales tamén se expandiron ao plástico de cultivo. A día sete, mediuse a circularidade das células dos enxertos creados mediante enxeñaría de tecidos utilizando o programa Fiji, e a circularidade das células adheridas en plástico.

Unha circularidade nunhas células cun valor arredor de 0,8 considérase morfoloxía hexagonal. Os enxertos foron fixados para detectar as proteínas da unión estreita entre células ZO-1, e as proteínas das unións adherentes entre células N-cadherina e β-catenina. Ademais, foron contratinguidos coa faloidina para observar a actina do citoesqueleto das células endoteliais maila súa disposición.

As células endoteliais dos catro endotelios construídos mostraban unha morfoloxía de tipo fibroblástico, con valores de circularidade de entre 0,61 e 0,69. As células cultivadas sobre plástico mostraron unha circularidade con valores comprendidos entre 0,52 e 0,62. Isto corroborouse coa contratinguidura na inmunofluorescencia con faloidina, onde se observan fibras de actina alongadas, típicas de células migrantes. Só en dous dos catros enxertos para queratoplastia endotelial se aprecia un grupo de células con actina disposta en forma de anel no citoplasma. Respecto das proteínas que participan nas unións célula-célula para formar un endotelio, só nos mesmos enxertos onde había células endoteliais con actina disposta en forma de anel se expresou ZO-1 a nivel de membrana celular, mentres que non se aprecia ningunha expresión de N-cadherina e β-cateina a nivel de membrana en ningún dos catro enxertos xerados.

Os resultados que se obtiveron para o primeiro obxectivo mostraron que só o P1 proporcionou córneas criopreservadas con células endoteliais viables. Porén, a variabilidade dos resultados impide aplicar este protocolo na clínica, para o que é preciso realizar máis estudos onde se testen diferentes parámetros de criopreservación que permitan conservar a viabilidade endotelial e as células adheridas á membrana de

Descemet, e tamén conservar a estrutura xeral da córnea. Por exemplo, habería que evitar o posible estrés osmótico causado ás células durante a retirada do DMSO, utilizando solucións de lavado con concentracións decrecentes e cunha osmolalidade tamén decrecente respecto da última solución de criopreservación. Tamén se poderían probar diferentes ramplas de arrefriamento, con baixadas de temperatura máis suaves que poderían ser beneficiosas e controlar a formación de posible xeo intracelular. Respecto da utilización do modelo de queratoplastia penetrante *in vitro* para estudar o comportamento das células endoteliais da córnea criopreservada, non se puideron establecer as condicións óptimas debido á perda do endotelio e ao número reducido de córneas usadas.

Os resultados do segundo obxectivo mostraron que é posible crear un enxerto reciclando córneas descartadas. Non obstante, a curta duración deste estudo impediu que se crease un endotelio completamente funcional. Sería necesario aumentar o tempo de cultivo deste enxerto para permitir que as células endoteliais formen as unións célula-célula necesarias para a formación da monocapa endotelial.

Estas dúas prometedoras metodoloxías representan alternativas con que, nun futuro, se podería reciclar e incrementar o número de tecidos corneais que poidan ser transplantados, coque se poderían tratar más pacientes con enfermidades corneais.